

Prairie View A&M University

Digital Commons @PVAMU

All Theses

8-2024

An Experimental Investigation Of Printing Speed, Layer Thickness, And Nozzle Temperature On The Mechanical Properties Of Silk- Pla Printed Specimens

Razaul Islam

Follow this and additional works at: <https://digitalcommons.pvamu.edu/pvamu-theses>

AN EXPERIMENTAL INVESTIGATION OF PRINTING SPEED, LAYER
THICKNESS, AND NOZZLE TEMPERATURE ON THE MECHANICAL
PROPERTIES OF SILK-PLA PRINTED SPECIMENS

A Thesis

by

RAZAUL ISLAM

Submitted to the Office of Graduate Studies of
Prairie View A&M University
in partial fulfillment of the requirements for the degree of

MASTER OF SCIENCE

August 2024

Major Subject: Mechanical Engineering

AN EXPERIMENTAL INVESTIGATION OF PRINTING SPEED, LAYER
THICKNESS, AND NOZZLE TEMPERATURE ON THE MECHANICAL
PROPERTIES OF SILK-PLA PRINTED SPECIMENS

A Thesis

by
RAZAUL ISLAM

Submitted to the Office of Graduate Studies of
Prairie View A&M University

in partial fulfillment of the requirements for the degree of

MASTER OF SCIENCE

Approve as to style and content by:

Jeajong Park
Chair of Committee

Xiaobo Peng
Co-Chair of Committee

Lai Jiang
Member

Jeffrey Streator
Head of Department

Pamela Obiomon
Dean, College of Engineering

Tyrone Tanner
Dean, Graduate School

August 2024

Major Subject: Mechanical Engineering

ABSTRACT

An Experimental Investigation of Printing Speed, Layer Thickness, and Nozzle Temperature on the Mechanical Properties of Silk-PLA Printed Specimens.

(August 2024)

Razaul Islam, B.Eng., Shenyang Aerospace University

Chair of Advisory Committee: Dr. Jaejong Park

Co-Chair of Advisory Committee: Dr. Xiaobo Peng

Fused Deposition Modeling (FDM) is a popular 3D printing technique used across various industries. Choosing the right printing parameters is essential for ensuring the overall quality and integrity of 3D-printed products. These parameters greatly affect the quality and strength of 3D-printed items. The focus of this study was the influence of printing parameters such as layer thickness, nozzle temperature, and printing speed on the mechanical behavior of 3D-printed silk polylactic acid (PLA). Tensile tests were conducted on a universal testing machine to analyze the mechanical behavior of the printed materials. Moreover, Digital Image Correlation (DIC) analyses were utilized on the tested specimens to determine the displacement and strain across the entire surface area. The test specimens were printed with layer thicknesses of 0.1mm, 0.15mm, and 0.2 mm. The temperatures of the nozzle used during printing varied from 200°C, 210°C, and 220°C, whereas print speeds of 100 mm/s, 120 mm/s, and 140 mm/s were considered. The other printing parameters were kept consistent for all specimens. The tensile specimen, adhering to ASTM D638 standards, was designed using SolidWorks CAD software. In this study, the

maximum UTS was observed at 40.68 MPa at 0.2mm layer thickness, 220°C nozzle temperature, and 120mm/s print speed, whereas a layer thickness of 0.2mm, nozzle temperature of 200°C, and print speed of 120mm/s demonstrated the lowest tensile stress, measuring 25.79 MPa. The analysis of variance (ANOVA) indicated that the interaction between layer thickness, nozzle temperature, and printing speed significantly affected the tensile strength and Young's modulus of Silk-PLA. This study revealed that nozzle temperature was the most critical parameter regarding the ultimate tensile strength and Young's modulus, providing crucial insights for optimizing 3D printing parameters, whereas DIC results showed comprehensive insights into the deformation and full field strain distribution of the 3D-printed materials.

Index Terms- Additive manufacturing, FDM, mechanical properties, Silk-PLA, DIC.

DEDICATION

I decided to dedicate this to my father, Mr. Anwarul Islam, and my mother, Mrs. Rezia Akter, for their boundless love and unwavering sacrifices. I also extend my heartfelt gratitude to my two elder sisters, Nasrin Ruma and Nazma Lupin, for their continuous support, encouragement, and affection have been a constant source of strength throughout this journey. I am deeply grateful for all of your presence in my life, for believing in my dreams, and for being my unwavering pillar of strength. Thank you.

ACKNOWLEDGMENTS

I want to express my heartfelt thanks to my faculty advisors- Dr. Jaejong Park and Dr. Xiaobo Peng, for their immeasurable support and guidance throughout my master's program. I would like to express my sincere gratitude to Dr. Lai Jiang for being a part of my thesis committee. I sincerely thank the National Science Foundation awards #2110760, #2107140, and the Department of Energy award #DENA0003987. Moreover, I am also grateful to Prairie View A&M University's (RISE) and (PRISE) programs for funding this research work.

TABLE OF CONTENTS

	Page
ABSTRACT.....	iii
DEDICATION.....	v
ACKNOWLEDGMENTS	vi
TABLE OF CONTENTS.....	vii
LIST OF FIGURES	ix
LIST OF TABLES.....	xiv
CHAPTER	
1. INTRODUCTION	1
1.1. Motivation.....	1
1.2. Thesis Objective.....	2
1.3. Road Map of the Thesis	4
2. LITERATURE REVIEW	5
2.1. Additive Manufacturing.....	5
2.2. Rapid Prototyping Process.....	6
2.3. Fused Deposition Modeling (FDM).....	7
2.4. Mechanical Properties Analysis of FMD Printed Material.....	8
2.5. Digital Image Correlations.....	16
2.6. Uniqueness of this research	18
3. METHODOLOGY	20
3.1. Materials	21
3.2. Fabrication of Test Specimen	22
3.3. Selected Printing Parameters	26
3.3.1. Layer Thickness.....	26

3.3.2. Nozzle Temperature	28
3.3.3. Printing Speed	29
4. RESULTS AND DISCUSSION	30
4.1. Tensile Testing.....	30
4.2. Optimizing the Printing Parameter	38
4.2.1. Analysis of Variance for Ultimate Tensile Strength	38
4.2.2. Analysis of Variance for Young's Modulus.....	51
4.3. DIC Experiment	61
4.3.1. 3D Printing for DIC.....	61
4.3.2. Sample Preparation.....	62
4.3.3 Experimental Setup	63
4.3.4. Image Acquisition	67
4.4. DIC Data Analysis	68
4.4.1. DIC Multiple Point Strain Analysis	68
4.5. DIC Result Analysis	85
5. CONCLUSION AND FUTURE WORKS	87
5.1. Conclusion	87
5.2. Printing Challenges.....	89
5.3. Future work	90
REFERENCES	91
CURRICULUM VITAE.....	101

LIST OF FIGURES

FIGURE		Page
1.	Outline of proposed research work.	3
2.	Flow chart of different states involved in the 3D printing processes [2].....	7
3.	(a) Illustration of the FDM technique [6], (b) INTAMSYS Funmat HT FDM 3D printer.	7
4.	Tensile stress vs different printing angle curves for different layer thicknesses [5].	9
5.	The mechanical properties exhibited by natural PLA (left side) and carbon-fiber-reinforced PLA (right side) are affected by different nozzle temperatures [12]...	10
6.	Stress-strain curve for three different printing speeds [19].	11
7.	Part printed using a 0.4 mm nozzle, a) 20 % infill, and b) 40 % infill [28].....	13
8.	Different build orientation of tensile specimens [5].	14
9.	Infill of 25 %, 50%, 75%, and 100 % [30], and diffrent infill pattern [31].	14
10.	a) Five different materials' tensile modulus, b) tensile modulus (MPa) for different infill for PLA material [36].....	16
11.	a) DIC set up with MTS Universal Testing machine, b) An illustration of the DIC technique.	18
12.	Flow chart of the research methodology.....	21
13.	Silk-PLA filament.....	22
14.	a) ASTM D638 Type I Tensile testing specimens (units in millimeters) [67], b) CAD design tensile specimens.....	22
15.	INTAMSYS FUNMAT HT 3D Printer.	23
16.	a) Tensile Specimen in Intamsuit Software, b) 27 types of different parameters printed tensile specimen.....	26
17.	Sample of three different layer thicknesses of 3D printed material, a) 0.05mm, b) 0.10mm, and c) 0.15mm [69].....	27

18.	a) Intamsys funmat HT 3D Printer with 0.4 mm nozzle, and b) Markforge X7 3D printer with 0.4mm nozzle.	28
19.	MTS E42 Universal Testing Machine during tensile testing.....	30
20.	Twenty-seven (27) different parameters in a total of 135 fractured specimens after tensile testing.	32
21.	Sample 1-9 Tensile Stress vs Strain graph (Layer thickness - 0.10mm).	32
22.	Sample 10-18 Tensile Stress vs Strain graph (Layer thickness- 0.15mm).	34
23.	Sample 19-27 Stress vs Strain graph (Layer thickness- 0.2mm).	35
24.	Tensile Stress vs Strain Curve for the Specimen- L3T1P3 with the lowest UTS. 36	
25.	Tensile Stress vs Strain Curve for the Specimen- L3T3P2 with the highest UTS.	36
26.	Tensile Strength (MPa) vs Sample Number graph.	37
27.	Young's Modulus (MPa) vs Sample Number graph.....	37
28.	A main effects plot illustrating the variations in Ultimate Tensile Strength (MPa).	40
29.	Residual plot of ultimate tensile strength at 95% confidence interval a) Normal plot for residuals, (b) Versus fits plot for residuals, (c) Histogram plot for residuals, and (d) Versus order plot for residuals.	42
30.	Interaction Plot between the three printing parameters.	43
31.	Contour Plot of UTS (MPa) vs Nozzle Temperature (°C), Layer thickness (mm).	45
32.	Contour Plot of UTS (MPa) vs Print Speed (mm/s), Layer Thickness (mm).....	46
33.	Contour Plot of UTS (MPa) vs Print Speed (mm/s), Nozzle Temperature (°C). .	47
34.	Ultimate Tensile Strength (MPa) in a 3D surface plot vs Print Speed (mm/s), Layer Thickness (mm).	48
35.	Ultimate Tensile Strength (MPa) in a 3D surface plot vs Nozzle Temperature(°C), Layer Thickness(mm).	49
36.	Ultimate Tensile Strength (MPa) in a 3D surface plot vs Print Speed (mm/s), Nozzle Temperature(°C).	50

37.	A main effects plot illustrating the variations in Young's modulus.	52
38.	Plot of Young's Modulus at 95% of confidence interval; (a) Normal plot for residuals, (b) Versus fits plot for residuals, (c) Histogram order plot for residuals, and (d) Versus order plot for residuals.	53
39.	Interaction Plot between the significant parameters.	54
40.	Contour Plot of Young's Modulus (MPa) vs Nozzle Temperature (°C), Layer Thickness(mm).	55
41.	Contour Plot of Young's Modulus (MPa) vs Print Speed(mm/s), Layer Thickness(mm).	56
42.	Contour Plot of Young's Modulus (MPa) vs Print Speed (mm/s), Nozzle Temperature (°C).	57
43.	Young's Modulus (MPa) in a 3D surface plot vs Print speed (mm/s), Nozzle Temperature (°C).	58
44.	Young's Modulus (MPa) in a 3D surface plot vs Nozzle Temperature (°C), Layer Thickness (mm).	59
45.	Young's Modulus (MPa) in a 3D surface plot vs Print Speed(mm/s) Layer Thickness (mm).	60
46.	DIC process is outlined. From left, (a) Tensile specimens printed by FMD, (b) Create white and then black speckle pattern on the specimens, (c) Equipment set up	61
47.	a) A white base coat is first applied using an acrylic spray, b) Light black paint is sprayed to a crated speckle pattern. This speckle pattern is traced in DIC to capture the strain field.	62
48.	DIC experimental setup.	63
49.	Left and Right camera calibration before the DIC experiment process.....	64
50.	False color image of left and right camera.....	65
51.	Calibration images are taken in camera plate for nine different settings.....	66
52.	DIC left and right camera captures images in different measuring sequences.	67
53.	Strain (ϵ_{yy}) illustrated through contour plots for testing sample 3 L1T1P3 in the Y-direction.	68

54.	Time vs strain graph for point 1 and point 2 for testing sample 3.....	69
55.	Strain (ϵ_{xx}) illustrated through contour plots for testing sample 3 L1T1P3 in the X-direction.	70
56.	Strain illustrated through contour plots for testing sample 1.....	71
57.	Strain illustrated through contour plots for testing sample 2.....	71
58.	Strain illustrated through contour plots for testing sample 3.....	72
59.	Strain illustrated through contour plots for testing sample 4.....	72
60.	Strain illustrated through contour plots for testing sample 5.....	73
61.	Strain illustrated through contour plots for testing sample 6.....	73
62.	Strain illustrated through contour plots for testing sample 7.....	74
63.	Strain illustrated through contour plots for testing sample 8.....	74
64.	Strain illustrated through contour plots for testing sample 9.....	75
65.	Strain illustrated through contour plots for testing sample 10.....	75
66.	Strain illustrated through contour plots for testing sample 11.....	76
67.	Strain illustrated through contour plots for testing sample 12.....	76
68.	Strain illustrated through contour plots for testing sample 13.....	77
69.	Strain illustrated through contour plots for testing sample 14.....	77
70.	Strain illustrated through contour plots for testing sample 15.....	78
71.	Strain illustrated through contour plots for testing sample 16.....	78
72.	Strain illustrated through contour plots for testing sample 17.....	79
73.	Strain illustrated through contour plots for testing sample 18.....	79
74.	Strain illustrated through contour plots for testing sample 19.....	80
75.	Strain illustrated through contour plots for testing sample 20.....	80
76.	Strain illustrated through contour plots for testing sample 21.....	81

77.	Strain illustrated through contour plots for testing sample 22.....	81
78.	Strain illustrated through contour plots for testing sample 23.....	82
79.	Strain illustrated through contour plots for testing sample 24.....	82
80.	Strain illustrated through contour plots for testing sample 25.....	83
81.	Strain illustrated through contour plots for testing sample 26.....	83
82.	Strain illustrated through contour plots for testing sample 27.....	84
83.	Printing failure sample at 140mm/s printing speed.	89

LIST OF TABLES

TABLE	Page
1. 3D printing machine specification [68].	24
2. 3D printing process parameters and levels	24
3. Constant process parameter	24
4. Layer thickness with printing parameters.	25
5. Results of the tensile experiment	31
6. Analysis of the variance table for ultimate tensile strength.....	39
7. Analysis of the variance table for young's modulus.....	51

CHAPTER 1

INTRODUCTION

1.1. Motivation

The rapid advancement of technology in the 21st century has significantly revolutionized various sectors, particularly in the realm of manufacturing. One such groundbreaking technology is Additive Manufacturing (AM), commonly known as 3D printing. Additive manufacturing produces a part layer by layer, which differs from traditional manufacturing, like the CNC machining process that removes materials from bulk materials. Due to this, 3D printing minimizes material waste and can print intricate shapes, thereby conserving a significant amount of raw materials throughout the printing process. 3D printing components have become widely used in industries including biomedicine, aerospace, automotive engineering [1], civil engineering, food industry, and so on.

There are a total seven different types of 3D printed technology invented so far. They are Directed energy deposition (DED), Sheet Lamination (SHL), Binder Jetting (BJT), Vat Photopolymerization (VPP), Material Jetting (MJT), Material Extrusion (MEX), Powder Bed Fusion (PBF) [2]. Vat Photopolymerization (VPP), which includes processes like Stereolithography (SLA) and Material Jetting (MJT), are liquid-based techniques, while the others are solid-based.

This thesis follows the style of the *IEEE*.

Among them, FDM is considered the most used technique, and it is predominantly used for polymer-based materials. FDM systems operate by feeding filament into the liquefier through a motor, where it is melted. Once the material is melted, deposits layer by layer until a complete part is finished. One of the benefits of using the FDM technique is its simplicity and flexible ability to fabricate products without creating a physical mold tailored to the desired shape. Many studies have been conducted on various materials to assess their suitability for use in FDM printing. However, PLA is frequently used as a thermoplastic material because of its low cost and biodegradable properties, making PLA a popular option for many applications.

In additive manufacturing (3D printing), printing parameters are considered one of the most crucial factors in the creation of high-quality 3D printed products. The quality and strength of 3D printed products can be greatly impacted by printing parameters, including the nozzle diameter, thickness of layers, different infill patterns, extruder or nozzle temperature, raster angle, and printing head speeds. By optimizing these parameters, the 3D-printed parts can have better surface quality, cost-effectiveness, and enhanced mechanical performance.

1.2. Thesis Objective

Until now, many studies have revealed the process parameter optimization for FMD 3D printing, but there has been less emphasis on studying the mechanical properties of Silk-PLA printed materials, and their deformation response was analyzed employing an optical system known as a Digital Image Correlation (DIC) method. This study delved into the mechanical response of 3D-printed Silk-PLA under varying processing conditions, specifically focusing on three distinct settings. Three distinct layer thicknesses were

employed for the specimens. The nozzle temperatures used for printing were between 200°C and 220°C in 10°C increments, while the corresponding printing speeds were 100 mm/s, 120 mm/s, and 140 mm/s, respectively. To assess the mechanical behavior of the specimens, tensile testing was performed with a universal testing machine, and each sample of a total of 27 printing specimens was tested with a DIC.

By doing so, the research sought to establish a definitive correlation between the process parameters and the mechanical strength of silk PLA materials. To identify the printing settings that had the greatest influence on the Silk-PLA specimens, a statistical analysis was conducted. The image-based strain analysis method known as DIC was analyzed for the complete deformation and strain fields of a testing sample.

By understanding the FDM process parameters with silk PLA, this study aimed to optimize printing parameters, which will lead to enhanced product quality, reduced costs, and improved mechanical performance. Ultimately, these advancements will further promote the widespread adoption of FDM technology and Silk-PLA materials in various industries. The outline of the proposed research work is given in Fig. 1.

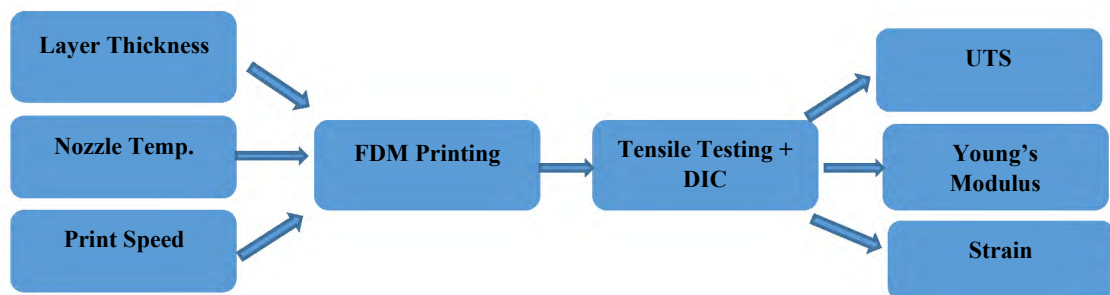


Fig. 1 Outline of proposed research work.

1.3. Road Map of the Thesis

This study is structured into five chapters, each addressing specific sections of the thesis. Chapter 1 studied the introduction and objectives of this research, and Chapter 2 explains the literature review focusing on Fused Deposition Modeling (FDM), mechanical characteristics analysis on FDM printed materials, and the recent application of digital image correlation techniques. Further, Chapter 3 describes the methodology of research, procedures for experimentation, collection of data, and statistical data analysis methods. Chapter 4 delves into the Image correlation technique, experimental procedures, and the analysis of DIC data. Finally, Chapter 5 summarizes the thesis findings, highlights the uniqueness of this research, and suggests some future work.

CHAPTER 2

LITERATURE REVIEW

2.1. Additive Manufacturing

Additive Manufacturing (AM), or Rapid Prototyping, represents a revolutionary approach to product development and manufacturing in the last few decades. AM debuted in 1987 with the introduction of stereolithography (SL) by 3D Systems, and SLA-1 holds the distinction of being the first commercial additive manufacturing (AM) system available in history [3]. Initially, AM was dominated by American companies like Stratasys, 3D Systems, and Z Corp, [2] but the AM landscape has expanded globally with significant contributions from Europe, led by companies like EOS in Germany, and in 2012, Israel company Objet joined with Stratasys Inc., becoming the largest manufacturing company in the history of additive manufacturing [3]. Further, China developed a 3D printing system that can produce large objects recently [4].

The advancements in additive manufacturing (AM) methods for creating small to medium and large-scale scale during the last few decades revolutionized the manufacturing industry. It has increasingly gained popularity because AM enables the creation of complex and customized 3D objects directly from CAD data. It constructs complex parts layer upon successive layers, removing the necessity for expensive tooling and minimizing material waste. As a result, it significantly reduced the time and cost associated with traditional manufacturing. Therefore, it has been utilized in various industries, with an emphasis on fast production and iterative design processes.

2.2. Rapid Prototyping Process

3D printing, or rapid prototyping, utilizes a multi-stage process to transform CAD models into physical objects shown in Fig. 2. The process begins with the design of the initial 3D model in CAD software. The CAD model is then converted into stereolithography (STL) format. Finally, the STL file is sent to the core program [2], with each stage playing a crucial role in the 3D printing process.

Step 1 CAD Design: by using CAD software packages like AutoCAD, NX, and SolidWorks the desired parts/ products can be drawn for 3D printing. Step 2 STL file Generation: following that, the CAD file is converted and saved in the stereolithography (STL) format. Using Cura software like Intamsuite, slice the 3D design parts and convert them to G code to understand the 3D printer. The slicing software processes the 3D model layer by layer, creating a toolpath for the 3D printer to follow. Step 3 File Transfer: the converted STL file requires uploading to the 3D printer for the printing process. Step 4 Machine Setup: before starting the printing, bed auto-leveling, default bed temperature, and some other printing setup would be done automatically. Before initiating the build process, it is essential to configure additional build parameters. Step 5 Build: the nozzle is designed to move freely along the X, Y, and Z axes within a designated build volume and feed materials through one or multiple nozzles. The parts are built sequentially, with each layer added according to the 3D CAD model and its stereolithography information. Step 6 Remove: after the 3D printed part is done, it should be taken out of the machine. Step 7 Post-processing: in some cases, post-processing steps like surface coating, smoothing, support removal, etc., are necessary before using the 3D-printed part. Step 8 Application:

ready for use. However, some parts may need to be assembled with other parts to complete the final part.

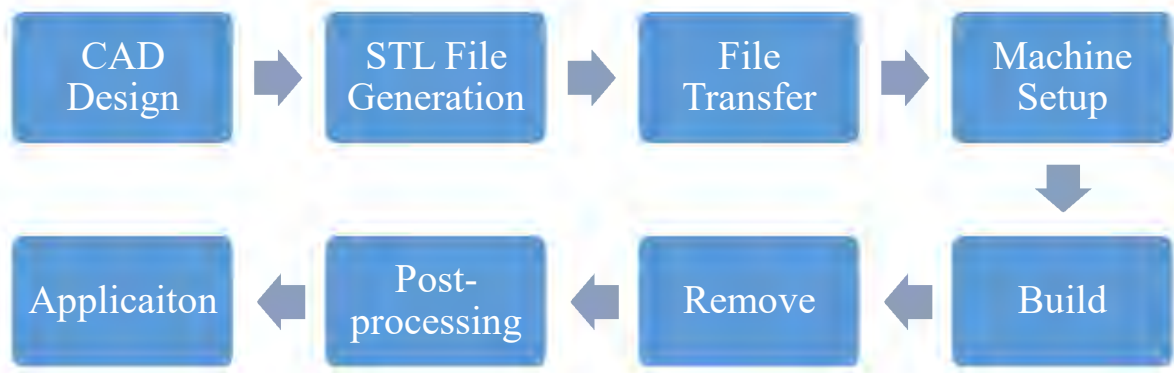


Fig. 2 Flow chart of different states involved in the 3D printing processes [2].

2.3. Fused Deposition Modeling (FDM)

Fused Deposition Modeling (FDM) was first invented by S. Scott Crump in 1988 and became popular with Stratasys Inc. [5]. FDM builds parts by depositing molten filament layer-by-layer until the part is completed. Initially, the raw material is pushed through the guided nozzle, as shown in Fig. 3(a) and (b), where it transitions from a filament form to a semi-liquid state. Subsequently, the semi-liquid substance is applied

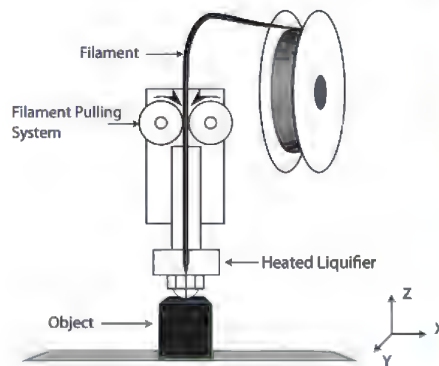


Fig. 3(a) Illustration of the FDM technique [6], (b) INTAMSYS Funmat HT FDM 3D printer.

over the former layer, then it cools down, hardens, and merges with the materials around it. Once an entire layer has been applied, the platform holding the object lowers by the thickness of one layer, allowing the printing of the subsequent layer until it completes the full part [5]. Nowadays, due to material diversity, cost-effectiveness, user-friendliness, and accessibility, FMD 3D printers have become more and more popular in many sectors.

2.4. Mechanical Properties Analysis of FMD Printed Material

Mechanical characteristics of materials produced through Fused Deposition Modeling, including strength, stiffness, and impact durability, are crucial elements in determining the structural integrity of the 3D printed parts. Therefore, numerous researchers have undertaken various efforts to enhance the properties and quality of 3D-printed parts. Several factors significantly impact the quality of a 3D-printed part. These include layer thickness, nozzle temperature, printing speed, infill density, that is, how much material is inside, build orientation, how the object is positioned during printing, raster angle, direction of material lines within each layer, raster gap, spacing between the lines, and so on. Therefore, the modification of FDM technique process parameters has been a major focus of many researchers. For instance, R Murugan et al. [7] investigated to determine how different parameters influence 3D-printed structures.

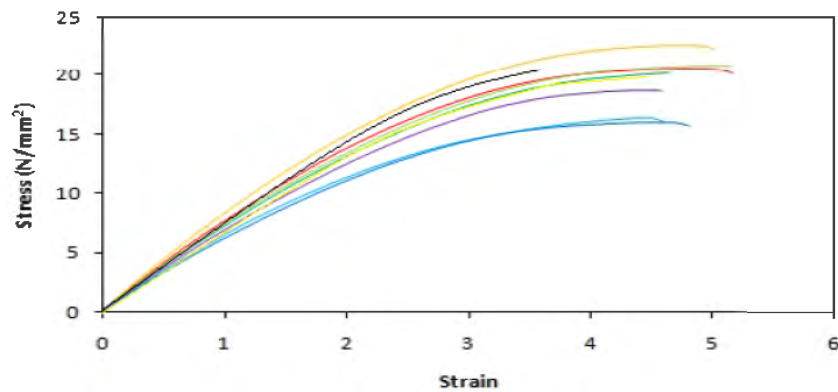


Fig. 4 Stress-strain curve derived from a tensile testing [7].

Their investigation demonstrated that the layer height notably influences the mechanical properties, as shown in Fig.4, and printing duration, whereas the temperature of extrusion is vital for determining the elastic modulus.

Vaibhav Bhosale et al. [8] studied how process parameters affect mechanical properties. According to their findings, layer height and infill percentage, as process parameters, are vital for determining the strength and surface roughness. By printing with a thinner layer thickness, FDM's tensile strength and surface roughness improved.

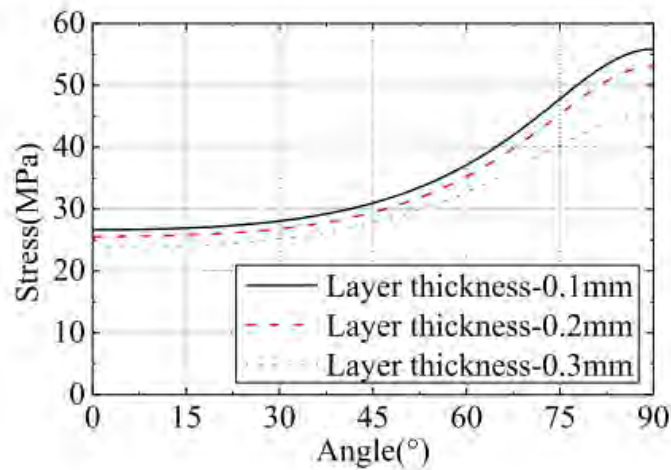


Fig. 5 Tensile stress vs different printing angle curves for different layer thicknesses [5].

Tianyun Yao et al. [5] analyzed FDM printed materials mechanical characteristics at seven distinct angles and three different layer thicknesses of PLA. They discovered that increased thickness of layer to 0.3 mm leads to lower tensile strength, as shown in Fig. 5. The same conclusion was reported by V. Durga Prasada and coworkers [9], highlighting that the optimal tensile strength was observed with a layer thickness of 0.1 mm. Lanzotti and coworkers [10] investigated the influence of changes in layer thickness alongside other process parameters and considered layer thickness between 0.1mm and 0.2mm. By analyzing various parameters, they predicted the optimum combinations that would yield

the highest ultimate tensile strength and strain. Researchers like J.M. Chacón and his team [11] revealed that thicker layers lead to improvement in mechanical properties. Moreover, greater strength and stiffness were demonstrated by samples in on-edge and flat orientations printed material, whereas those with upright orientations demonstrated the weakest mechanical properties. Further, Magri and his team [12] examined how different nozzle temperatures affect mechanical characteristics, as shown in Fig. 6. Their observation was that the maximum tensile properties of PLA parts were achieved by elevating the nozzle temperature to 230°C.

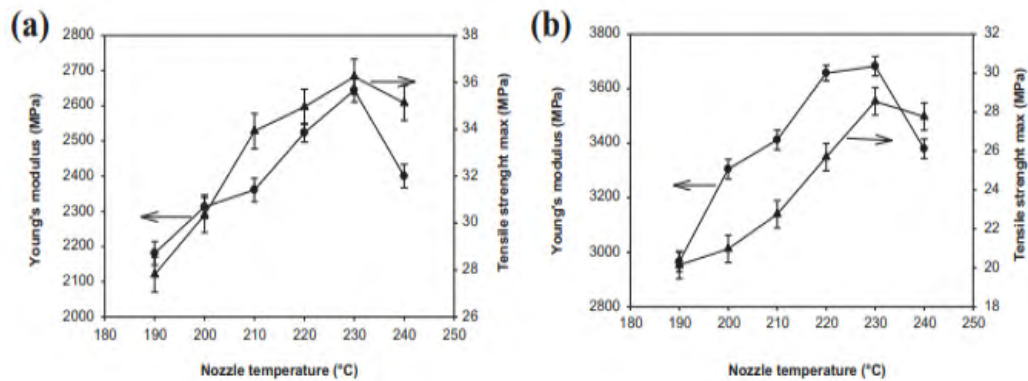


Fig. 6 The mechanical properties exhibited by natural PLA (left side) and carbon-fiber-reinforced PLA (right side) are affected by different nozzle temperatures [12].

For FDM-printed PLA material, Maguluri et al. [13] suggest a nozzle temperature of 220°C. This was supported by Alsoufi et al. [14] who set the nozzle temperature at 220°C for printing parts with 100% infill. The temperature of the nozzle is much more significant and sensitive than its printing speed when considering the strength of printed PLA specimens. When the nozzle temperature was raised from 180°C to 220°C, the highest tensile strength was seen [15].

Furthermore, the work by Yang et al. [16], and Heidari-Rarani et al. [17] supported the significance of optimizing the printing speed for FMD 3D printing. Both of this researcher's investigations examined how the combination of FDM printing speed and other parameters impact PLA printed materials and the conclusion has been reached that optimizing printing speed is essential for achieving better mechanical properties in FDM-printed PLA parts. Moreover, some researchers studied the feasibility of FDM printing speed when it exceeded 100 mm/s for Polylactic Acid (PLA). Similarly, Nabavi-Kivi and coworkers [18] reported that the most significant elongation and optimal tensile strength is achieved through printing at 70 mm/s. In Napolitano et al's [19] research, they analyzed the mechanical properties of PLA in a series of experiments that involved varying FDM parameters, including printing speed at 110mm/s. According to their findings, as illustrated in Fig. 7, a printing speed of 110 mm/s results in the highest tensile strength for PLA materials.

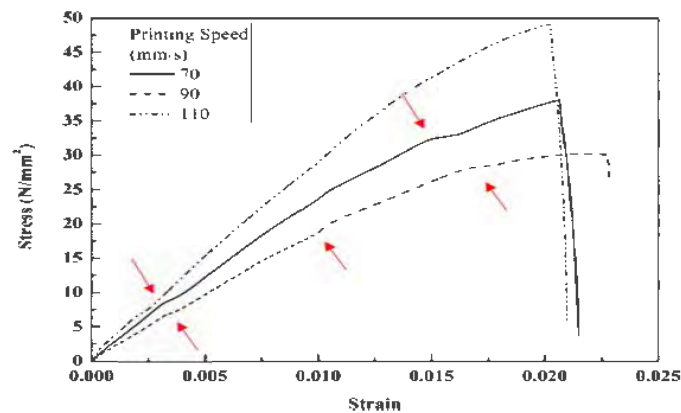


Fig. 7 Stress-strain curve for three different printing speeds [19].

Nonetheless, according to Łukasz Miazio et al. [20] and Mohammad Reza Khosravani et al. [21], PLA materials tend to decrease tensile strength as printing speeds increase. Another researcher, Rezaeian and his coworkers [22] examined printing speeds

at four varying rates for ABS material. The most optimal results were obtained when printing at a speed of 70 mm/s, exhibiting the highest elongation and fracture resistance. Changes in raster layout and printing speed were investigated by Khosravani et al. [23] as they fabricated 3D-printed parts. This study showed that increased raster angle resulted in a decrease in the mechanical properties of the examined specimens. The orientation of the raster considerably impacts the robustness of the specimen [21].

According to Mohammad Reza Khosravani et al. [23], the mechanical properties are decreased when the raster angle is increased. Recent studies by Xinzhou Zhang et al. [24] explained that the highest tensile strength shows the tensile specimens printed with 0° raster angle, whereas the lowest is at 90° raster angle. Mohammed Algarni [25] investigated how three distinct raster angles affect the mechanical behavior of PLA. Notably, their study identified parts printed with a 90° raster angle exhibited a 36% increase in maximum tensile strength compared to those printed with a 0° orientation.

Nozzle diameter significantly influences the 3D-printed parts. The most used nozzle diameters in the FDM printer are 0.3, 0.4, 0.5, 0.6, and 0.8 mm, and they could be altered according to the demand of the printed part. Sudin et al. [26] found that adjusting the nozzle diameter can be a way to influence the mechanical strength of the printed part. The head of the FDM 3D printer was tested with seven different printing nozzle diameters studied by Wojciech Kiński and coworkers [27]. According to their finding, a 0.5 mm nozzle diameter was the best choice for maximizing the printed material's strength, and superior surface quality was observed as the printing nozzle's diameter increased, and the printing time decreased.

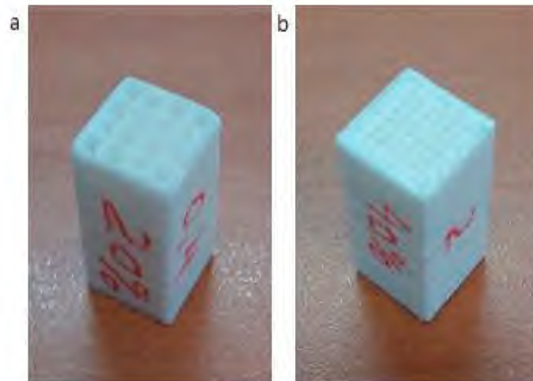


Fig.8 Part printed using a 0.4 mm nozzle, a) 20 % infill, and b) 40 % infill [28].

Buj-Corral and coworkers [28] studied how varying nozzle diameters and infill densities influence, as shown in Fig.8, and concluded that with increasing the infill values, pore size decreases, and the higher the nozzle diameter, the higher the pore size was observed. In FMD 3D printing, building orientation significantly impacts its final strength and functionality in FDM 3D printing. The arrangement of different angles can notably influence mechanical properties like strength, durability, and dimensional accuracy. Researchers conducted studies, such as Tianyun Yao et al. [5] studied the impact of seven different angles, as shown in Fig. 9, and three-layer thicknesses on PLA materials, concluding that the mechanical properties of the 3D printed material underwent significant changes with variations in the printing angle. Moreover, in 2016 Mst Faujiya Afrose et al. [29] found that the X direction (PLA-X) has a maximum tensile strength of 38.7 MPa compared to the other two directions, Y and 45, respectively.

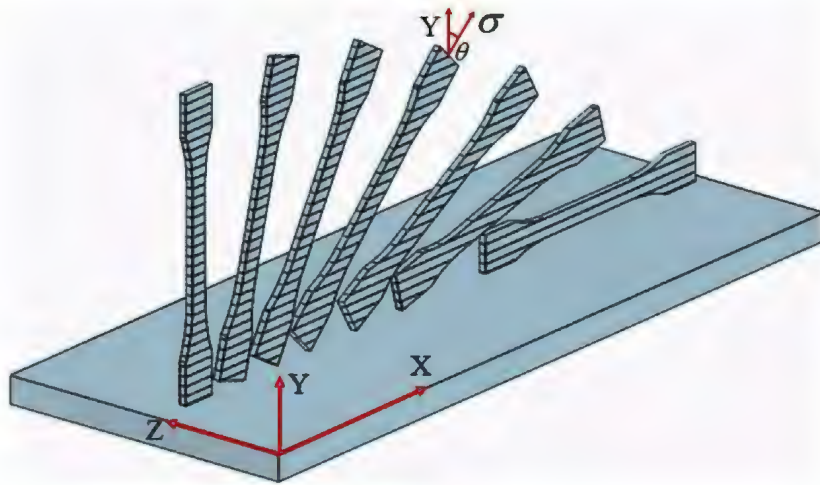


Fig.9 Different build orientation of tensile specimens [5].

In 3D printing, infill describes the internal latticework that determines how densely the material fills the inside of a printed object. The Percent of infill changes significantly influences properties like mechanical strength, print time, and overall cost of the 3d printed parts. Seol et al. [30] studied the infill of 25 %, 50%, 75%, and 100 % with different internal shapes like line, lattice, concentric, crystal (I), and crystal (II) parts as shown in Fig. 10(a) and (b). The study found that increasing infill density significantly strengthens the printed part. They observed a 2.5 times increase in tensile strength (to 50 MPa) when using 100% infill compared to 25% infill.

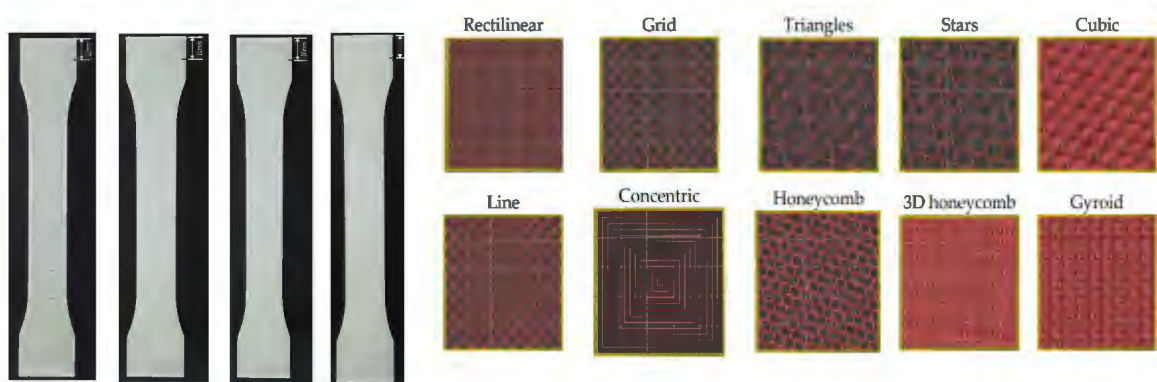


Fig.10 Infill of 25 %, 50%, 75%, and 100 % [30], and different infill pattern [31].

Moreover, in 2016 Miguel et al. [32] found that a change in the infill percentage causes a change in the maximum tensile strength of the 3D printed parts, and the highest tensile strength was found on 100 percent infill density. Recently, Gunasekaran and his coworker [33] studied the PLA printed materials under different infill densities. They conducted mechanical testing, and they asserted that the higher infill density resulted in better mechanical properties. Mahmoud Moradi and his team [34] studied the different infill patterns of FDM 3D-printed structures and determined that among various patterns and found that a triangular infill pattern exhibits mechanical properties. Other researchers like Christian Lubombo et al. [35] revealed that maintaining the same number of perimeter shells while changing infill patterns could lead to a twofold increase in stiffness and an 82 percent boost increase in strength.

K.N. Gunasekaran et al. [33] and Kyoung-SU Seol et al. [30] studied FDM across various infill percentages, and their findings indicated that a higher infill density of the printed specimens led to a significant improvement in tensile strength. Chamil Abeykoon and co-authors [36] examined the effects of different processing conditions along with using PLA and ABS materials in 3D printing, as illustrated in Fig.11 (a) and (b). Their research revealed that the maximum Young's modulus was obtained from 100% infill density, and 215° C was the most suitable temperature for the PLA filament.

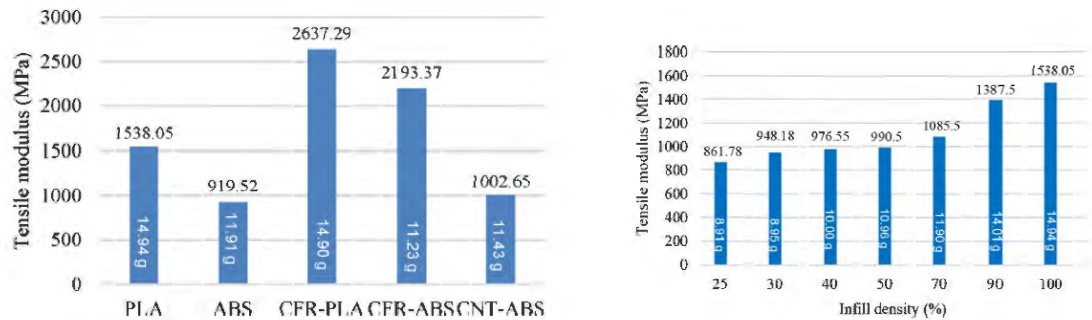


Fig.11 a) Five different materials' tensile modulus, b) tensile modulus (MPa) for different infill for PLA material [36].

M. Samykano and colleagues [37] looked into the consequences of varying different process parameters. In general, tensile strength was enhanced through the adoption of 0.5mm layer thickness, a raster angle set at 65° , and an infill level of 80%. They concluded that the predicted optimized parameter combinations could lead to higher tensile properties. João Francisco et al. [38] recommended a higher infill density and concluded that 60% of infill density has the best mechanical properties.

2.5. Digital Image Correlations

Digital Image Correlations (DIC) has made significant progress over the past 20 years due to the advantage of its non-contact approach. This is a novel method for measuring major deformation or strain, but it is appealing because it can measure displacement at numerous points distributed across the surface of the sample. The key advantage of DIC over other techniques, such as laser-based methods, is its use of standard white light sources, and a correlation algorithm is employed to trace the location of multiple surface points in two consecutive images to measure displacement.

After the CCD cameras are familiarized with image data, these images are stored in a computer for analysis [39]. DIC analyzes the deformation mechanisms in various materials, including metals, composites, polymers, wood, and biological materials [40] [41] [42] to investigate the stress-strain deformation behavior of materials [43], assess residual stresses [44], fracture [45] [46] and study the progression of cracks [47]. Many researchers have used the DIC alongside tensile testing [48]. For example, Kevin Schnittker and his team [49] examined the uses of DIC for strain measurements and highlighted the need for improved printing parameters. Zhuo Xu et al. [50] studied FDM printed three different scales of PLA fabricated specimens' mechanical behavior. The complete deformation and strain fields of a sample were measured using DIC. As per their conclusion, specimens with downscaled displayed lower ultimate tensile strength and decreased elongation at failure. Some researchers have successfully conducted experiments using the DIC to examine the strain fields of composite materials [51] and transverse strain and longitudinal strain [52].

Additive manufactured honeycomb structures created using different materials like ABS and carbon fiber-reinforced polyamide had their strain behavior evaluated using digital image correlation during tensile tests [53]. Schnittker [54] explored the accurate strain measurement in large 3D-printed components. Using DIC, researchers have also worked on creating a database detailing the structural performance of large polymer additive manufacturing components [55]. Additionally, some other researchers examined the cracking behavior of stainless-steel alloy across different 3D printing build orientations [56]. Taking advantage of DIC, Y. H. Wang and his colleagues [57] investigated the sheet-metal tensile test.

Despite many studies being conducted to investigate the tensile properties of different types of 3D-printed materials [58], minimal research has been conducted on implementing DIC analysis with mechanical testing of Silk-PLA materials. Therefore, this research aimed to examine the mechanical characteristics of Silk-PLA 3D-printed materials by utilizing different process parameters. Fig. 12 (a) illustrates the DIC setup with the MTS universal testing machine, and Fig. 12 (b) shows an illustration of the DIC technique during the tensile loading condition.

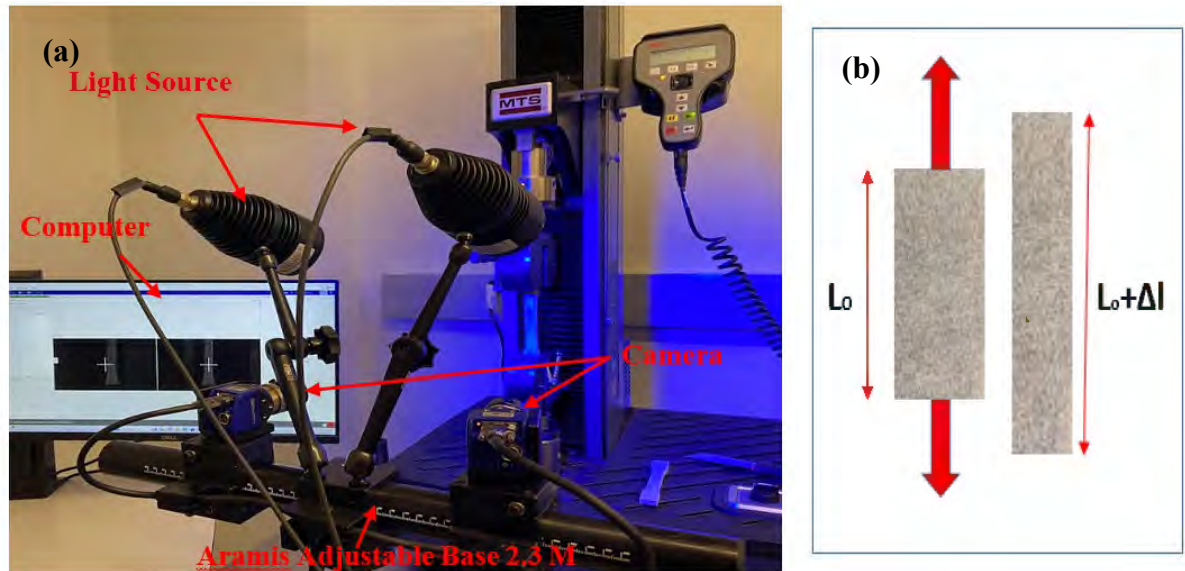


Fig.12 a) DIC set up with MTS Universal Testing machine, b) An illustration of the DIC technique.

2.6. Uniqueness of this research

PLA, the most used material for FDM, offers many advantages, including biodegradability, ease of processing, renewability, and commercial availability. However, it also has certain drawbacks, such as brittleness and low thermal stability [59]. Silk PLA maintains all the benefits of regular PLA while overcoming those drawbacks by producing

prints that are stronger and more rigid than pure PLA. However, fewer studies have been conducted on Silk-PLA. This study explored Silk-PLA instead of pure PLA materials with high-speed printing parameters.

For PLA, printing speed is one of the critical parameters. When discussing the specific print speeds of 120mm/s and 140mm/s, these are considered higher than the typical printing speeds for normal PLA materials. In general, FDM 3D printers are considered for the lower printing speeds [60]. Many research studies considered printing speeds to be less than 100 mm/s [23] [60] [61] [20] [62] [63] [13] [64]. Therefore, exploring higher printing speeds, like 120mm/s and 140mm/s, can be valuable findings for PLA or Silk-PLA materials by providing insights into the limits of certain types of materials and can help in understanding the modifications in the printing speeds with other process parameters.

CHAPTER 3

METHODOLOGY

In this chapter, the methodology process of this study is explained, which involves multiple stages, as shown in Fig. 13. Starting from the CAD design of the tensile testing specimen according to ASTM D638 tensile specimens to ensure reliable and standardized results. The CAD file was saved in stereolithography (STL) format. Then, using Cura software, such as Intamsuite, to slice 3D design parts and convert them into G code to understand the 3D printer. The slicing software processes the 3D model layer by layer, creating a toolpath for the 3D printer to follow. The converted STL file is transferred to the 3D printer machine. Setting up other fixed parameters as necessary before the build process.

Printing parameters included three distinct layer thicknesses, L1-0.1mm, L2-0.15mm, and L3-0.20mm, which were chosen for the specimens, nozzle temperatures range from 200°C to 220°C (increasing by 10°C each time), and corresponding print speeds of 100 mm/s, 120 mm/s, and 140 mm/s. This created 27 different printing parameter combinations and a total of 135 tensile specimens. An MTS E42 universal testing machine was employed to conduct the tensile tests on the specimens, and all 135 sample specimens' raw data were collected. Digital image correlation analyses were conducted on each of the 27 unique tensile specimens. The final step involves evaluating the mechanical properties through tensile testing and analyzing full-field strain and displacement values using DIC data.

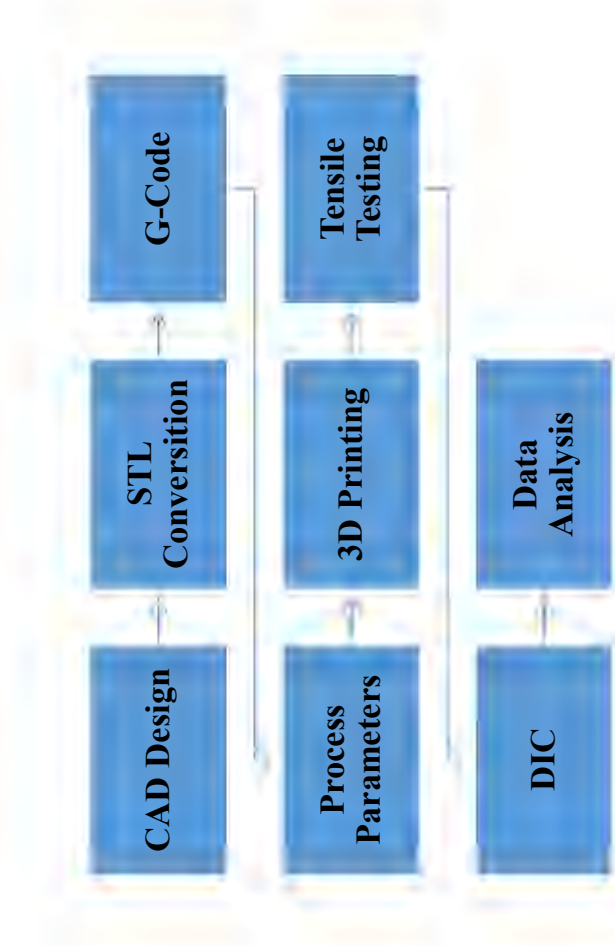


Fig. 13 Flow chart of the research methodology.

3.1. Materials

Polylactic Acid (PLA) is an eco-friendly thermoplastic polymer originating from renewable sources, like corn starch or sugarcane [65]. PLA materials are considered the most used material in FDM. Although PLA has advantages, including biodegradability, processing ease, renewability, and commercial availability, it still has specific characteristics like brittleness and low thermal stability [59]. Due to this, silk-PLA material, a natural fiber that comes from animals, could be an alternative to PLA. Silk PLA still retains all the advantages of regular PLA but produces stronger, more rigid prints than PLA [66]. Therefore, in this work, instead of pure PLA filament, silk-PLA material, as shown in Fig.14, was considered and has a diameter of 1.75 mm. The melting temperature of Silk-PLA filament ranges from 190°C and 220°C.



Fig.14 Silk-PLA filament.

3.2. Fabrication of Test Specimen

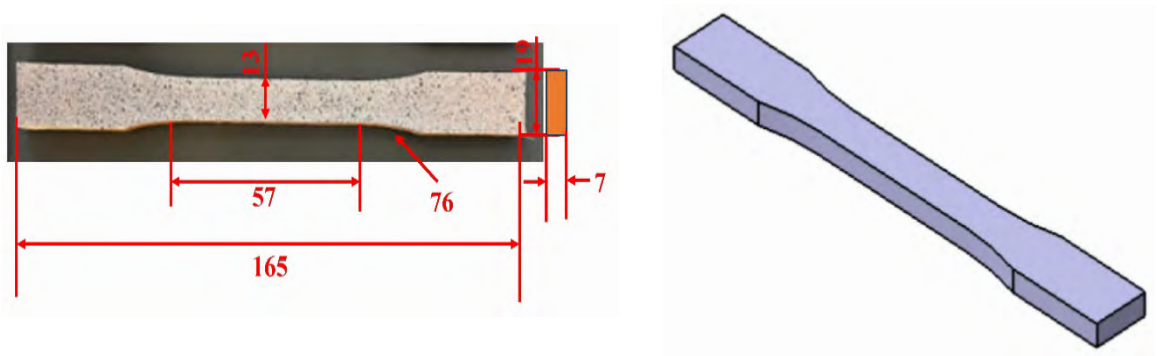


Fig.15 a) ASTM D638 Type I Tensile testing specimens (units in millimeters) [67], b) CAD design tensile specimens.

The tensile specimen was designed using SolidWorks software following the specifications of ASTM D638 Type I, as shown in Figure 15 (b). Figure 15 (a) illustrates the dimensions of the design specimens. The cross-section is 13 mm wide and 7 mm thick. The gauge length is 50 mm, the total length is 165 mm, and the width measures 19 mm,

respectively. Designing the 3D model was transformed into an STL file format, and Cura software was utilized to convert it into G code before inputting it into the printer.

All specimens were fabricated using the FDM Intamsys FUNMAT HT 3D printer, as shown in Fig. 16, and specifications are detailed in Table 1. The specimens were fabricated with three distinct layer thicknesses L1-0.1mm, L2-0.15mm, and L3-0.20mm.

The extrusion or nozzle temperatures varied between 200°C and 220°C, increasing by 10°C for each setting, and corresponding printing speeds were set at 100 mm/s, 120 mm/s, and 140 mm/s according to Table 2. The study utilized Silk-PLA material throughout. Other parameters, such as the infill density of 100%, build plate temperature of 40°C, raster angle of 45°, chamber temperature of 25°C, and the printing orientation, are kept constant for all specimens according to Table 3. This resulted in 27 unique combinations depicted in TALE IV, totaling 135 specimens.



Fig.16 INTAMSYS FUNMAT HT 3D Printer.

TABLE I
3D PRINTING MACHINE SPECIFICATION [68].

Printer Specifications	
Extruder	Single
Extruder Diameter	0.4mm
Layer Height	0.05-0.4mm
Print Speed	30-200mm/s
Filament Diameter	1.75mm
Build Volume	260*260*260mm
Dimensions	530*490*645mm
Heated-Plate Temperature (MAX)	160°C/320°F
Extruder Temperature (MAX)	450°C/842°F
Heated Chamber (MAX)	90°C/194°F

TABLE II
3D PRINTING PROCESS PARAMETERS AND LEVELS

Parameters	Notation	Level 1	Level 2	Level 3
Layer thickness	L(mm)	L1- 0.1	L2- 0.15	L3- 0.2
Nozzle Temperature	T(°C)	T1-200	T2- 210	T3-220
Printing Speed	P(mm/s)	P1-140	P2-100	P3-120

TABLE III
CONSTANT PROCESS PARAMETER

Parameters	Set value
Build plate temperature	40 °C
Chamber temperature	25°C
Raster angle	45°
Printing pattern	Lines
Infill density	100%
Nozzle diameter	0.4 mm

TABLE IV
LAYER THICKNESS WITH PRINTING PARAMETERS.

Sample No.	Code	Layer thickness (L) in mm	Nozzle Temperature(T) in °C	Printing Speed (P)in mm/s
1.	L1T1P1	0.1	200	100
2.	L1T1P2	0.1	200	120
3.	L1T1P3	0.1	200	140
4.	L1T2P1	0.1	210	100
5.	L1T2P2	0.1	210	120
6.	L1T2P3	0.1	210	140
7.	L1T3P1	0.1	220	100
8.	L1T3P2	0.1	220	120
9.	L1T3P3	0.1	220	140
10.	L2T1P1	0.15	200	100
11.	L2T1P2	0.15	200	120
12.	L2T1P3	0.15	200	140
13.	L2T2P1	0.15	210	100
14.	L2T2P2	0.15	210	120
15.	L2T2P3	0.15	210	140
16.	L2T3P1	0.15	220	100
17.	L2T3P2	0.15	220	120
18.	L2T3P3	0.15	220	140
19.	L3T1P1	0.2	200	100
20.	L3T1P2	0.2	200	120
21.	L3T1P3	0.2	200	140
22.	L3T2P1	0.2	210	100
23.	L3T2P2	0.2	210	120
24.	L3T2P3	0.2	210	140
25.	L3T3P1	0.2	220	100
26.	L3T3P2	0.2	220	120
27.	L3T3P3	0.2	220	140



Fig.17 a) Tensile Specimen in Intamsuit Software, b) 27 types of different parameters printed tensile specimen.

All the tensile specimens were printed, as illustrated in Fig. 17(a). They were then separated by plastic bags, as shown in Fig. 17(b). To prevent moisture from altering the material properties, a silica gel packet was included in each plastic bag.

3.3. Selected Printing Parameters

3.3.1. Layer Thickness

In additive manufacturing, parts are created by adding material layer by layer. The thickness of the layer, also known as its height, is a crucial parameter in additive manufacturing. The different types of layer thickness shown in Fig. 18, determine the resolution of the printed object and can significantly influence its mechanical properties, surface finish, and printing time. Therefore, it essentially defines the vertical dimension of each layer of material deposited during printing.

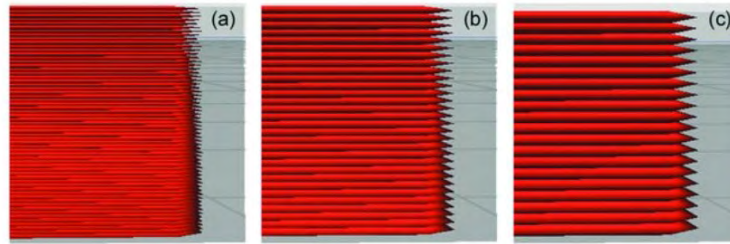


Fig.18 Sample of three different layer thicknesses of 3D printed material, a) 0.05mm, b) 0.10mm, and c) 0.15mm [69].

Many studies reveal that optimizing the layer thickness improves mechanical properties in the final product [69]. It is found that smaller layer thicknesses significantly enhance the material's strength for PLA-printed materials [9]. Tahseen Fadhil et al. [70] revealed that the final product's strength and impact resistance are greatly influenced by layer thickness. Yanping Liu and coworkers [71] noticed that the increased thickness of the layer caused decreased tray strength and improved time efficiency without affecting dimensional accuracy. However, discrepancies seem to be found in some of the results obtained from the studies on the different layer thicknesses.

For instance, according to Rajpurohit and coworkers [72] higher tensile strength was observed with a smaller thickness layer, J. Santhakumar et al. [73] also addressed the same conclusion that increased layer thickness leads to lower tensile strength; however, according to Sood et al. [74] initially increasing the thickness of the layers reduced tensile strength, but further increases in thickness led to an improvement in strength. Therefore, a thorough investigation of the FDM parameters like layer thickness is required to address the disparity in results. The goal of this investigation was to determine the optimal layer thickness for achieving the intended mechanical properties in 3D-printed PLA parts, using insights from previous research and to clarify the connection between layer thickness, other process parameters, and material strength. This research is unique in its aim of addressing

discrepancies found in previous studies and improving our understanding of FDM printing methods.

3.3.2. Nozzle Temperature

In FDM 3D printing, the nozzle temperature refers to the heat setting of the extruder nozzle from which the filament is extruded onto either the build platform or previous layers of the print. Figure 19 (a) shows the Intamsys Funmat HT 3D printer, and Figure 19 (b) displays the Markforged X7 3D printer. Both 3D printers are equipped with a 0.4 mm nozzle. Nozzle temperature in the FDM process directly influences both the printing process itself and the quality of the printed object.

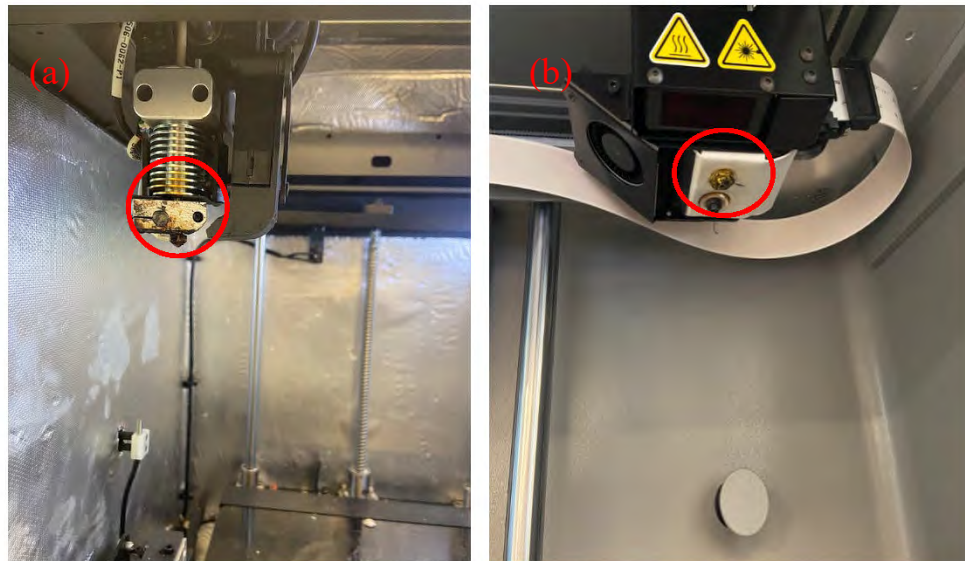


Fig.19 a) Intamsys funmat HT 3D Printer with 0.4 mm nozzle, and b) Markforge X7 3D printer with 0.4mm nozzle.

The temperature of the nozzle is much more significant and sensitive when considering the strength of printed PLA specimens. Research suggests a potential link between higher nozzle temperature and improved mechanical strength in PLA prints [75]. The nozzle temperature increased to 220°C, resulting in the tensile strength of PLA materials reaching their peak, compared to a lower temperature of 180°C [15], and a nozzle

temperature of 220°C is recommended for FDM-printed PLA material [13, 76]. Moreover, Magri and his team [12] examined how different extrusion temperatures affect mechanical characteristics. Their observation was that the maximum tensile properties of PLA parts were achieved by elevating the extrusion temperature to 230°C. Therefore, this study explored how three different nozzle temperatures affect the mechanical properties of Silk-PLA printed materials in light of these findings. This study is crucial for the advancement of 3D printing technology and for improving the quality of PLA-printed parts.

3.3.3. Printing Speed

Print speed defines the extruding nozzle's traveling speed along the platform, and it greatly influences the quality of 3D-printed components. The printing speed can be varied according to the different types of 3D printers, the type of material used, and the complexity of the printed model. The traditional operating speeds of FDM 3D printers, which are commonly used for PLA printing, are typically low, less than 100 mm/s [60].

For instance, researchers like AA Ansari et al.'s [61] study found higher tensile strengths when the printing speed is higher, at 50mm/s, compared to lower tensile strengths at 40mm/s. Until now, many researchers used a printing speed of below 100mm/s; however, few researchers, like Napolitano et al. [19] analyzed PLA's mechanical properties at a printing speed of 110mm/s. According to their findings, higher printing speed led to the highest tensile strength for PLA materials. Therefore, exploring higher speeds is crucial for understanding how PLA materials perform under conditions of increased velocity. Expanding the research on higher printing speeds could result in enhanced material properties, reduced printing times, and broader applications for PLA materials in 3D printing.

CHAPTER 4

RESULTS AND DISCUSSION

4.1. Tensile Testing

The tensile test was conducted on an MTS E42 UTM as shown in Fig. 20 which has up to 5 KN load capacity. The tensile test specimens were created following ASTM D638 Type-I [77] guidelines. In each relevant orientation, five specimens were fabricated for tensile testing. Data from these five samples were recorded, and the closest average values were selected to determine the elasticity modulus and peak tensile strength. A total of 135 specimens (Fig. 21) were tested at a constant speed of 5 millimeters per minute. The MTS system was configured to automatically capture the raw tensile stress-strain data in a comma-separated values (.csv) format. The UTS was assessed by measuring the peak tensile stresses achieved during the tests, whereas the slopes of the tensile stress-strain curves were utilized to calculate the elastic modulus shown in Table 5.

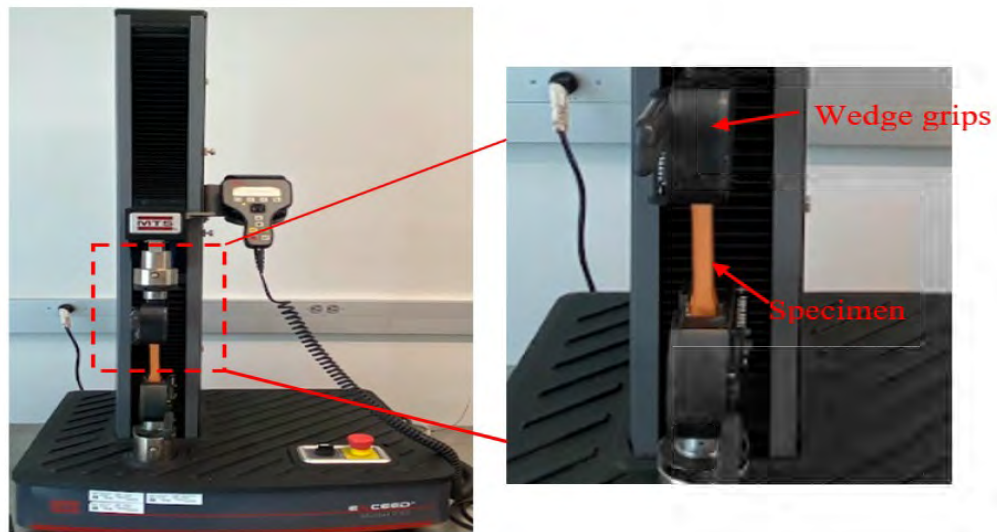


Fig. 20 MTS E42 Universal Testing Machine during tensile testing.

TABLE V
RESULTS OF THE TENSILE EXPERIMENT

Sample No.	Code	Average Weight (g)	Mean Tensile Strength (MPa)	Young's modulus (MPa)
1.	L1T1P1	19.74	31.95	877.09
2.	L1T1P2	19.90	36.21	965.46
3.	L1T1P3	20.30	34.03	874.29
4.	L1T2P1	20.40	34.11	994.20
5.	L1T2P2	20.86	36.51	1054.51
6.	L1T2P3	20.52	32.67	893.71
7.	L1T3P1	20.22	29.05	854.71
8.	L1T3P2	20.90	35.49	1027.84
9.	L1T3P3	20.50	36.09	998.32
10.	L2T1P1	19.56	29.27	730.09
11.	L2T1P2	20.46	37.48	981.22
12.	L2T1P3	20.12	30.59	842.26
13.	L2T2P1	20.90	31.61	890.23
14.	L2T2P2	20.80	37.22	1001.89
15.	L2T2P3	20.52	37.45	999.00
16.	L2T3P1	20.66	36.91	982.06
17.	L2T3P2	20.80	37.77	999.60
18.	L2T3P3	20.74	37.48	920.42
19.	L3T1P1	20.90	36.79	785.40
20.	L3T1P2	20.00	25.79	687.84
21.	L3T1P3	20.78	32.59	779.73
22.	L3T2P1	20.78	36.23	900.71
23.	L3T2P2	20.94	37.70	972.30
24.	L3T2P3	21.22	35.87	1066.16
25.	L3T3P1	21.16	32.72	828.71
26.	L3T3P2	21.16	40.68	1041.69
27.	L3T3P3	21.12	37.00	941.55

Table Representation symbol-

- Layer Thickness: L1- 0.1mm, L2-0.15mm, and L3- 0.2mm
- Nozzle Temperature: T1-200°C, T2- 210°C, and T3- 220°C
- Print Speed: P1- 100mm/s, P2- 120mm/s, and P3- 140mm/s

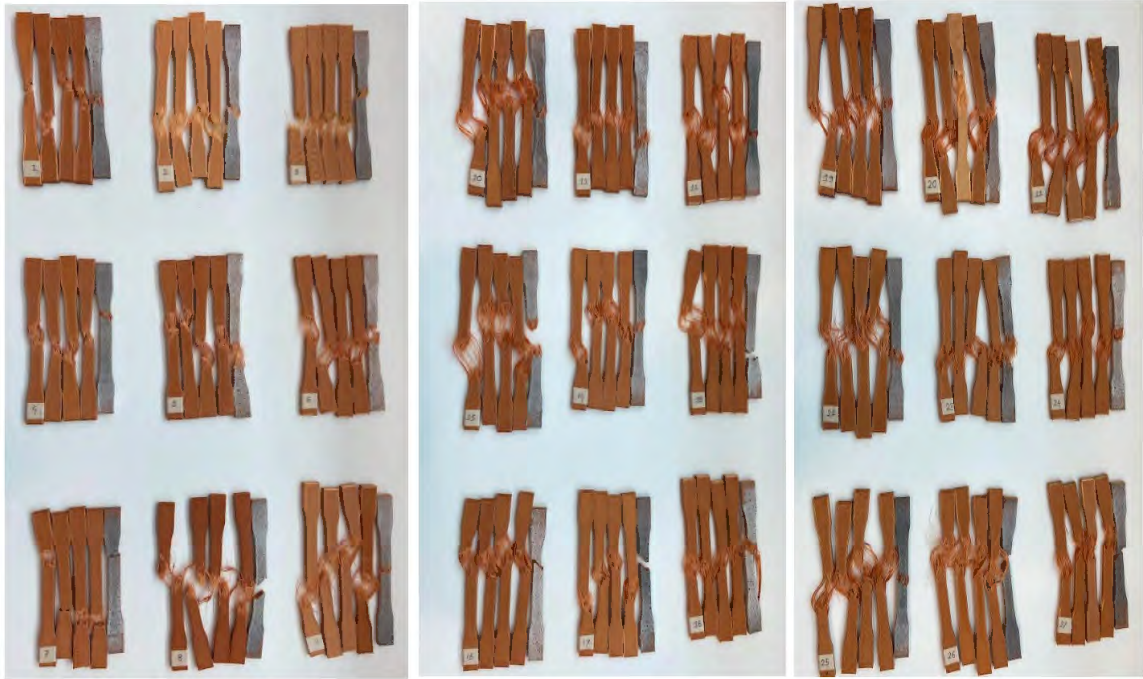


Fig. 21 Twenty-seven (27) different parameters in a total of 135 fractured specimens after tensile testing.

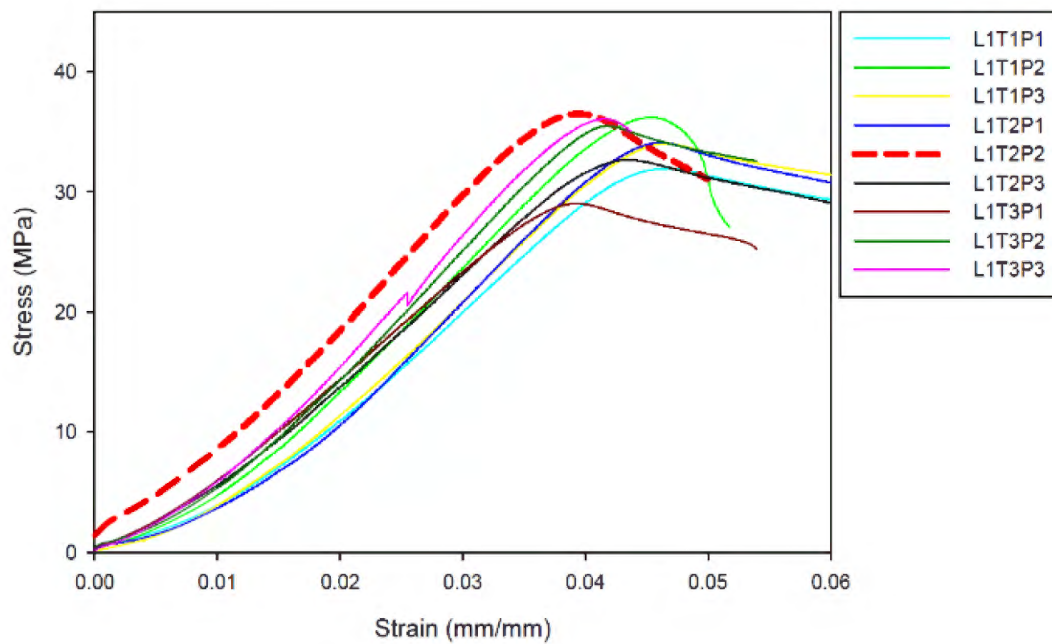


Fig. 22 Sample 1-9 Tensile Stress vs Strain graph (Layer thickness - 0.10mm).

Fig. 22 shows the Tensile Stress versus Tensile Strain graph for the first nine specimen samples. According to ASTM standards, five specimens were printed in each

orientation. The average values of those five samples were recorded, and one of the closely averaged values of the five samples was plotted. For instance, in testing sample 1- L1T1P1, the tensile strength of five samples is recorded as 30.959 MPa, 29.945, MPa 30.894, MPa, 32.973 MPa, and 31.95 MPa. The average of those values is 31.4 MPa. Therefore, the mean tensile strength value of these samples was chosen 31.95MPa.

Another example is sample, 2- L1T1P2, in which tensile strength values are 36.978 MPa, 35.018 MPa, 36.21 MPa, 36.777 MPa, 35.06 MPa, and the average value is 36.0096MPa. Therefore, the mean value of these samples is 36.21 MPa was considered. In Fig. 22, a thickness for each layer of 0.1 mm, a nozzle heat setting at 210 °C, and a printing speed of 120 mm/s exhibited the maximum tensile strength at 36.51MPa. Similarly, two other samples such as L1T1P2 and L1T3P31 also demonstrated the tensile stress around 36 MPa. However, where thickness for each layer of 0.1mm, the nozzle heat setting at 220 °C, and the print speed of-100mm/s recorded the lowest tensile strength of 29.05 MPa compared with the other eight samples.

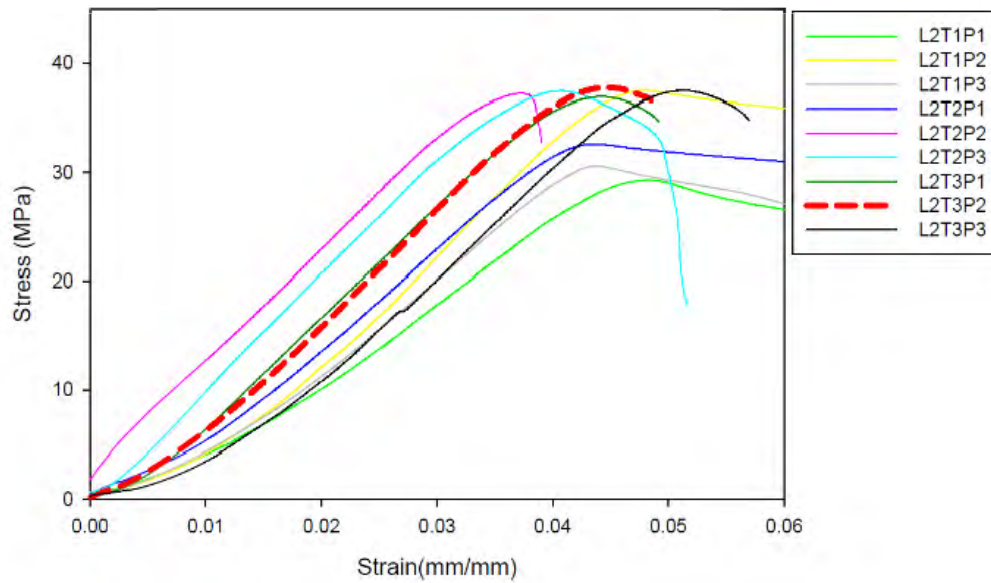


Fig.23 Sample 10-18 Tensile Stress vs Strain graph (Layer thickness- 0.15mm).

Fig. 23 shows the plot of nine samples with a fixed layer thickness of 0.15 mm. Each sample plot graph value was taken with the close average value of the five samples. Sample 18- L2T3P2, where L2 is set at 0.15 mm, T3 is adjusted to 220 °C, and P2 is 120 mm/s, has the highest tensile strength of 37.77 MPa and several other samples, including L2T1P2, L2T2P2, L2T2P3, and L2T3P3 exhibits the similar tensile strength levels, all hovering around 37 MPa. The lowest tensile strength was observed in these nine samples at testing sample 10- L2T1P1 when layer thickness, L2- 0.2mm, nozzle temperature T1- 200 °C and printing speed, P1-100mm/s at 29.27MPa, which is approximately 22.47% lower than higher tensile strength at sample 17.

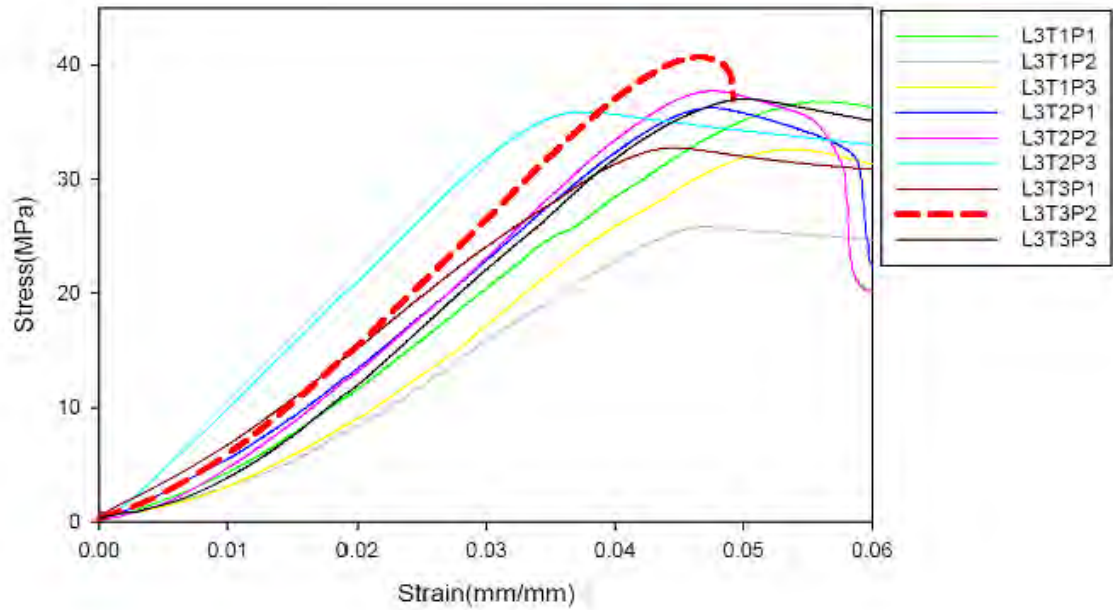


Fig. 24 Sample 19-27 Stress vs Strain graph (Layer thickness- 0.2mm).

Fig. 24 displays a 0.2 mm fixed-thickness sample. Each sample plot value was derived from the close average of five samples. As shown in Fig. 24, testing sample 26, denoted as L3T3P2 (L3: 0.2mm, T3: 220°C, P2: 120mm/s), achieved a tensile strength of 40.68 MPa, the highest value among all the samples tested. In contrast, sample 20 (see Fig. 25) labeled L3T1P2 (L3- 0.2 mm, T1- 200 °C, and P2- 120 mm/s) demonstrates the lowest tensile strength, measuring 25.79 MPa, which is approximately 36.60% lower than that of sample 26 which is shown in Fig. 26. In both samples, a significant change in mechanical properties was noticeable by altering the nozzle temperature by 20°C, even with the same layer thickness and printing speed, 0.2 mm and 120mm/s, respectively. As observed, the higher temperature in sample 26 would most likely enhance the bonding between the layers, resulting in a higher tensile strength which agrees with [78] [79]. Moreover, this emphasizes the importance of optimizing printing conditions to achieve 3D printed parts' desired strength and reliability.

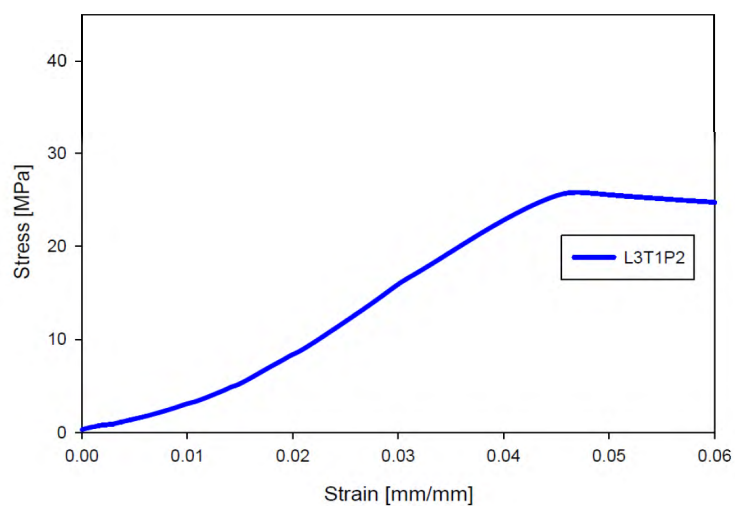


Fig. 25 Tensile Stress vs Strain Curve for the Specimen- L3T1P3 with the lowest UTS.

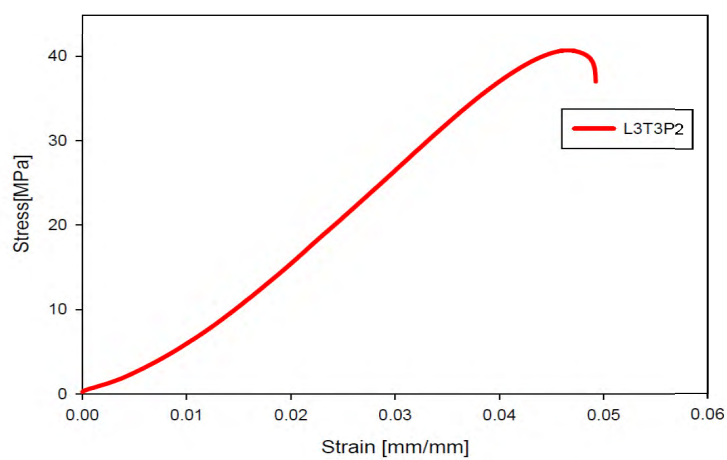


Fig. 26 Tensile Stress vs Strain Curve for the Specimen- L3T3P2 with the highest UTS.

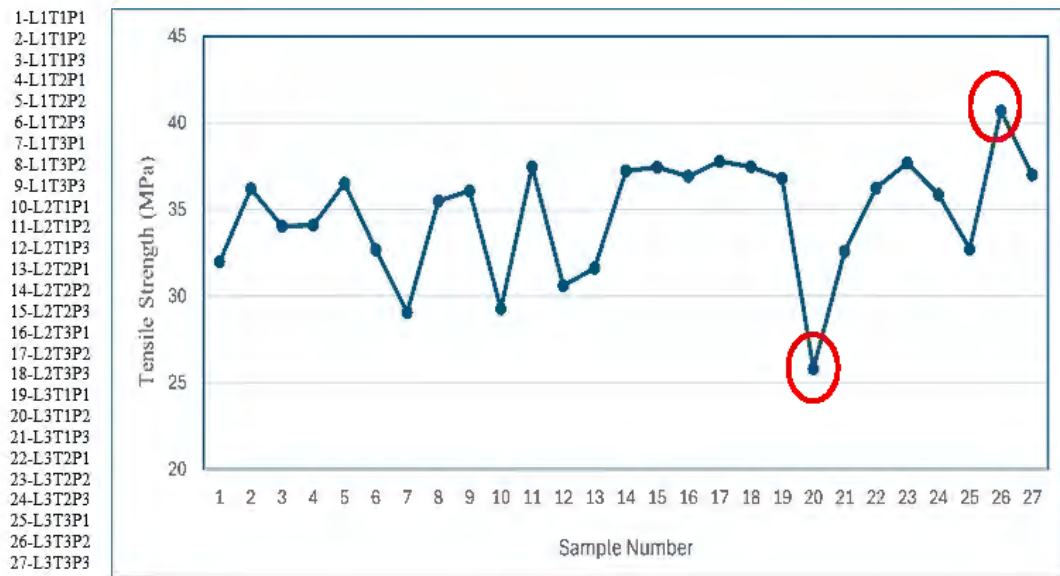


Fig. 27 Tensile Strength (MPa) vs Sample Number graph.

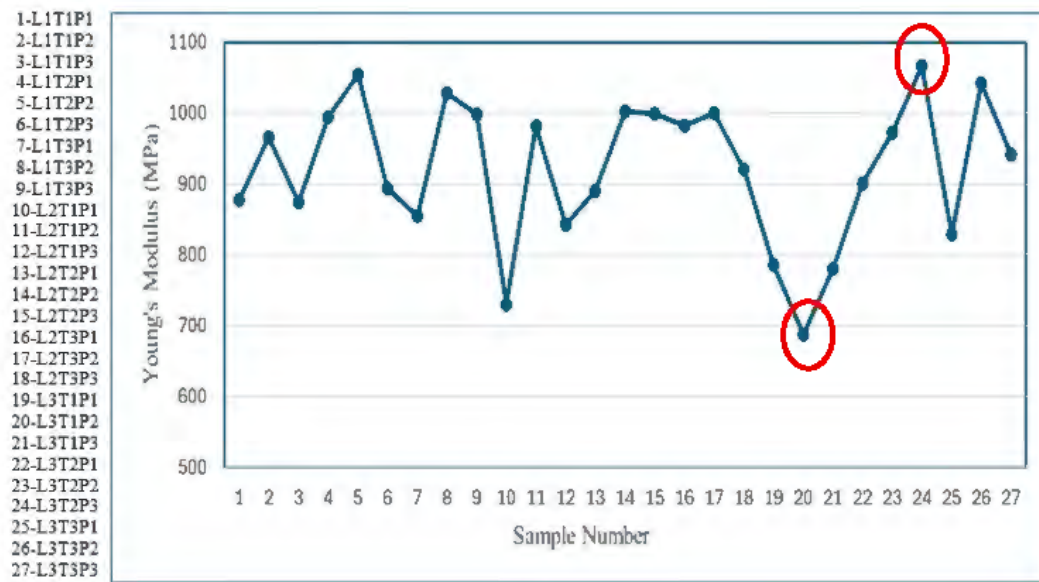


Fig. 28 Young's Modulus (MPa) vs Sample Number graph.

Based on the data in Table 3, Fig. 27 demonstrates that there is significant variation in tensile strength among the 27 samples, with values ranging from 25 MPa to 41 MPa. A significant change in mechanical properties was observed between sample 20, with the lowest tensile strength, and sample 26, with the highest tensile strength. Moreover, Fig. 28 depicts Young's modulus values for 27 tested samples. The highest Young's modulus value of 1066.16 MPa was recorded for sample 24, which is approximately 55% higher than the lowest value of 687.84 MPa for sample 21.

4.2. Optimizing the Printing Parameter

DOE, or Design of Experiment, utilizes statistical analysis to better grasp the combined effects of each factor in the experimental setup. The outcomes or processes of these experiments are typically influenced by multiple input parameters or factors. This study explored the effect of printing parameters on Silk-PLA's mechanical properties using MINITAB 17 software, and response surface methodology (RSM) was also performed.

4.2.1. Analysis of Variance for Ultimate Tensile Strength

Analysis of Variance, commonly referred to as ANOVA, is a statistical approach used to examine variations between the mean values of groups within a sample. It is frequently used to compare three or more groups to identify whether there are statistically significant variances among them. An ANOVA table analyzes how three printing settings affect Silk-PLA's tensile strength, with all obtained data falling within the 95% confidence interval.

TABLE VI
ANALYSIS OF THE VARIANCE TABLE FOR ULTIMATE TENSILE STRENGTH

Source	DF	Adj SS	Adj MS	F-Value	P-Value
Regression	3	319.03	106.342	16.71	0.000
L	1	109.46	109.465	17.20	0.000
T	1	180.09	180.091	28.30	0.000
P	1	29.47	29.4471	4.63	0.033
L*L	1	87.30	87.300	13.72	0.000
N*N	1	81.65	81.646	12.83	0.000
P*P	1	215.14	215.130	33.81	0.000
L*N	1	92.37	92.374	14.52	0.000
L*P	1	17.99	17.988	2.83	0.095
N*P	1	41.78	41.781	6.57	0.012
Error	125	795.41	6.363		
Total	134	1650.65			

DF (Degrees of Freedom); Adj SS (Adjusted Sum of Squares); Adj MS (Adjusted Mean Square); F-Value (F statistic); P-Value (Probability value)

Table 6 shows ANOVA in the tensile test results section in the MINITAB, and in the source column L represents Layer Thickness, T stands for Nozzle Temperature, and P denotes Printing Speed. The p-value, or probability value, revealed the significant influence of parameters on the output, in this case, ultimate tensile strength. The process parameter statistical significance is indicated by a p-value less than 0.05 [80] [81]. From the Table, it is indicated that Layer Thickness (L) and Nozzle Temperature(T) have a probability value of 0.000 and 0.000, which is less than 0.05 and this is considered the statistically significant parameter for ultimate tensile strength. Print Speed has a higher p-value of 0.033 which is less significant to tensile strength. From Table 6, it is noticeable that all parameters, except for L*P, have p-values below 0.05.

4.2.1.1. Main effect plot for UTS

From experimental data, the maximum tensile strength, recorded at 40.68 MPa, was achieved with L2- 0.2mm, T3- 220°C, and P2- 120mm/s. Fig. 29 depicts a main effects plot illustrating the variations in Ultimate Tensile Strength (MPa). The process parameters are displayed on a horizontal axis, while the mean Ultimate Tensile Strength is shown on the vertical axis as shown in Fig.b29. The trend line for the layer thickness is nearly horizontal; therefore, there is no statistically significant impact of layer thickness on UTS within the range examined. However, the nozzle temperature trend line displays a positive slope, suggesting that an upward trend in UTS was observed with increasing nozzle temperature (200°C to 220°C). This relationship is statistically significant.

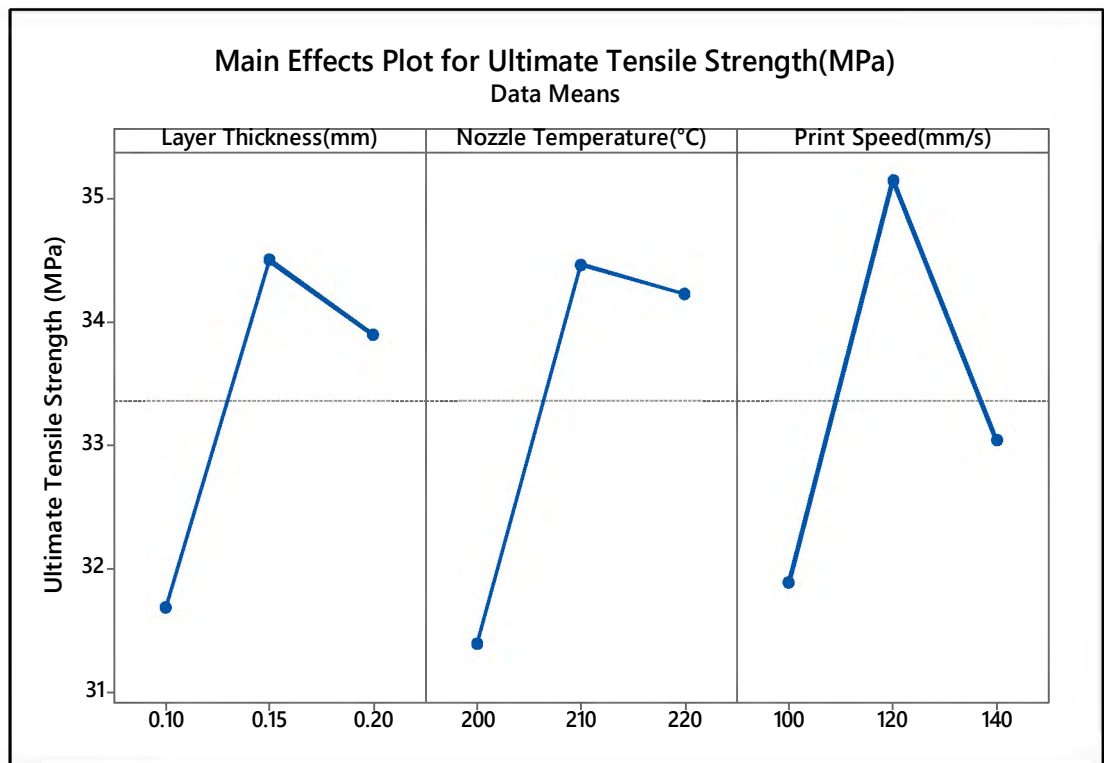


Fig. 29 A main effects plot illustrating the variations in Ultimate Tensile Strength (MPa).

The slope line for printing speed is slightly positive, with tensile strength peaking at 120 mm/s. However, when the printing speed is increased to 140 mm/s, the tensile strength drops sharply, falling below the mean value. The conclusion drawn is that at a temperature of 220°C (T3) and a printing speed of 120 mm/s (P2), Silk-PLA exhibits higher tensile strength.

4.2.1.2. Residuals plot for UTS

The normal probability plot and the histogram are used to test the assumption of normality of the residuals. Fig. 30 (a) plot shows that the residuals mostly follow the line and have a mean close to zero. It means that the residuals are approximately normally distributed. Fig. 30 (c) histogram plot provides the visual representation of the distribution of residuals. The plot of residuals versus fits Fig. 30 (b) helps assess the validity of the assumption regarding the constant variance of the residuals, and the absence of a pattern indicates that the residuals are likely independent. There has been no unexpected change in residuals over time, as revealed by the plot Fig. 30 (d) residuals versus observation order.

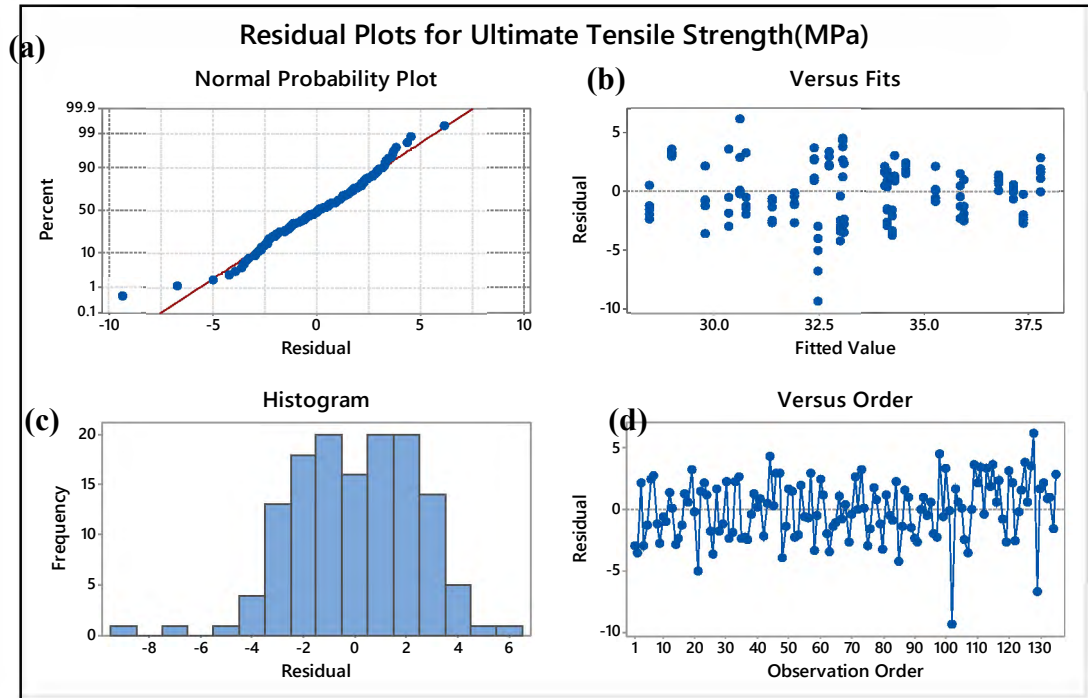


Fig. 30 Residual plot of ultimate tensile strength at 95% confidence interval a) Normal plot for residuals, (b) Versus fits plot for residuals, (c) Histogram plot for residuals, and (d) Versus order plot for residuals.

4.2.1.3. Interaction Plot for UTS

The interaction plot is a powerful tool for identifying how multiple factors influence a response variable simultaneously. Fig. 31 presents an interaction plot, visualizing how three printing parameters influence the average tensile strength (MPa) of Silk-PLA materials. In an interaction plot, parallel lines indicate the absence of any interaction, whereas different slope lines indicate that interaction might be present.

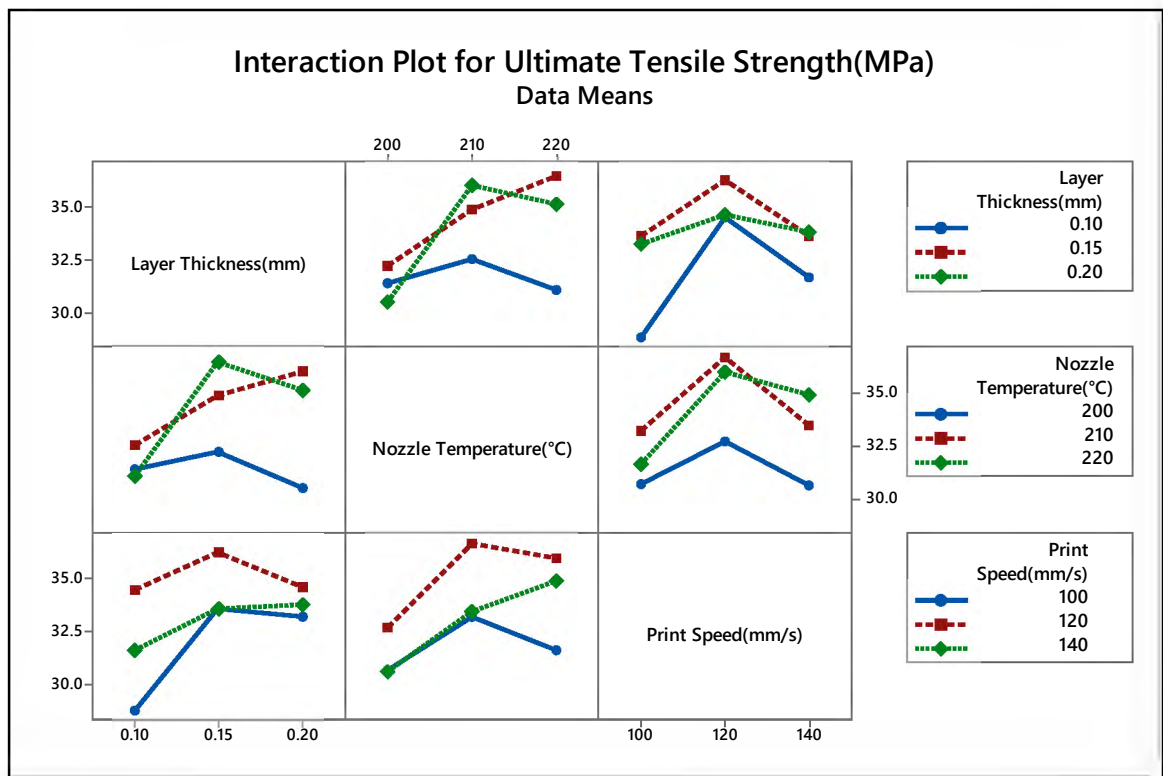


Fig. 31 Interaction Plot between the three printing parameters.

The top-left graph in Fig. 31 shows a noticeable correlation between the layer thickness and nozzle temperature. The tensile strength alters with different nozzle temperatures as layer thickness changes from 0.1mm to 0.2mm, except for the 0.1mm thickness, which has a lower tensile strength. The ultimate tensile strength will increase

with an increase in the nozzle temperature in this case and reach the maximum when the layer thickness is at 0.15mm with a nozzle temperature of 220°C.

Using the middle graph in Fig. 31, tensile strength varies with temperature changes. However, there is a significant interaction exists between layer thickness and nozzle temperature. Therefore, it is difficult to conclude which parameters have the most influence. Generally, a higher temperature of 220°C with a layer thickness of 0.15 mm results in a tensile strength of over 35 MPa.

Using the bottom graph Fig. 31, it is noticeable that increasing print speed to 140 mm/s seems to reduce tensile strength across most conditions, but mostly parallel lines indicate the absence of any interaction in these two Figs. Nonetheless, the plot suggests that 120 mm/s print speeds might be beneficial for maximizing tensile strength to more than 37MPa, particularly at a print speed of 120mm/s and nozzle temperatures of 210°C.

4.2.1.4. Contour Plots for UTS

Contour plots, or level plots, allow data visualization in three dimensions on a two-dimensional surface. These plots were created using MINITAB software to investigate the relationship between tensile strength and three selected process parameters. The contour plots are shown in the subsequent images. Contour plots provide a clear visual representation of how specific selected parameters and any parameters between specific parameters can impact the tensile strength.

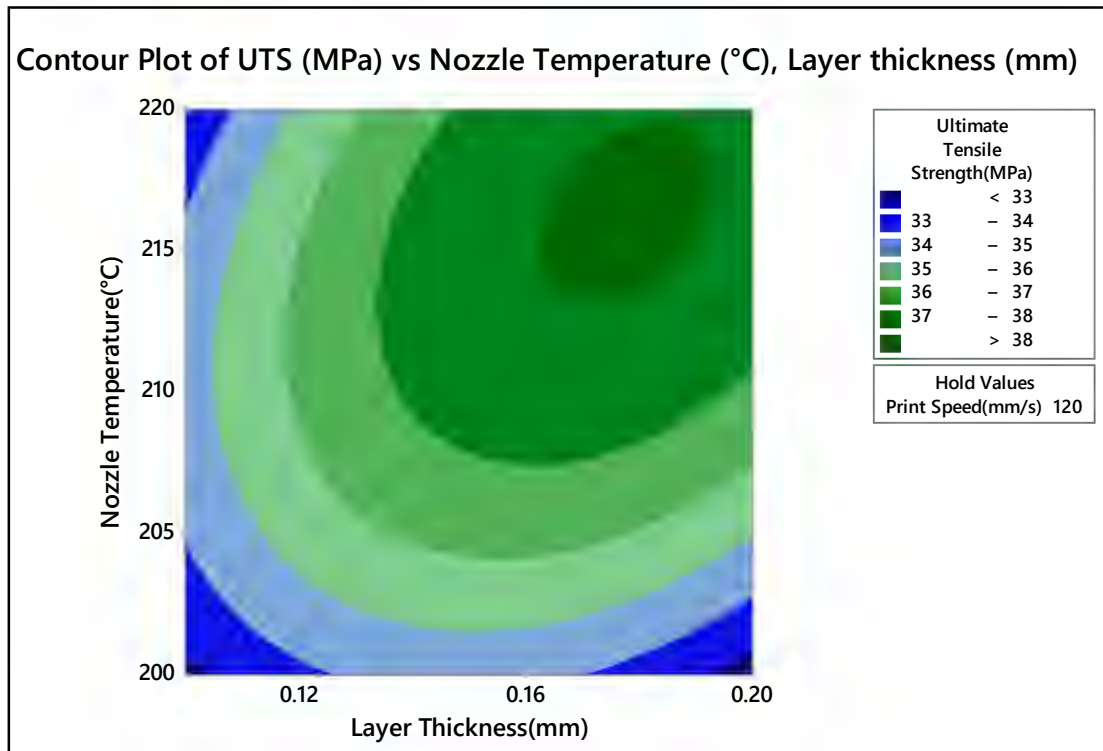


Fig. 32 Contour Plot of UTS (MPa) vs Nozzle Temperature (°C), Layer thickness (mm).

For instance, in Fig. 32, the contour plot of Ultimate Tensile Strength (MPa) as a function of Nozzle Temperature (°C) and Layer Thickness (mm), with the printing speed fixed at 120 mm/s. The layer thickness (L) is considered between 0.10 mm and 0.20mm, but using the contour visual plots, one can delve into alternative layer thicknesses such as 0.12mm or 0.18mm and nozzle temperature between 205 °C and 215 °C finding the ultimate tensile strength of this range. By maintaining a moderate speed of 120 mm/s while adjusting the temperature between 213°C to 219°C and using a moderate layer thickness of 0.16 above, a higher tensile strength can be obtained.

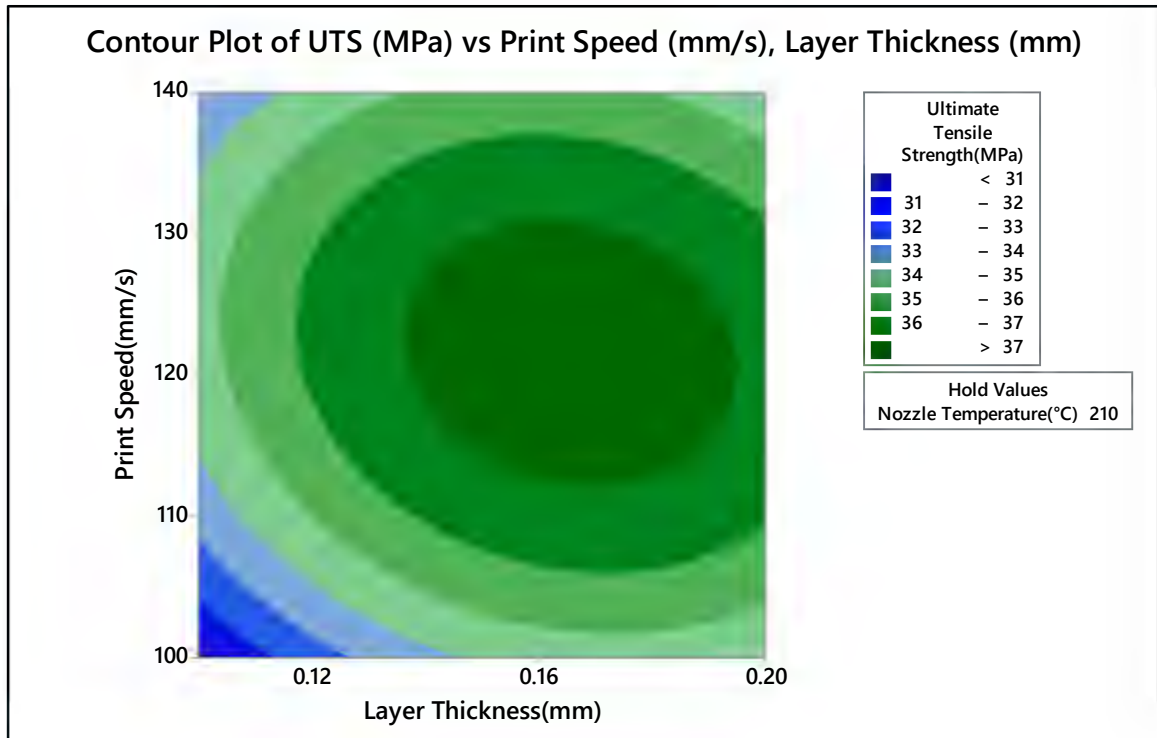


Fig. 33 Contour Plot of UTS (MPa) vs Print Speed (mm/s), Layer Thickness (mm).

Referring to Fig. 33, the contour plot that illustrates UTS (MPa). This plot explores how UTS is affected by both Print Speed (mm/s) and Layer Thickness (mm). It is important to note that the nozzle temperature for this specific plot is fixed at 210°C. Fig. 33 shows that a printing speed of 120 mm/s in conjunction with a layer thickness of 0.14 mm and higher ultimate tensile strength were observed at more than 37 MPa. Conversely, at lower print speeds like 100 mm/s and higher speeds like 140 mm/s, using a layer thickness of around 0.1 mm results in tensile strengths of 32 MPa or lower.

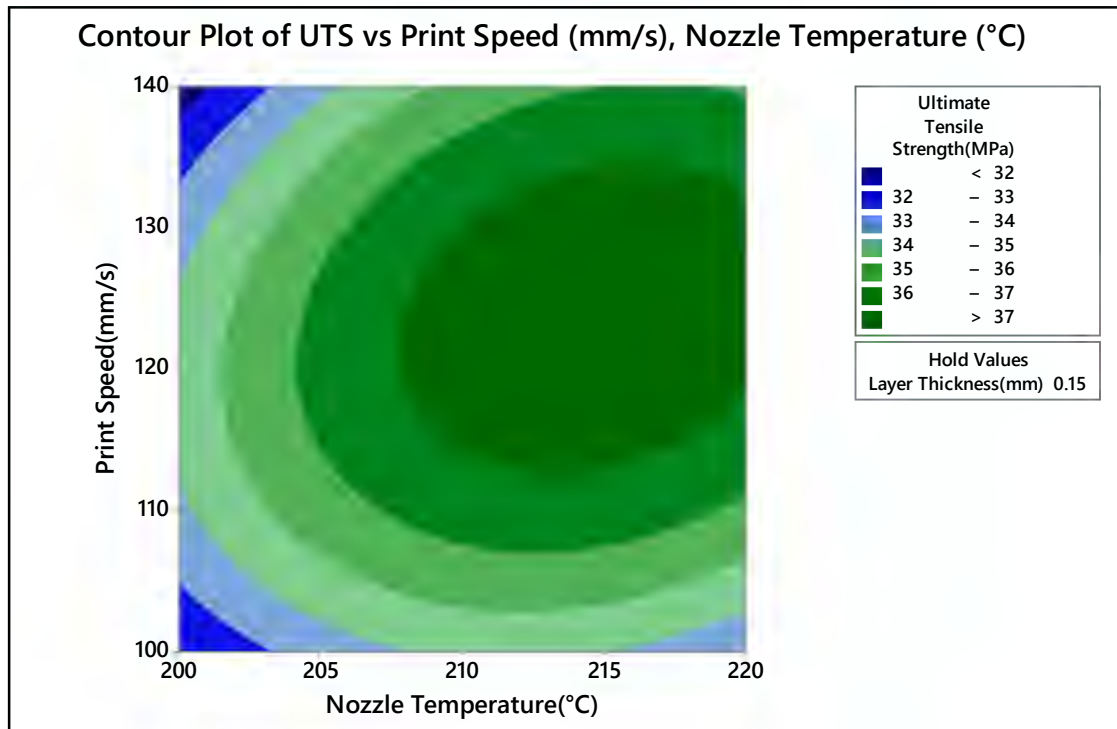


Fig. 34 Contour Plot of UTS (MPa) vs Print Speed (mm/s), Nozzle Temperature (°C).

Referring to Fig. 34, the contour plot illustrates UTS (MPa). This plot explores how UTS is affected by both print speed (mm/s) and nozzle temperature (°C). It is important to note that the value of the layer thickness holds at 0.15mm. It shows that with nozzle temperatures ranging from 210°C to 220°C and printing speeds between 110 mm/s and 130 mm/s, the ultimate tensile strength can exceed 37 MPa.

4.2.1.5. Surface Plots for UTS

Surface plots are graphical representations in three dimensions that are utilized to illustrate the correlation between a fixed variable, which is the dependent variable, and two additional independent variables. Figs. 35-37 provide comparable depictions of the outcomes derived from the response surface methodology (RSM) analysis within a three-dimensional plane. These planes exhibit the impact of two variables on the ultimate tensile strength while concurrently maintaining the average value of the third variable.

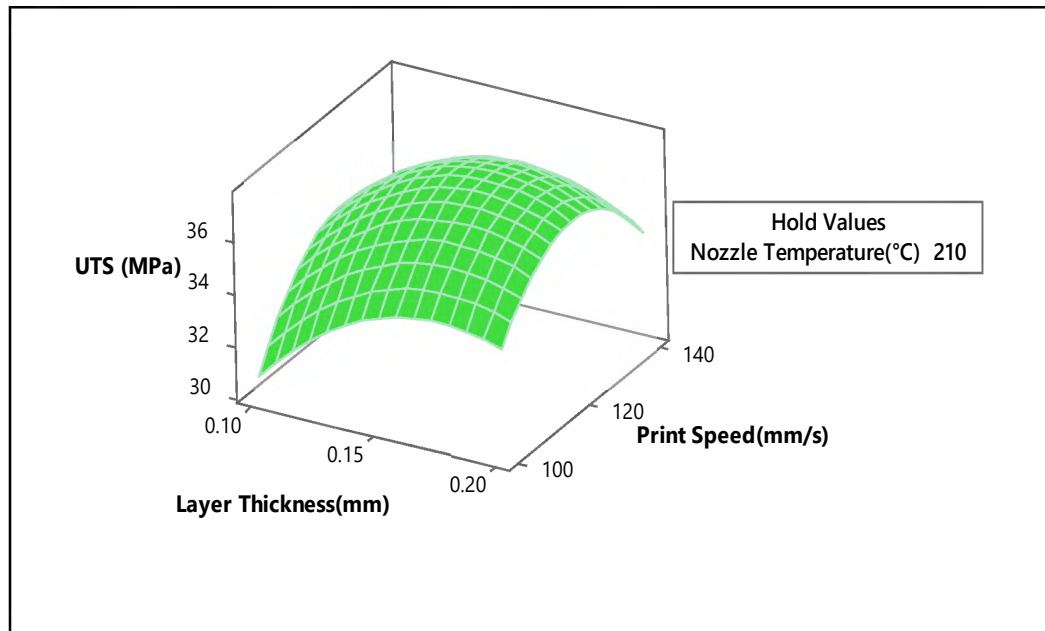


Fig. 35 Ultimate Tensile Strength (MPa) in a 3D surface plot vs Print Speed (mm/s), Layer Thickness (mm).

Fig.35 shows the Surface Plot of UTS (MPa) vs Print speed (mm/s) and Layer Thickness(mm) when the nozzle temperature is constant at 210 (°C). Print speed and layer thickness are independent variables, representing the horizontal axes, whereas the vertical axis represents the UTS in MPa. In this three-dimensional plane, it is evident that L2 (layer

thickness) -0.15 mm combined with P2 (printing speed)- 120 mm/s results in an increase in tensile strength.

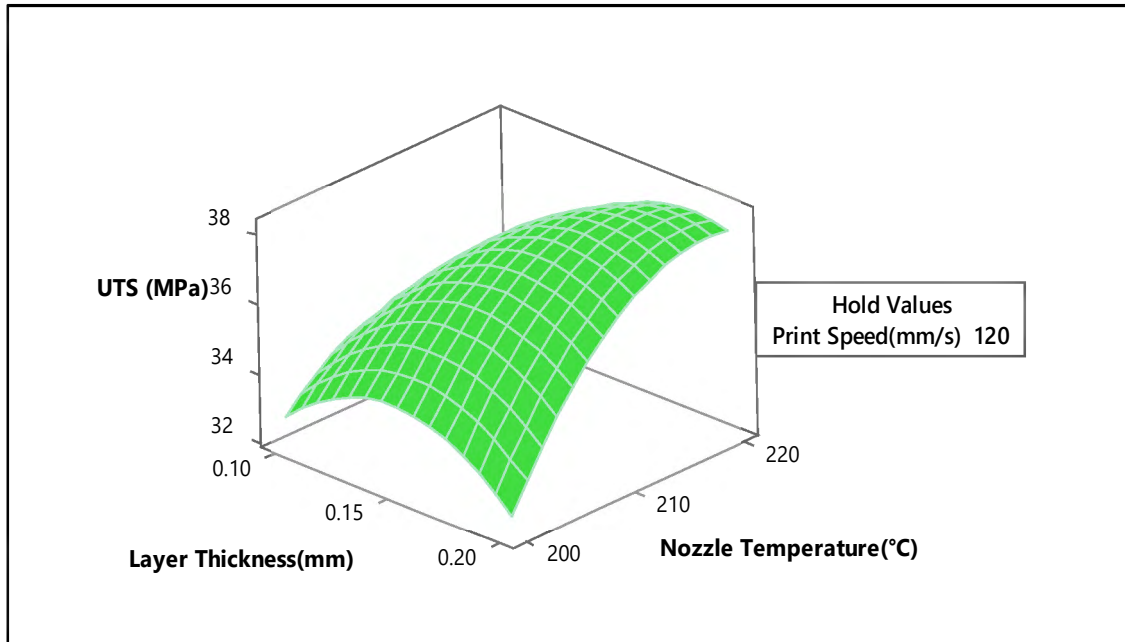


Fig. 36 Ultimate Tensile Strength (MPa) in a 3D surface plot vs Nozzle Temperature(°C), Layer Thickness(mm).

For instance, Fig. 36 shows the Surface Plot of UTS when the print speed is constant at 120mm/s. nozzle or extruder temperature and layer thickness are independent variables, representing the horizontal axes, whereas the vertical axis represents the UTS in MPa. The ultimate tensile strength (UTS) remains highest when the layer thickness is set to 0.15mm. Then, increasing the layer thickness to 0.2mm decreases the UTS to around 32MPa.

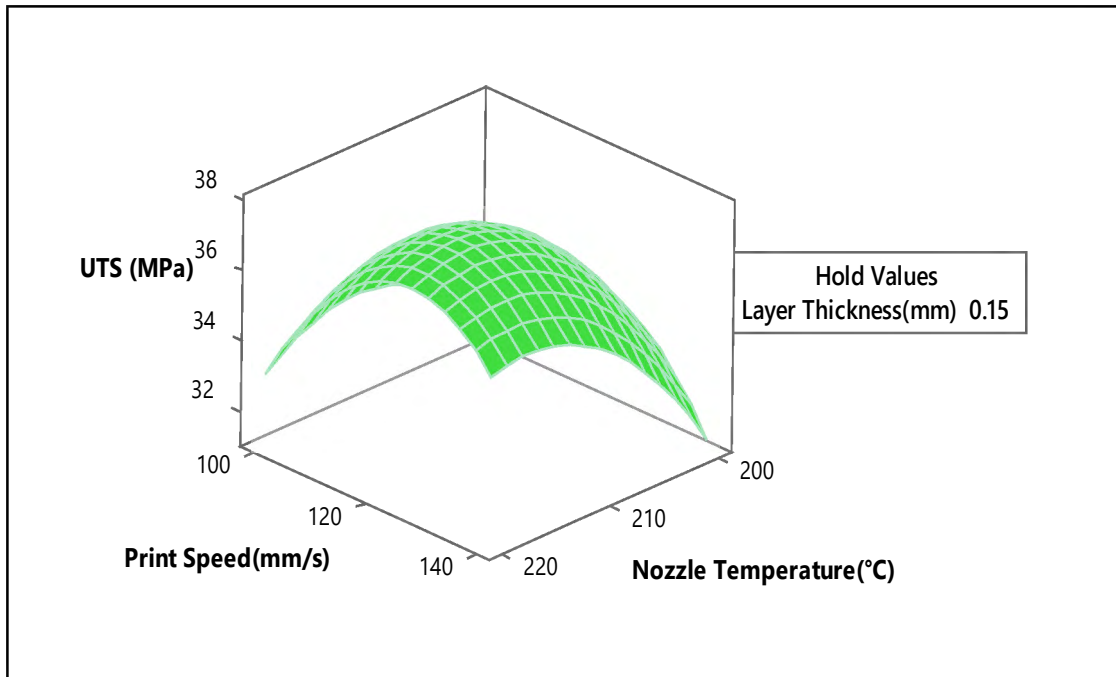


Fig.37 Ultimate Tensile Strength (MPa) in a 3D surface plot vs Print Speed (mm/s), Nozzle Temperature(°C).

Fig. 37 shows the 3D Surface Plot of UTS vs T (°C) and P (mm/s) when holding Layer Thickness at 0.15mm. The horizontal axis is represented by Print speed (mm/s), and Nozzle Temperature (°C), while the vertical axis represents the UTS in MPa. The relationship between nozzle temperature, print speed, and the material's ultimate tensile strength (UTS) is evident in this plot. Increasing the nozzle temperature to 220°C leads to a noticeable rise in UTS. Similarly, UTS reaches a peak value at a print speed of around 120 mm/s.

4.2.2. Analysis of Variance for Young's Modulus

TABLE VII
ANALYSIS OF THE VARIANCE TABLE FOR YOUNG'S MODULUS

Source	DF	Adj SS	Adj MS	F-Value	P-Value
Regression	3	92139	30713.0	6.38	0.004
L	1	15963	15863.3	3.32	0.086
T	1	63786	63786.4	13.25	0.002
P	1	12389	12389.5	2.57	0.127
L*L	1	413	412.9	0.09	0.773
N*N	1	37717	37717.2	7.84	0.012
P*P	1	31589	31588.8	6.56	0.020
L*N	1	12999	12998.8	2.70	0.119
L*P	1	4497	4496.9	0.93	0.347
N*P	1	692	691.8	0.14	0.709
Error	17	81818	4812.8		
Total	26				

L=Layer Thickness; T = Nozzle Temperature; P = Print Speed

ANOVA analysis was carried out on Young's modulus to gain insight into the importance of the process parameters. The p-value, also known as the probability value, serves to assess the significance of the influence that parameters have on the output variable, specifically on Young's modulus. From Table 7, layer thickness (L) has a probability value of 0.086, and printing speed (P) has a probability value of 0.127. Therefore, both layer thickness and printing speed had p-values higher than 0.05, indicating they do not have a significant impact on Young's modulus under the conditions studied. However, the nozzle temperature, as denoted as a T, has a probability of 0.002 which is less than the considered P value of 0.05 and has a significant parameter for the Young's modulus of the material. From Table 7, it can be seen that other combined parameters, except for N*N and P*P, have p-values more than 0.05.

4.2.2.1. Main effect plot for Young's Modulus

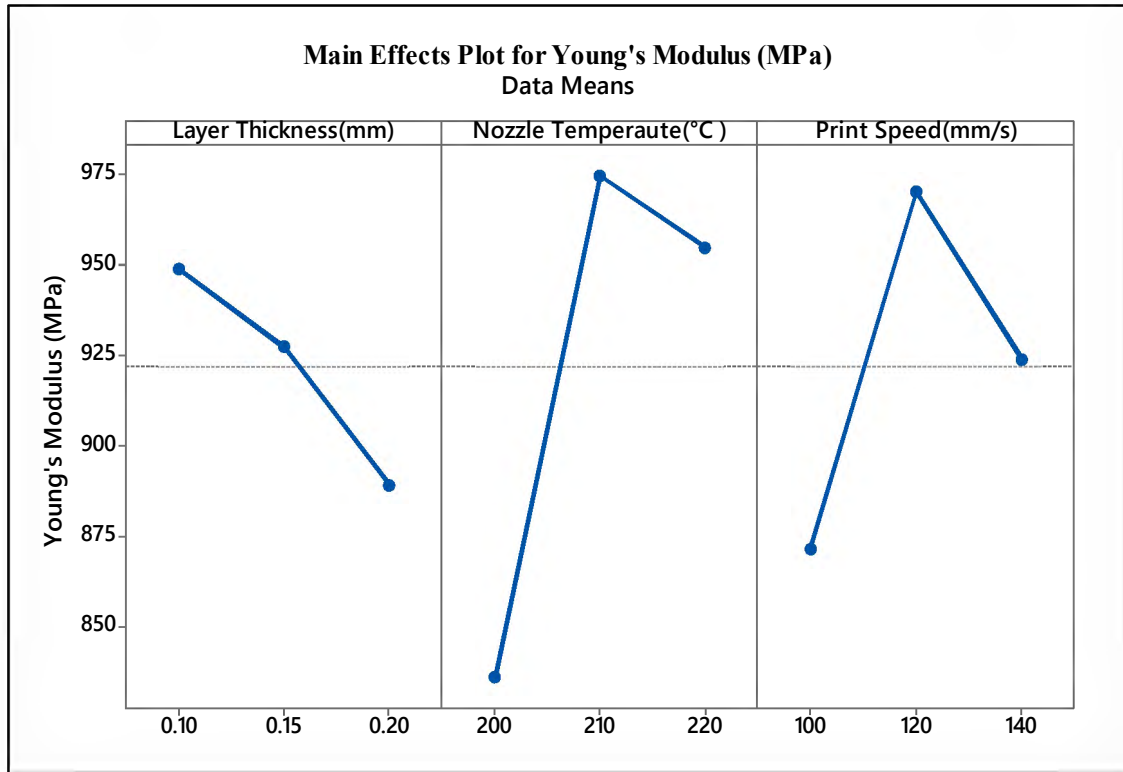


Fig. 38 A main effects plot illustrating the variations in Young's modulus.

A main effects plot illustrating the variations in Young's modulus is given in Fig. 38. As layers thicken from 0.10 mm to 0.20 mm, the graph indicates a decrease in the average Young's Modulus value. The thickness of the layer was 0.10mm, which led to the observation of the best Young's Modulus. It is observed that nozzle temperature significantly affects Young's modulus, i.e., when nozzle temperature increases 200°C to 210°C, it has the highest Young's modulus, but it drops gradually when nozzle temperature increases to 220°C. Therefore, the nozzle temperature increases to 210°C, which can significantly increase the young's modulus. The correlation between the printing speed and Young's Modulus demonstrates an initial rise as the printing speed increases from 100

mm/s to 120 mm/s, subsequently decreasing at 140 mm/s printing speed and reaching close to the mean value.

4.2.2.2. Residuals plot for Young's Modulus

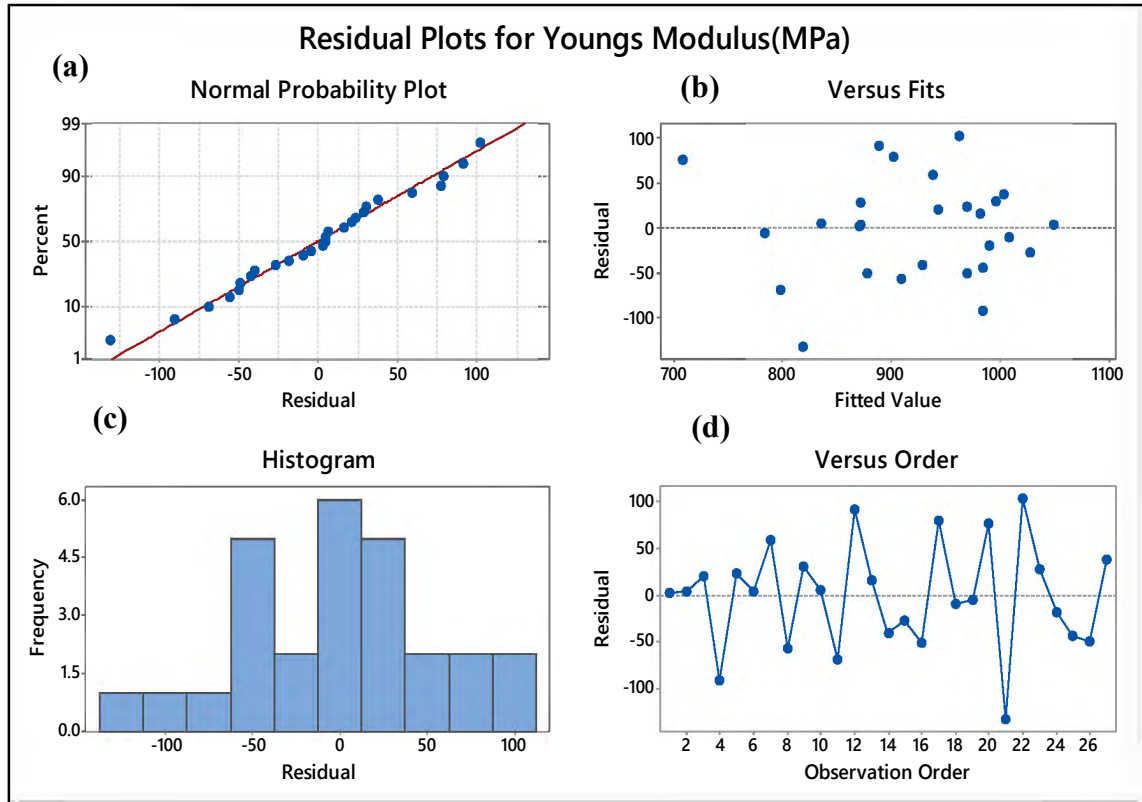


Fig. 39 plot of Young's Modulus at 95% of confidence interval; (a) Normal plot for residuals, (b) Versus fits plot for residuals, (c) Histogram order plot for residuals, and (d) Versus order plot for residuals.

Fig. 39 (a) The normal probability plot and (c) the histogram plot, which provides a visual representation of the distribution of residuals, shows that the residuals are relatively normal and have a mean close to zero. It means that the residuals are approximately normally distributed. The residuals are shown in plot (b) against the fitted values. The ideal outcome for this plot is to have no discernible pattern, which indicates that the model's predictions are consistent across all values, and according to the plot of

residuals versus observation order (d), there have been no unexpected changes in residuals over time.

4.2.2.3. Interaction Plot for Young's Modulus

The interaction plots for Young's modulus, as a function of significant parameters considered in this study, are shown in Fig. 40. In an interaction plot, parallel lines indicate the absence of any interaction. A line with different slopes line indicates that there might be interaction present.

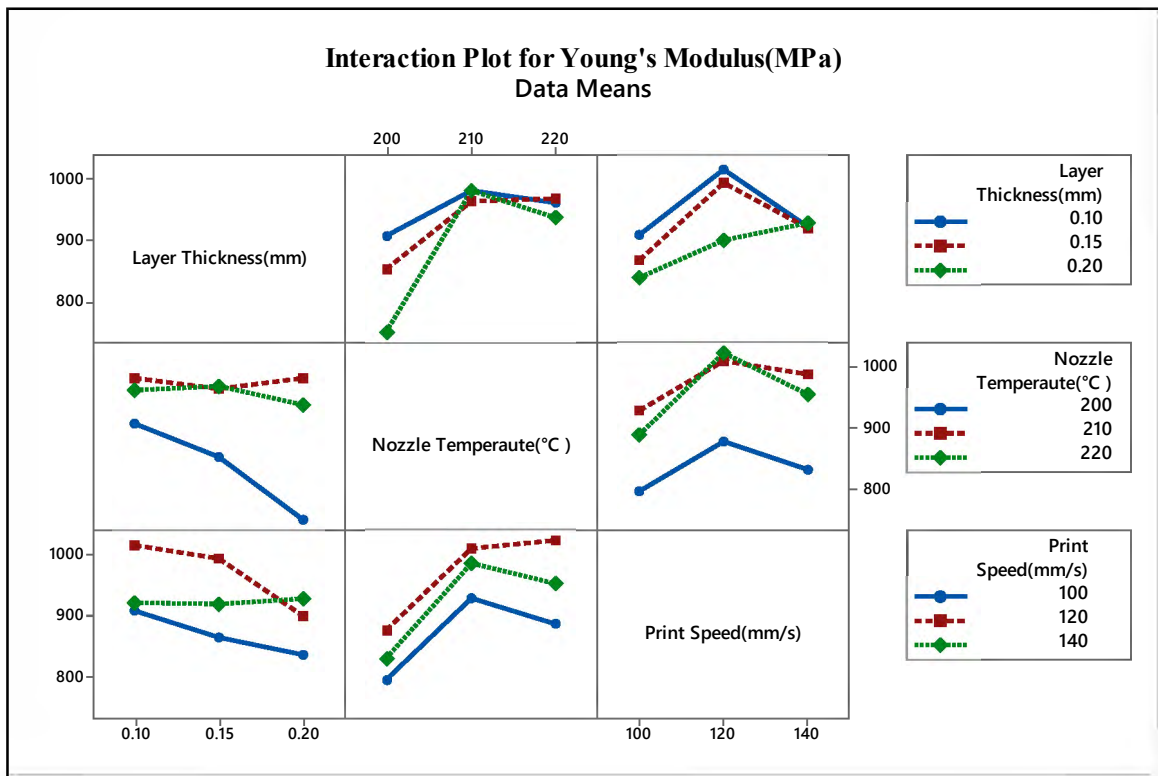


Fig. 40 Interaction Plot between the significant parameters.

The top-left graph in Fig. 40 reveals a strong interaction between layer thickness and nozzle temperature on Young's modulus (material stiffness). Interestingly, the combination of a 0.10mm layer thickness, 210°C nozzle temperature, and 120mm/s print speed yields the highest stiffness as shown in the graph. The middle left and right graphs

consistently show that a 200°C nozzle temperature results in the lowest Young's modulus compared to 210°C and 220°C. Using the bottom-left graph, it can be concluded that a printing speed of 120 mm/s and nozzle temperature of 220°C has a similar Young's modulus value and a layer thickness of 0.1mm. Additionally, in the graph below, it's evident that print speed and nozzle temperature have a very small effect, as seen by the nearly parallel lines.

4.2.2.4. Contour Plots for Young's Modulus

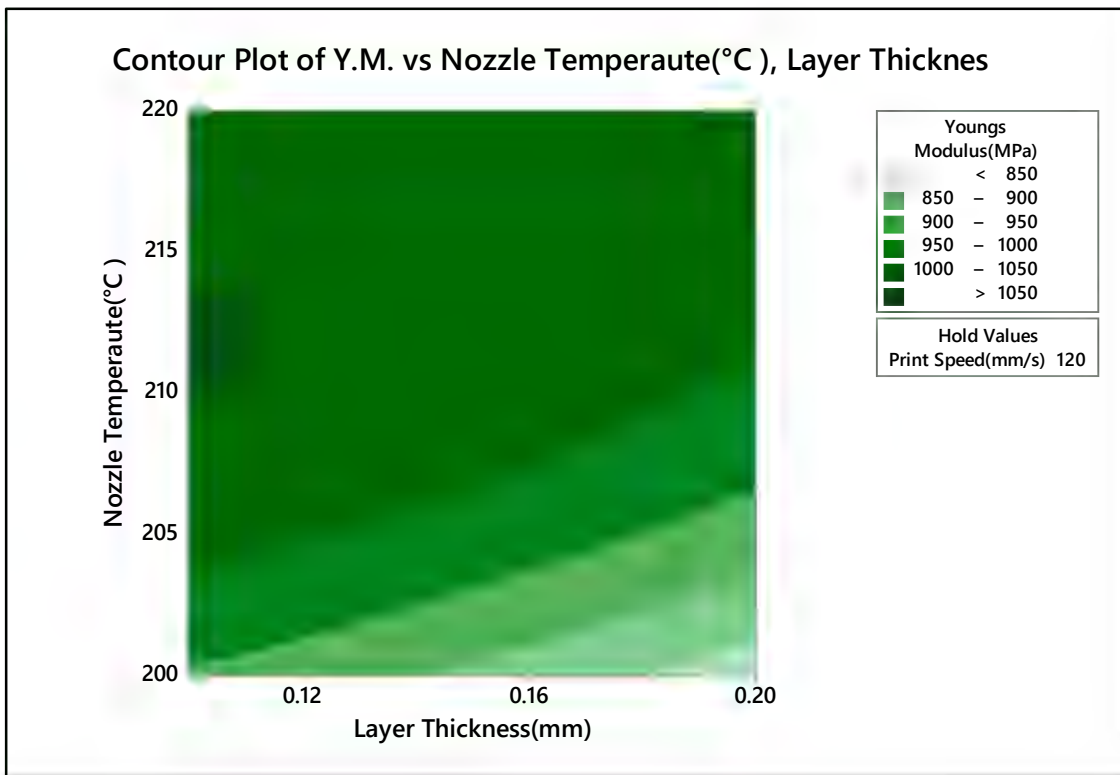


Fig. 41 Contour Plot of Young's Modulus (MPa) vs Nozzle Temperature (°C), Layer Thickness(mm).

Contour plots, or level plots, allow data visualization in three dimensions on a two-dimensional surface. These plots, Fig. 41-43 were created using MINITAB software to provide a clear visual representation of how specific selected parameters and any parameters between specific parameters can impact Young's modulus. For instance, Fig.

41 is a contour plot that shows Young's Modulus (material stiffness) in MPa as it varies with Nozzle Temperature ($^{\circ}\text{C}$) and Layer Thickness (mm). In this specific plot, the printing speed is fixed at 120 mm/s. The key takeaway from the lower left corner of the graph is that a combination of a lower layer thickness (0.1mm) and a higher nozzle temperature (around 205°C) leads to a high Young's Modulus, exceeding 1000 MPa.

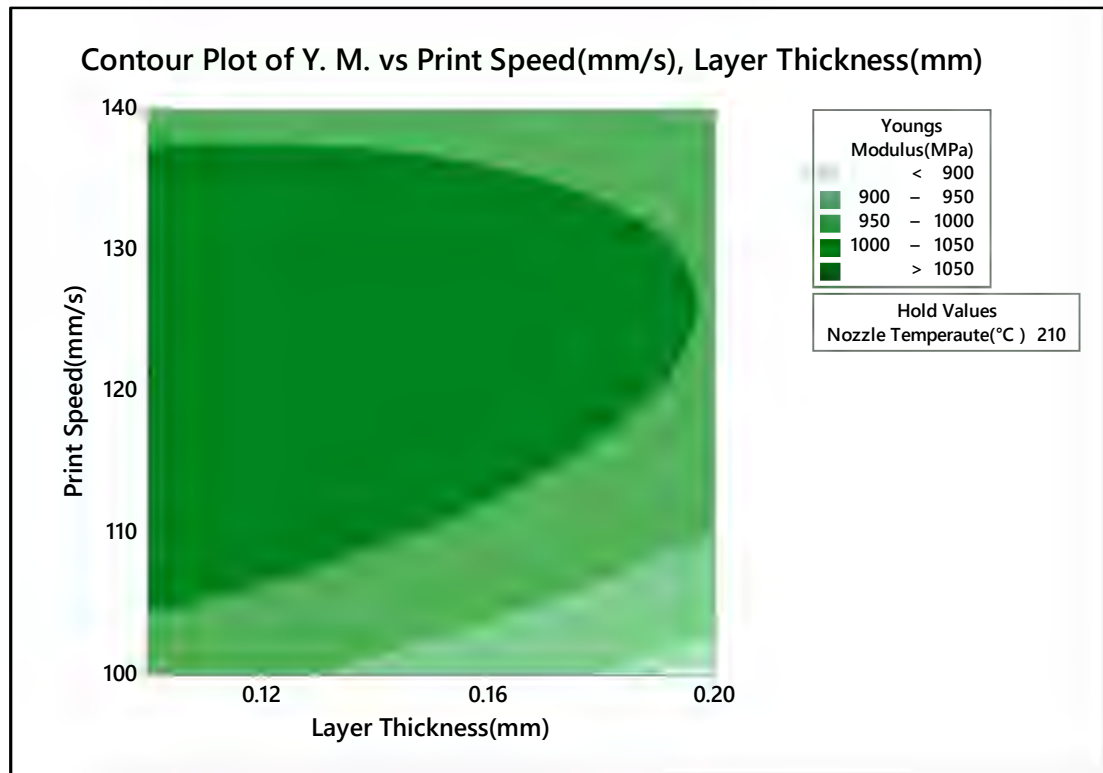


Fig. 42 Contour Plot of Young's Modulus (MPa) vs Print Speed(mm/s), Layer Thickness(mm).

Fig. 42 presents a contour plot visualizing Young's Modulus (MPa) as it is affected by Printing Speed (mm/s) and Layer Thickness (mm). In this case, the nozzle temperature is fixed at 220°C . The plot reveals that a higher Young's Modulus can be achieved with a printing speed between roughly 105mm/s and 137mm/s. Additionally, it is evident that Young's Modulus decreases as the layer thickness increases.

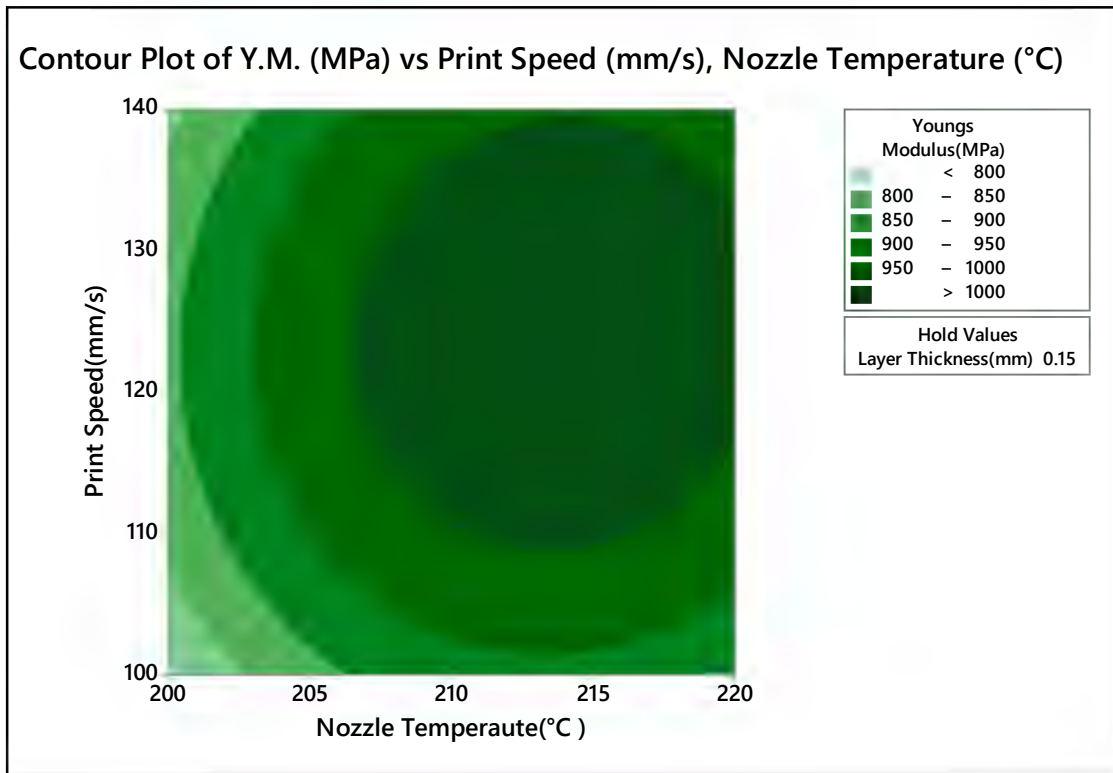


Fig. 43 Contour Plot of Young's Modulus (MPa) vs Print Speed (mm/s), Nozzle Temperature (°C).

Fig. 43 shows a contour plot that maps Young's Modulus (material stiffness in MPa) across variations in Print Speed (mm/s) and Nozzle Temperature (°C). In this plot, the layer thickness is held constant at 0.15 mm. Interestingly, the plot suggests that the most favorable combination for achieving a high Young's Modulus is a higher nozzle temperature (215°C) paired with a moderate print speed (approximately 120 mm/s to 130 mm/s).

4.2.2.5. Surface Plots for Young's Modulus

The correlation between a fixed variable and two additional independent variables can be depicted using surface plots, which are graphical representations in three dimensions, provided by Figs. 44-46. These plots demonstrate how two variables affect Young's modulus, while simultaneously keeping the average value of the third variable constant.

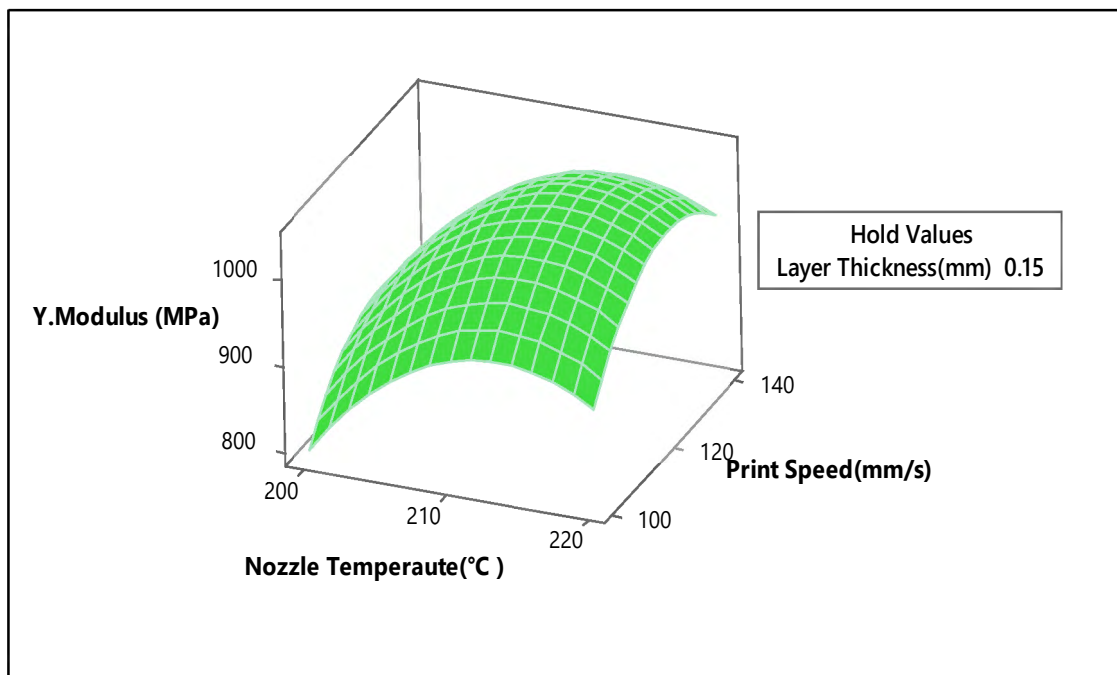


Fig. 44 Young's Modulus (MPa) in a 3D surface plot vs Print speed (mm/s), Nozzle Temperature (°C).

Fig. 44 visualizes Young's Modulus (MPa) in a 3D surface plot to show how it changes in relation to both Print Speed (mm/s) and Nozzle Temperature (°C). In this graph, the layer thickness is fixed at 0.15mm. Print speed and nozzle temperature are adjustable settings (independent variables) shown on the horizontal axes. The vertical axis represents Young's Modulus, measured in Megapascals (MPa). In Fig. 44, it is noticeable that

increasing the nozzle temperature to 210 °C and print speed to 120mm/s at horizontal axes result in a higher Young's Modulus value.

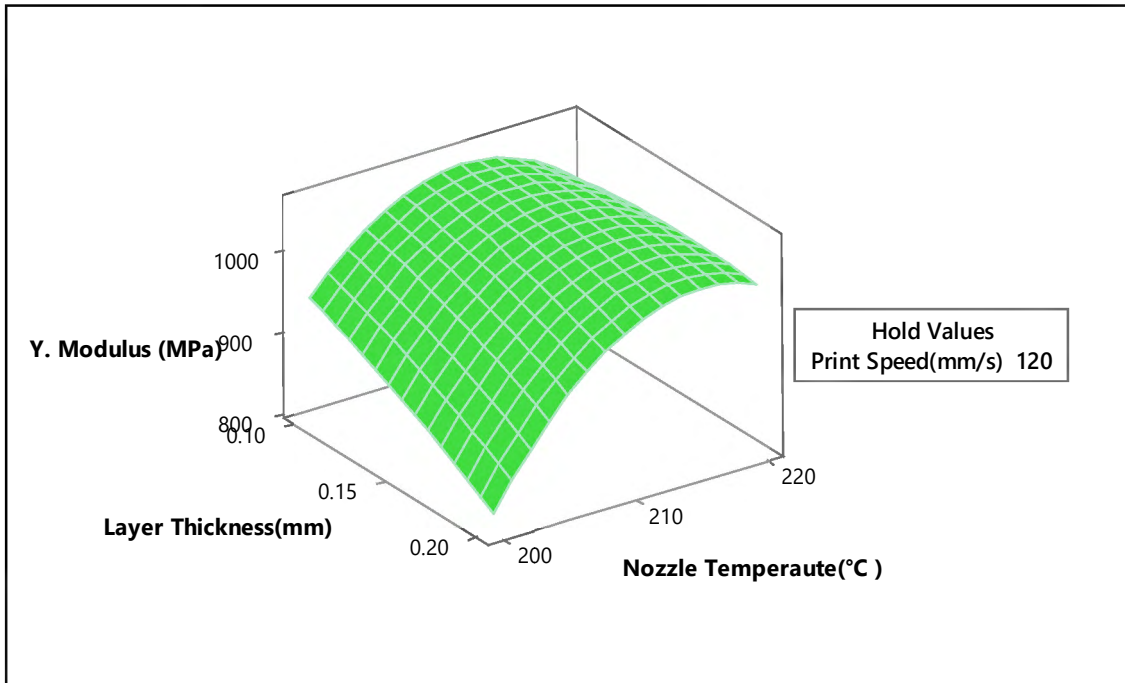


Fig. 45 Young's Modulus (MPa) in a 3D surface plot vs Nozzle Temperature (°C), Layer Thickness (mm).

The example of Fig. 45, illustrates that Young's Modulus varies with nozzle temperature (°C) and layer thickness (mm) while the print speed holds at 120mm/s. The data suggests thicker layers lead to a noticeable decrease in Young's Modulus. However, a higher nozzle temperature can counteract this effect, and result in a higher Young's Modulus.

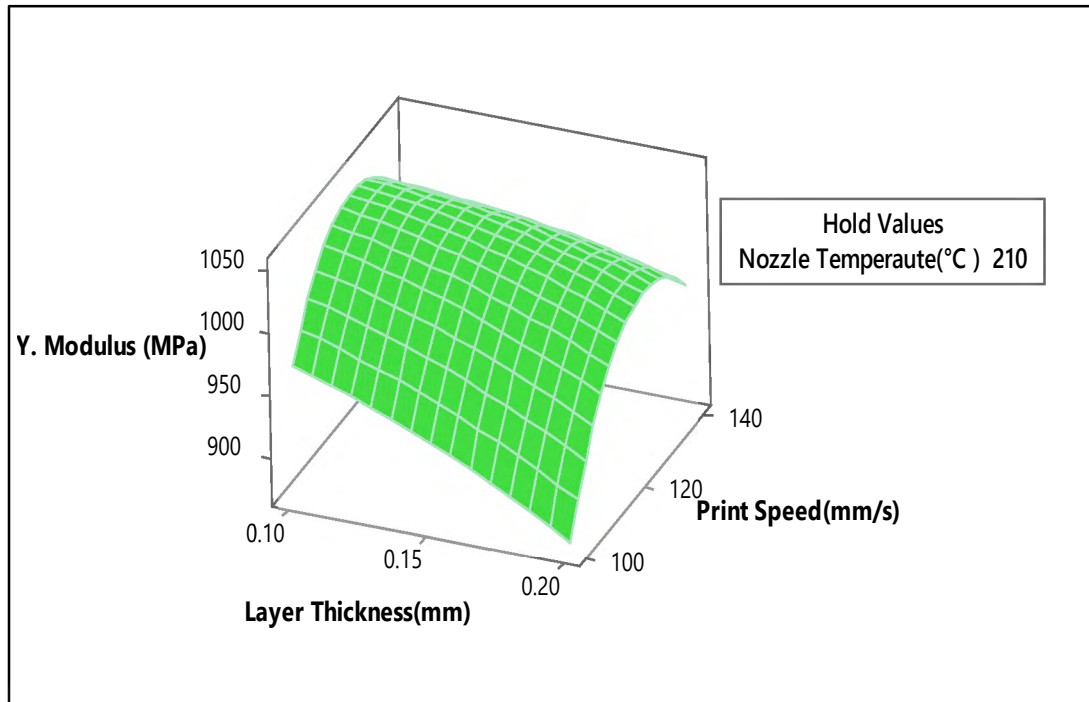


Fig. 46 Young's Modulus (MPa) in a 3D surface plot vs Print Speed(mm/s) Layer Thickness (mm).

Fig. 46 presents a 3D surface plot visualizing Young's Modulus (material stiffness in MPa) as it is affected by both Print Speed (mm/s) and Layer Thickness (mm). In this plot, the nozzle temperature is fixed at 210°C. The horizontal axes represent the printing parameters: speed (mm/s) on one axis and layer thickness (mm) on the other. The vertical axis represents the resulting Young's Modulus value in MPa. According to Fig. 46, if a decrease in layer thickness and print speed increases, the value of Young's modulus will increase as well. The data appears to show a positive correlation between print speed and thinner layers with increased material stiffness, as measured by Young's Modulus.

4.3. DIC Experiment

DIC is a widely used technique for measuring 2D and 3D displacement fields [82]. It has experienced a growing trend in its application in mechanical characterization [83] under various loading conditions, providing comprehensive insights into the deformation and strain distribution of the materials [84]. Furthermore, the combination of tensile test results with DIC data has enabled the approximation of in-plane elastic properties, and Poisson ratio, providing a holistic understanding of material behavior under tensile loading conditions [85]. Therefore, this study uses DIC during tensile testing to measure the major minor strain values and displacement. The DIC process is outlined shown in Fig. 47 below.

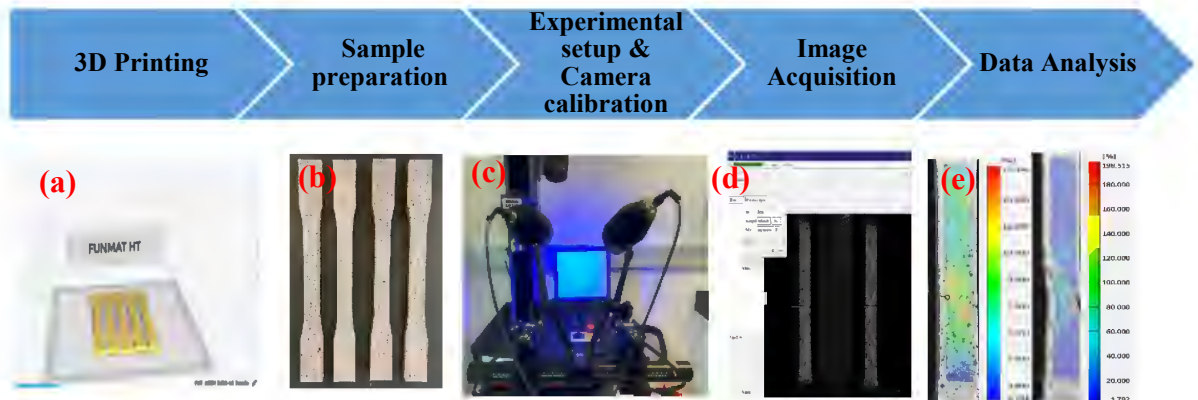


Fig. 47 DIC process is outlined. From left, (a) Tensile specimens printed by FMD, (b) Create white and then black speckle pattern on the specimens, (c) Equipment set up and camera calibration by using a Calibration Panel, (d) image capture by using GOM snap software, and (e) data analysis with GOM correlate software.

4.3.1. 3D Printing for DIC

Following ASTM D638 standards, tensile specimens were created using an FDM 3D printer. The printing process utilized three different layer thicknesses: L1-0.1 mm, L2-0.15 mm, and L3-0.2 mm. The nozzle temperatures varied between 200°C and 220°C, increasing by 10°C for each setting. Corresponding printing speeds were set at 100 mm/s, 120 mm/s, and 140 mm/s. This resulted in 27 unique combinations, totaling 135 specimens.

Of these, 27 were specifically prepared for tensile testing combined with Digital Image Correlation (DIC) analysis.

4.3.2. Sample Preparation

To perform a tensile testing experiment utilizing digital image correlation, it is imperative to initially meticulously and attentively prepare the samples. The process of sample preparation holds significant importance as it directly affects the precision and dependability of the results obtained from the tensile testing [86]. To enable the implementation of digital image correlation, at first, a background of white was spray painted on the tensile specimens, and then a black speckle pattern was applied to the specimens for high-speed camera identification, shown in Fig. 48 (a) and (b). In this study, out of 135 sample specimens, 27 were specifically prepared with a white and black speckle pattern for DIC analysis.

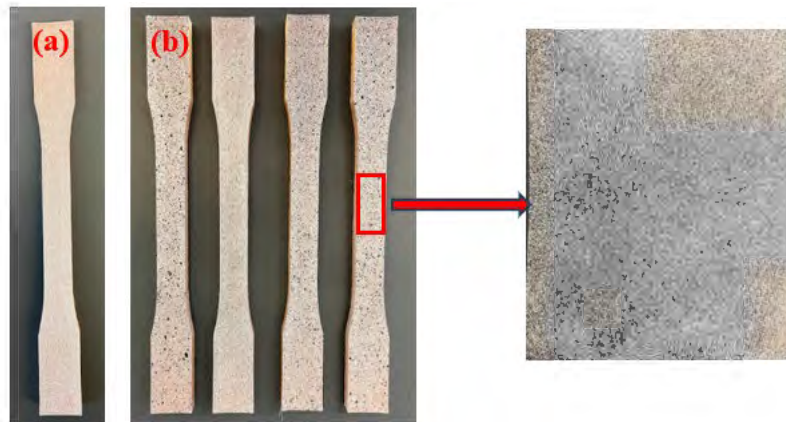


Fig. 48 a) A white base coat is first applied using an acrylic spray, b) Light black paint is sprayed to a crated speckle pattern. This speckle pattern is traced in DIC to capture the strain field.

4.3.3 Experimental Setup

4.3.3.1. DIC Equipment

The experimental setup of DIC, depicted in Fig. 49 consists of two CCD cameras at ARAMIS GOM GmbH, Germany. These cameras were arranged at an angle of 25° relative to each other and those are equipped with lens XENOPLAN 2.0/35-0903 (mvBlueFOX3, Germany) with a focal length of 35 mm. The calibration setup included a Calibration Panel Type /SN CP 40/170.

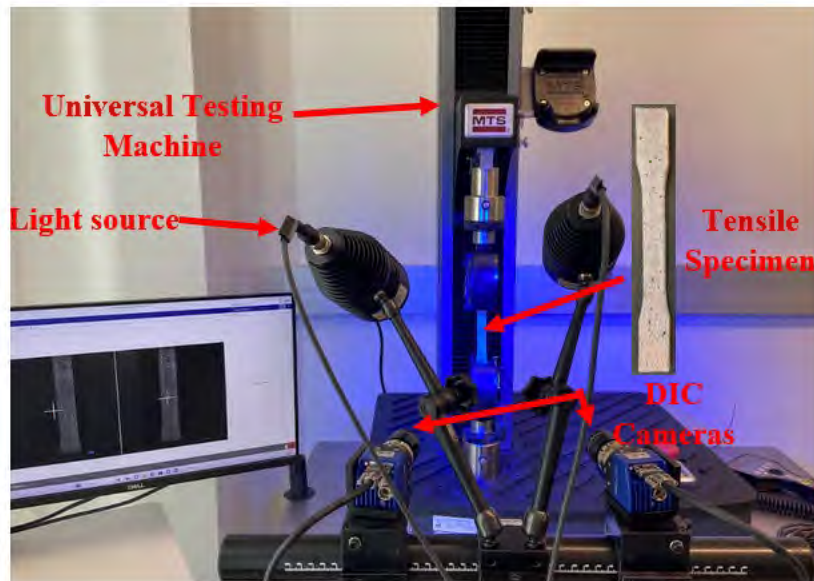


Fig. 49 DIC experimental setup.

4.3.3.2. DIC Software

GOM Snap, a 2D software, processed through GOM Correlate, is used to capture images during tensile testing. In contrast, GOM Correlate has been utilized to analyze digital images to determine material properties and validate and optimize numerical simulations. The GOM correlation software tracked how black and white dots moved on the X and Y axes and computed the associated strains.

4.3.3.3. Camera Calibration

This dual-camera arrangement is essential for 3D DIC systems because they enable the system to calculate 3D displacements and strains across the entire test object by analyzing the perspective differences between images taken from the two cameras. Here, Fig. 50 interface shows views from a left and right camera focusing on the Calibration Panel. The two cameras' slider distance is 178 mm, and the working distance between the calibration panel is 480mm.

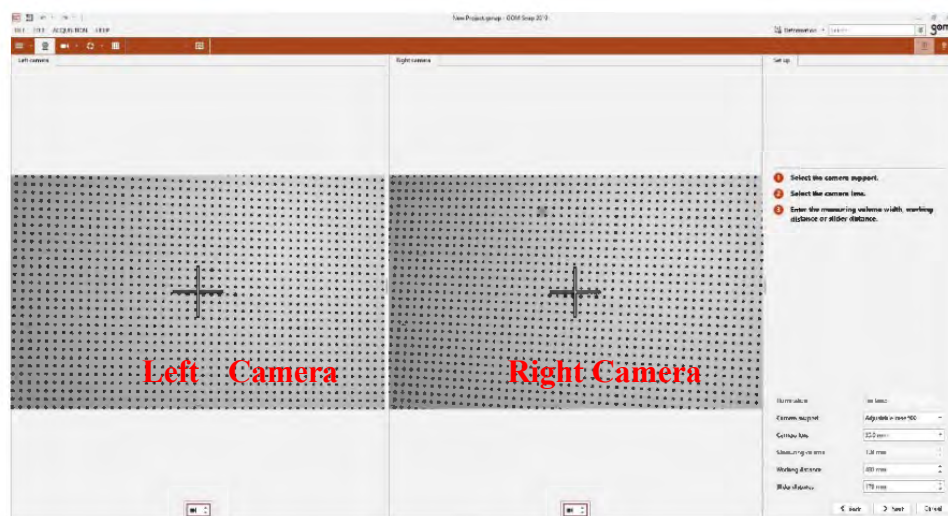


Fig. 50 Left and Right camera calibration before the DIC experiment process.

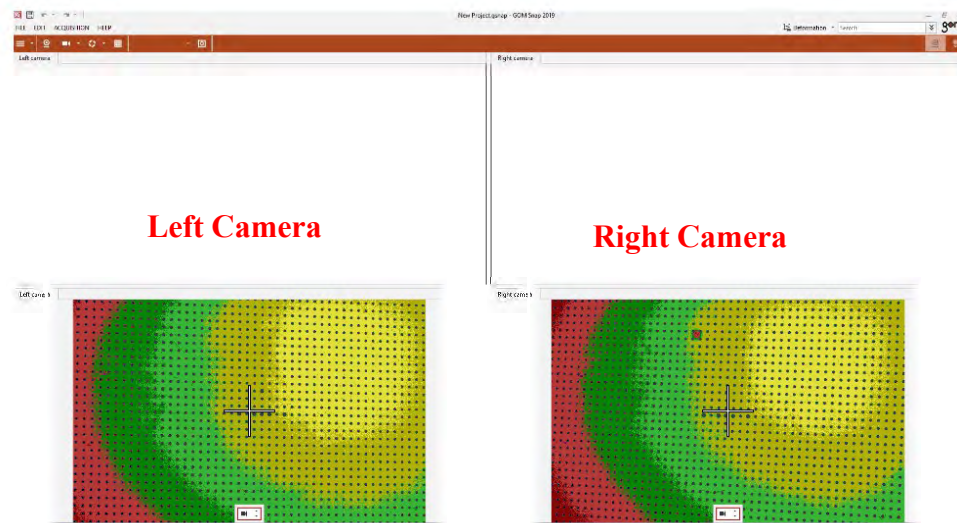


Fig. 51 False color image of left and right camera.

Fig. 51 shows views from a stereo DIC system's left and right cameras. The false color overlay indicates that the system analyzes the calibration quality across the field of view from both perspectives. In calibration, these colors may represent the deviation from expected positions or the quality of the calibration and can help in assessing the quality of the calibration by visually representing the discrepancies or errors between the observed and expected positions of a calibration target or a speckle pattern. During the calibration phase, two cameras capture images of calibration positions from nine different positions or angles, as shown in Fig. 52.

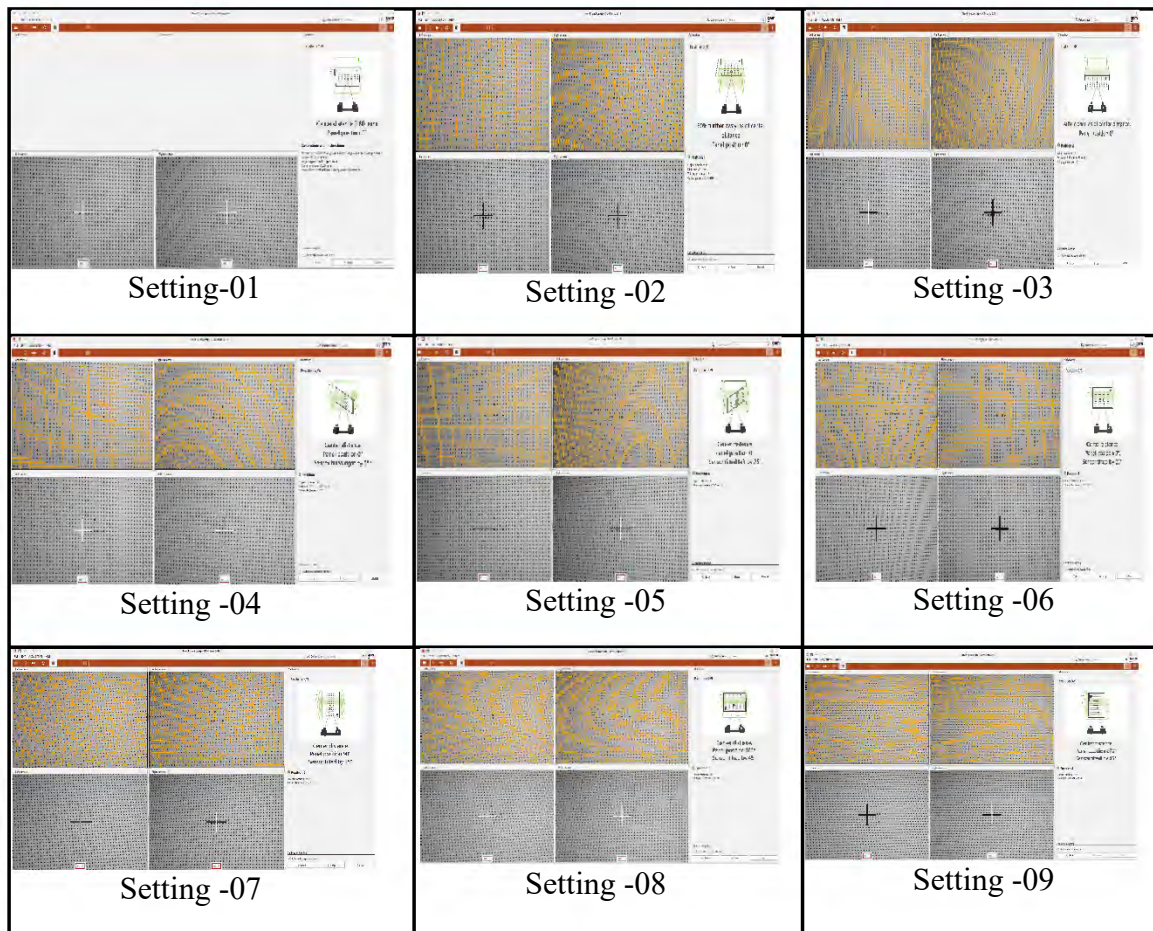


Fig. 52 Calibration images are taken in camera plate for nine different settings.

4.3.4. Image Acquisition

After the experimental setup, GOM Snap 2D free software was used to capture the $\frac{1}{2}$ Hz images shown in Fig. 53. Two high-speed CCD cameras were utilized to record the change in distance of surface speckles during tensile testing and to collect the strain data before being processed by GOM correlate software. The correlation parameters were configured with a facet dimension of 19 pixels and an inter-point spacing of 16 pixels. The DIC system recorded a 1280 x 860 pixel image of the specimen's surface and at a speed of 10 per second. The GOM Correlate software performed the post-processing analysis.

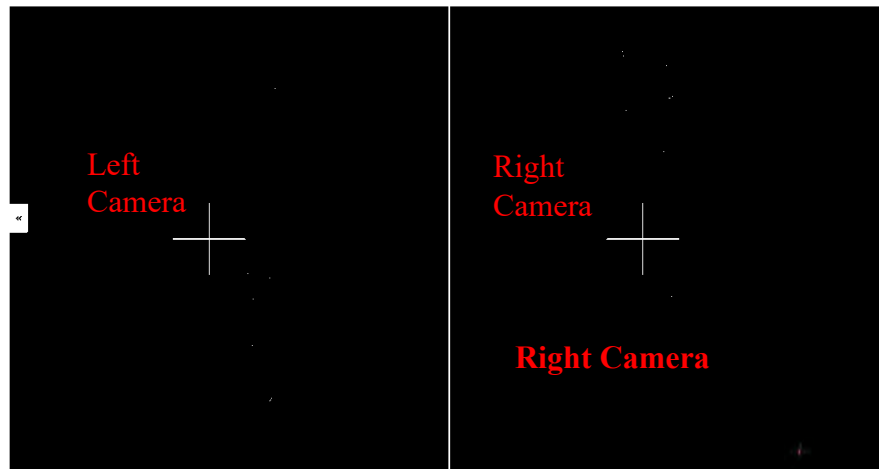


Fig. 53 DIC left and right camera captures images in different measuring sequences.

4.4. DIC Data Analysis

4.4.1. DIC Multiple Point Strain Analysis

In the DIC contour plots, the color scales are labeled with percentages, indicating the amount of strain in Figs. 54 and 56, corresponding to four distinct stages of tensile testing sample 3 L1T1P3 L1- 0.1mm, T1- 200°C, and P3- 140mm/s. Two points are randomly selected for the tensile specimen's full-field view to assess the strain (ϵ_{yy}) in the Y-direction and strain (ϵ_{xx}) in X-direction respectively.

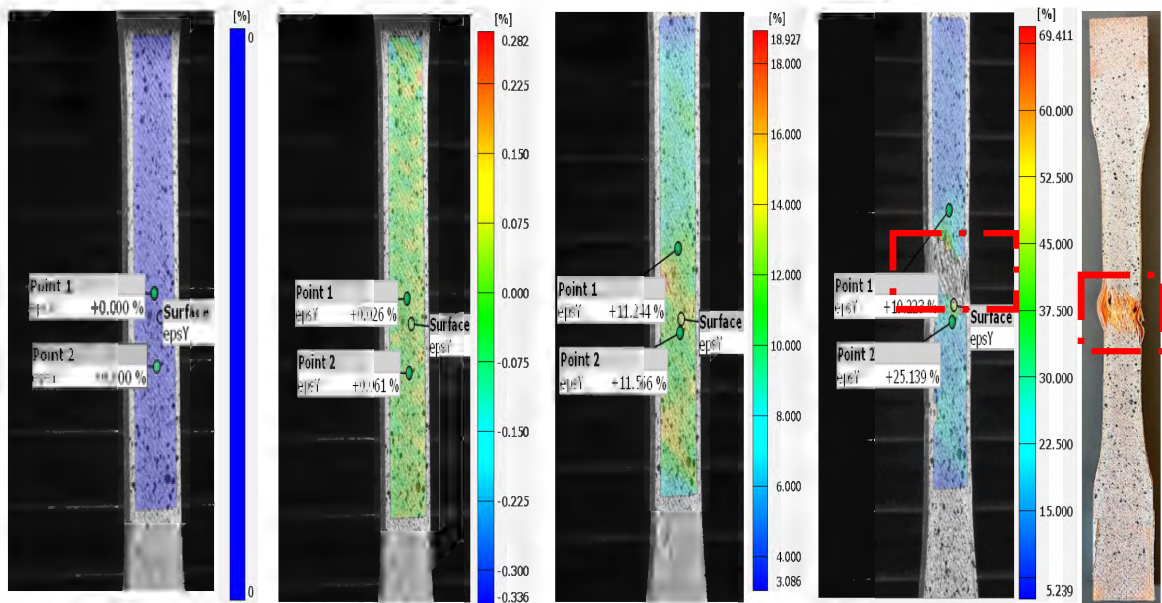


Fig. 54 Strain (ϵ_{yy}) illustrated through contour plots for testing sample 3 L1T1P3 in the Y-direction.

The scales vary significantly across the panels, with the leftmost panel showing the initial condition preceding the tensile test, the follow-up image shows in Fig. 54 the lower strain values of points 1 and 2 (0.026% and 0.061%), the middle panel showing moderate values of around 11% for both points and finally, the rightmost panel demonstrates strain

values, with point 1 exhibiting 19.223% and point 2 reaching 25.139%, thereby highlighting the material's response under substantial tensile strain.

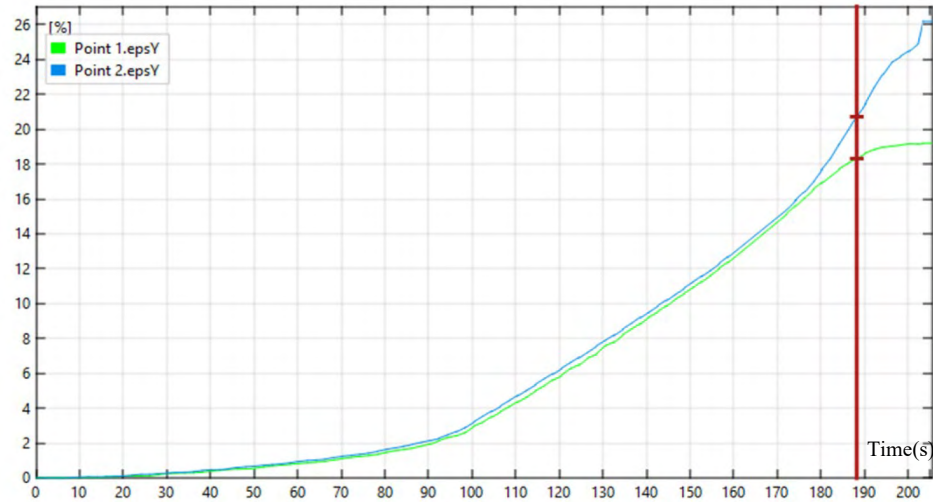


Fig. 55 Time vs strain graph for point 1 and point 2 for testing sample 3.

Furthermore, Fig. 55 illustrates a close observation of the Time versus strain graph for points 1 and 2 of testing sample 3. In the initial loading phase, points 1 and 2 exhibited nearly identical trends and strain values. However, approximately 180 seconds into the experiment, the strain values began to diverge, with the difference steadily increasing until the end of the experiment. This resulted in maximum strain values of approximately 26% and 19% for point 1 and point 2, respectively.

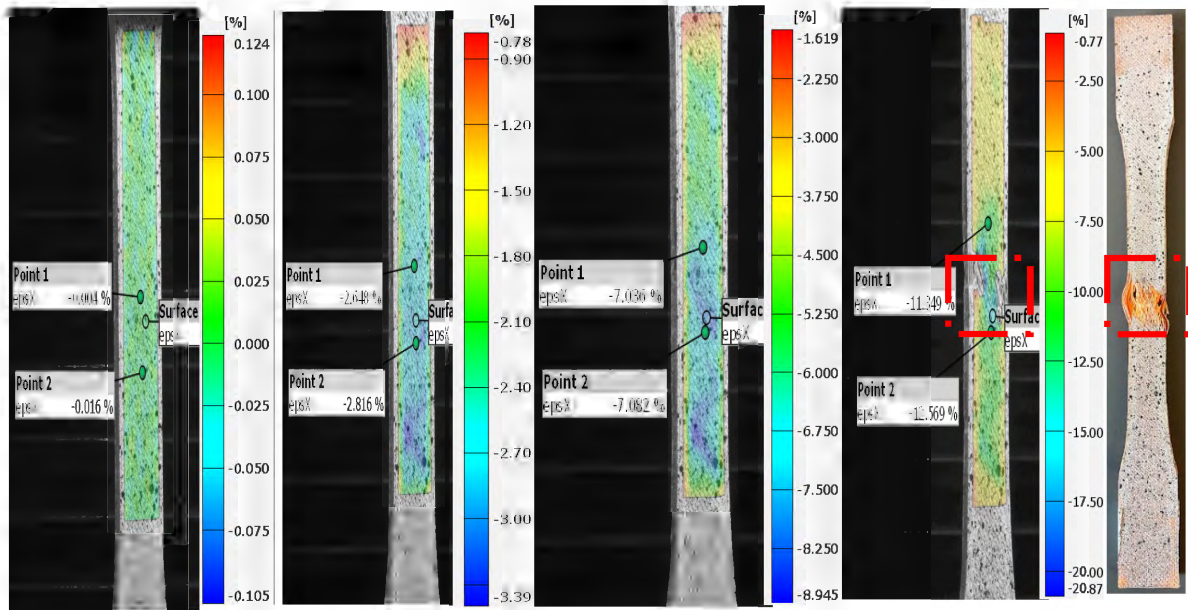


Fig. 56 Strain (ϵ_{xx}) illustrated through contour plots for testing sample 3 L1T1P3 in the X-direction.

Fig. 56 illustrates the strain (ϵ_{xx}) in the X-direction for the tensile testing sample 3. Here, the presence of a negative strain value in the data suggests the regions in the full specimens within the sample are experiencing compression or a reduction in strain due to Poisson's effect. The data shows the strain is not uniform across the surface of the material. The higher compression strain was observed for point 2 at strain (ϵ_{xx}) -0.016%. Notably, point 2 experiences a higher compression strain than point 1 from the beginning to the end of the tensile test.

4.4.1. Strain Maps for layer thickness 0.1mm Specimens

Sample 01: L1T1P1, L- 0.1mm, T- 200 °C, P- 100mm/s

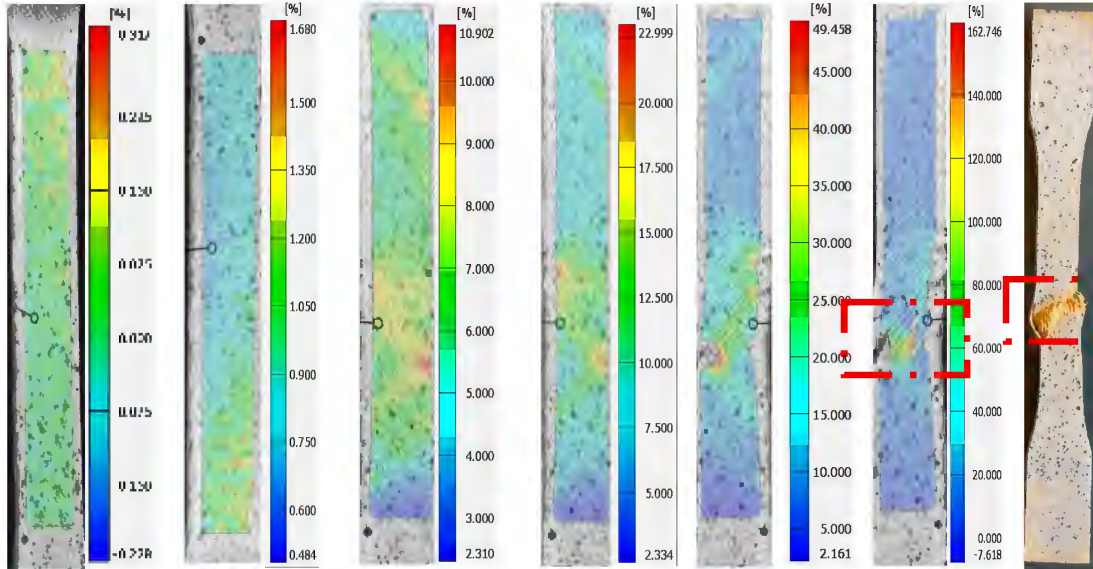


Fig. 57 Strain illustrated through contour plots for testing sample 1.

Sample 02: L1T1P2; L- 0.1mm, T- 200 °C, P- 120mm/s

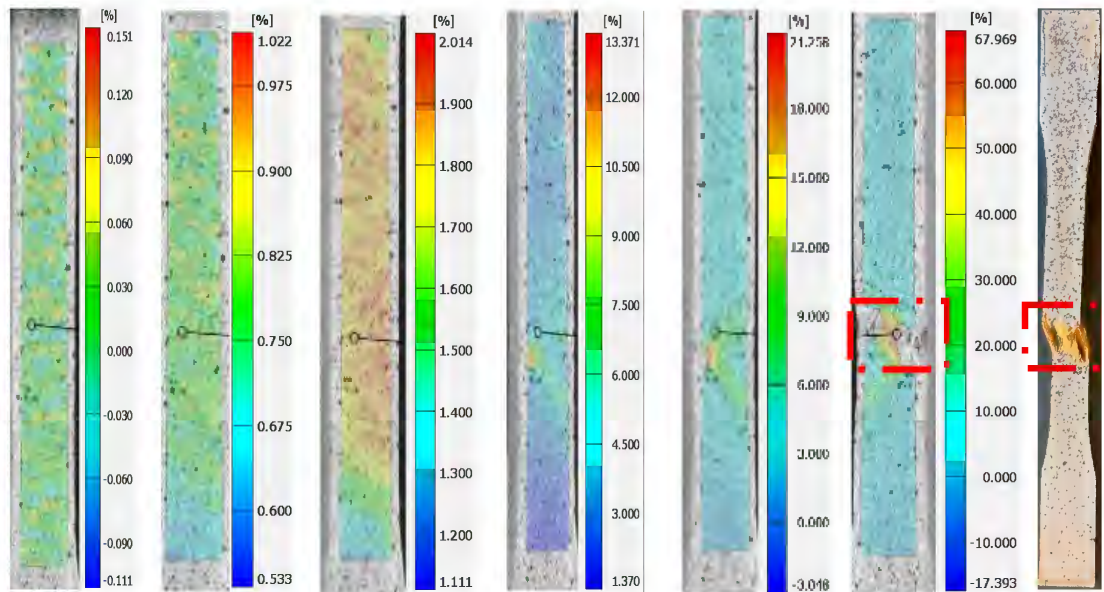


Fig. 58 Strain illustrated through contour plots for testing sample 2.

Fig.57 and Fig. 58 show the contour plots of strain for sample 1-L1T1P1 and sample 2-L1T1P2 in the Y-direction of DIC with tensile tests over time.

Sample 03: L1T1P3; L- 0.1mm, T- 200 °C, P- 140mm/s

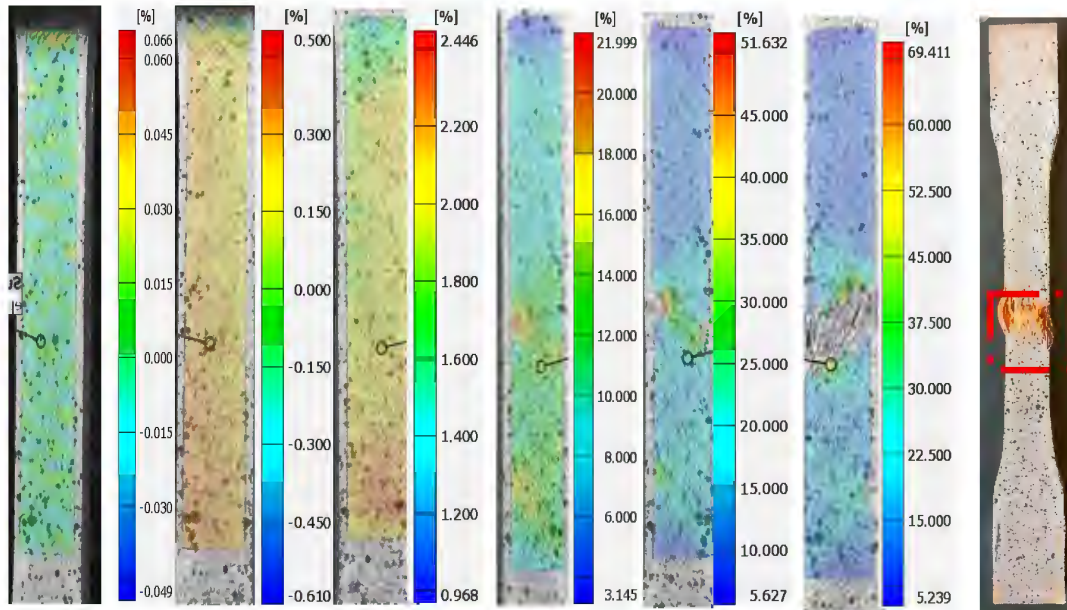


Fig. 59 Strain illustrated through contour plots for testing sample 3.

Sample 04: L1T2P1; L- 0.1mm, T- 210 °C, P- 100mm/s

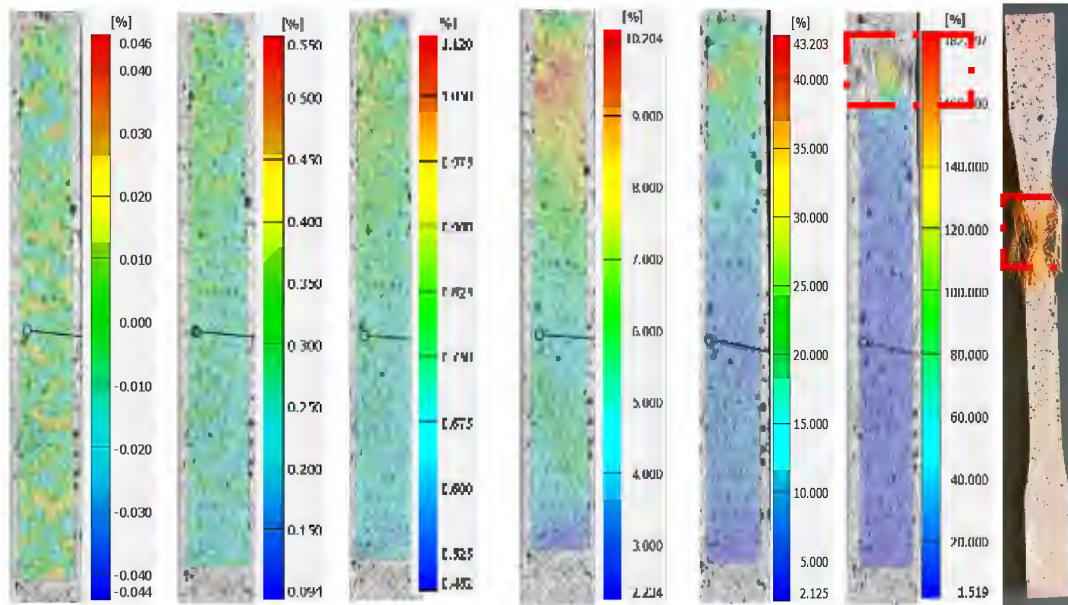


Fig. 60 Strain illustrated through contour plots for testing sample 4.

Fig. 59 and Fig. 60 show the contour plots of strain for sample 3- L1T1P3 and sample 4- L1T2P1 in the Y-direction of DIC with tensile tests over time.

Sample 05: L1T2P2; L- 0.1mm, T- 210 °C, P- 120mm/s

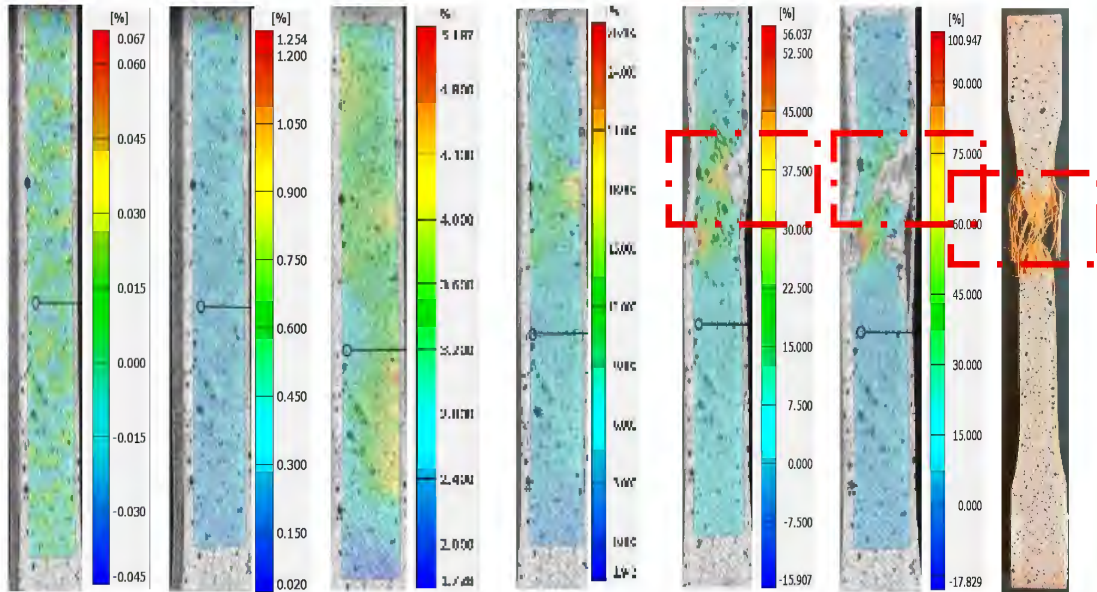


Fig. 61 Strain illustrated through contour plots for testing sample 5.

Sample 06: L1T2P3; L- 0.1mm, T- 210 °C, P- 140mm/s

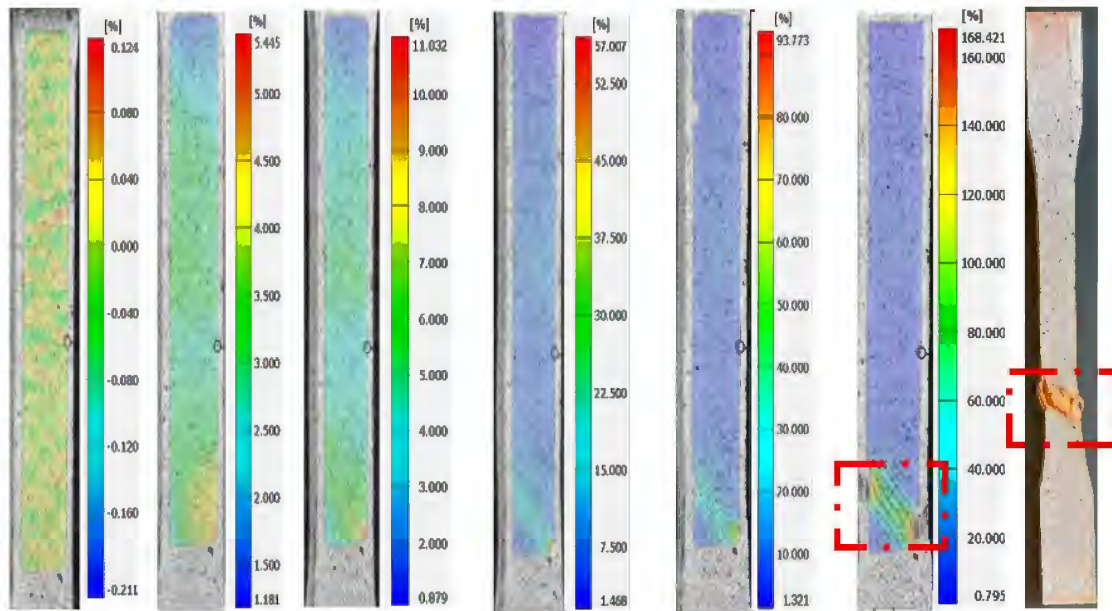


Fig.62 Strain illustrated through contour plots for testing sample 6.

Fig. 61 and Fig. 62 show the contour plots of strain for sample 5 L1T2P2, and sample 6 L1T2P3 in the Y-direction of DIC with tensile tests over time.

Sample 07: L1T3P1; L- 0.1mm, T- 220 °C, P- 100mm/s

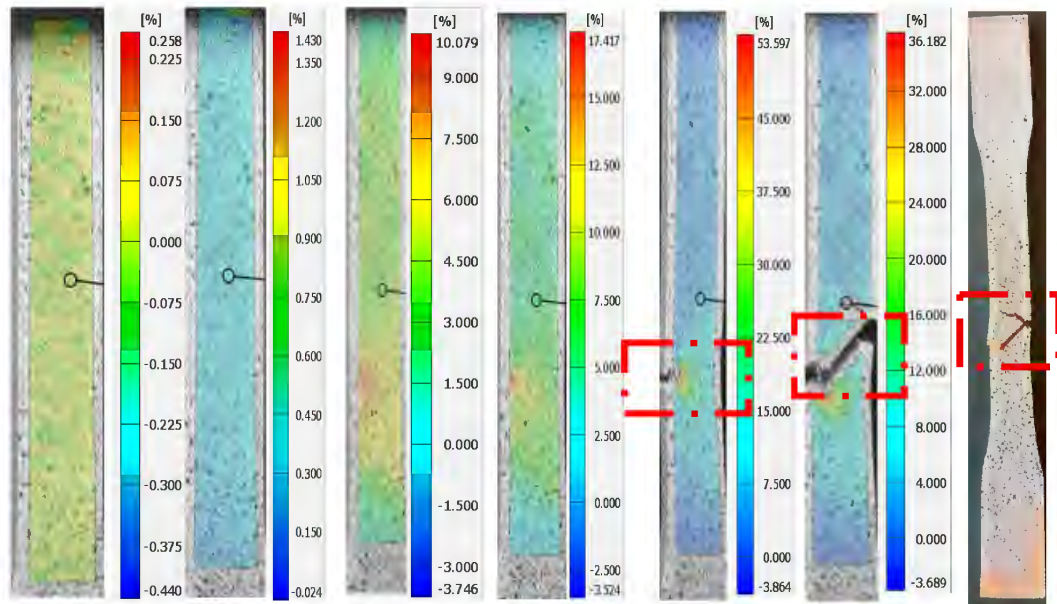


Fig. 63 Strain illustrated through contour plots for testing sample 7.

Sample 8: L1T3P2; L- 0.1mm, T- 220 °C, P- 120mm/s

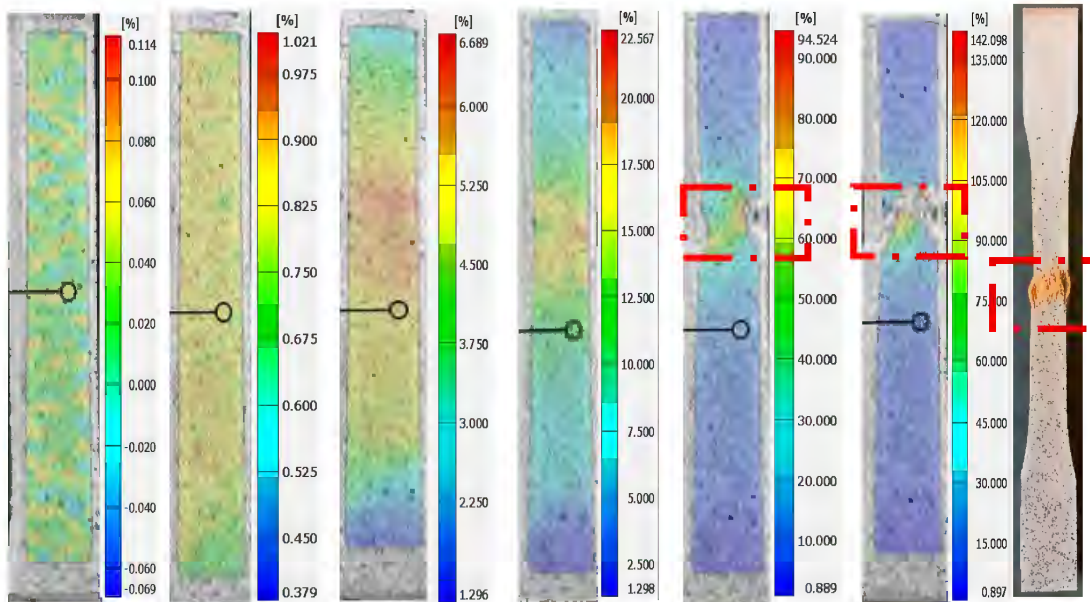


Fig. 64 Strain illustrated through contour plots for testing sample 8.

Fig. 63 and Fig. 64 show the contour plots of strain for sample 7 L1T3P1, and sample 8 L1T3P2 in the Y-direction of DIC with tensile tests over time.

Sample 09: L1T3P3; L- 0.1mm, T- 220 °C, P- 140mm/s

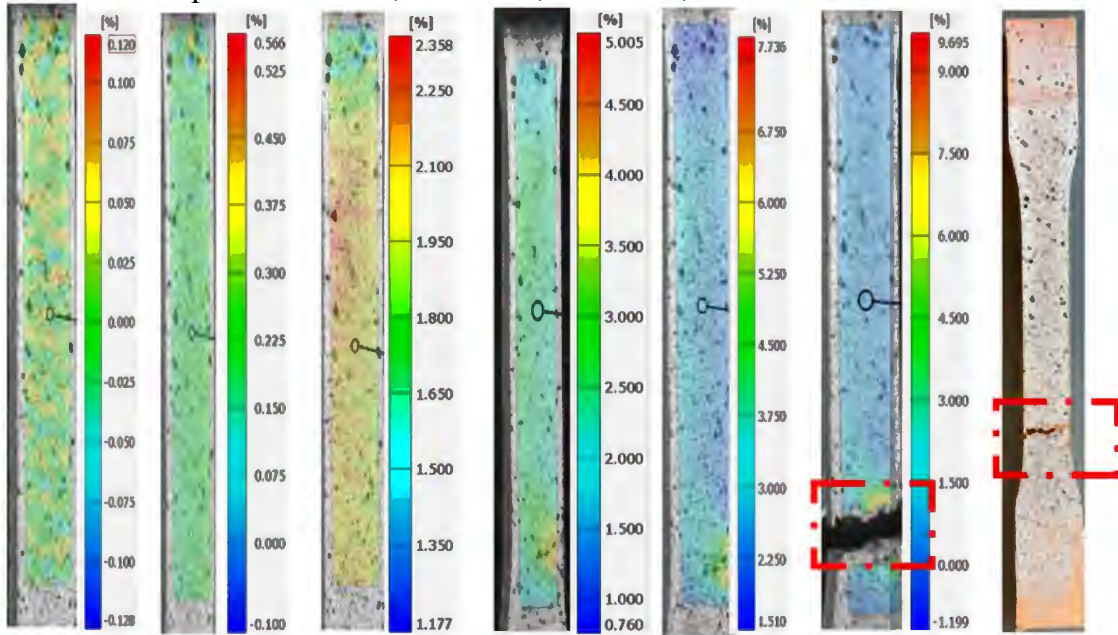


Fig. 65 Strain illustrated through contour plots for testing sample 9.

4.4.2. Strain Maps for layer thickness 0.15mm Specimens

Sample 10: L2T1P1; L- 0.15mm, T- 200 °C, P- 100mm/s

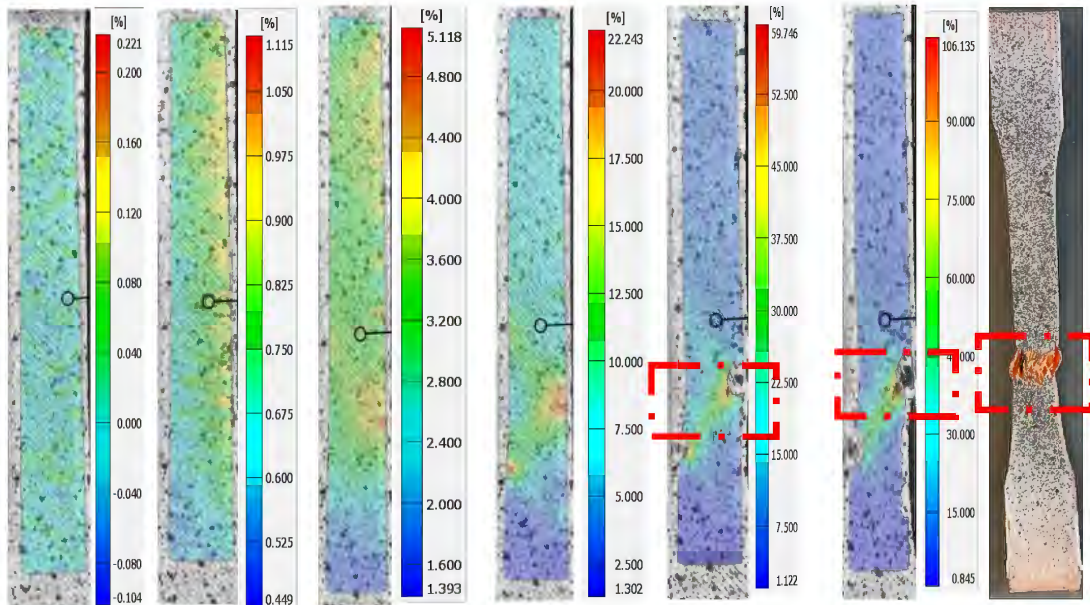


Fig.66 Strain illustrated through contour plots for testing sample 10.

Fig. 65 and Fig. 66 show the contour plots of strain for sample 9- L2T1P3 and sample 10- L2T1P1 in the Y-direction of DIC with tensile tests over time.

Sample 11: L2T1P2; L- 0.15mm, T- 200 °C, P- 120mm/s

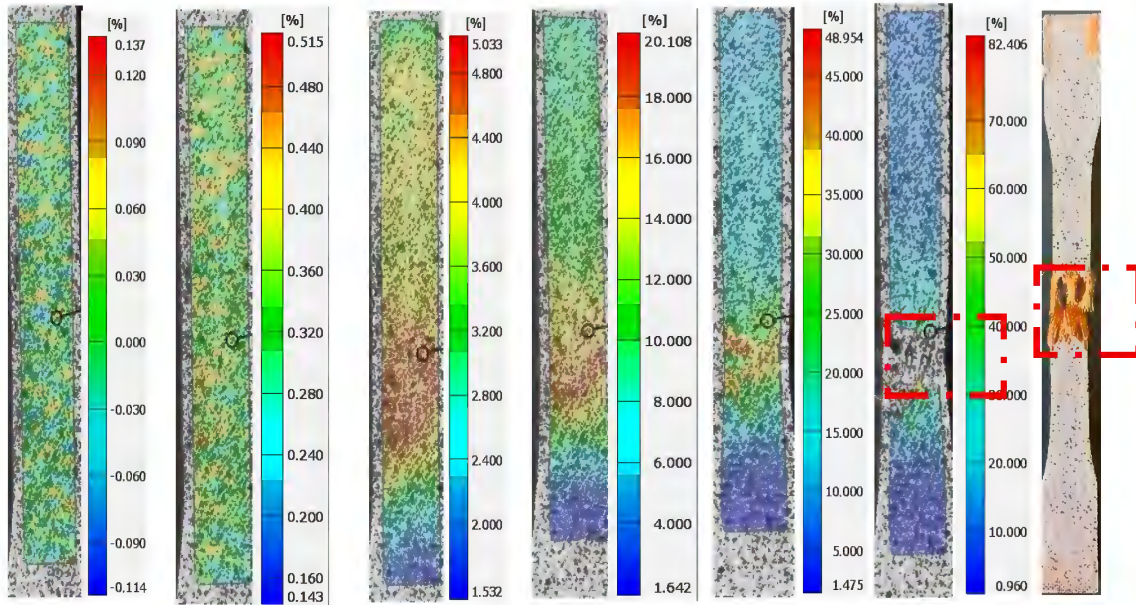


Fig. 67 Strain illustrated through contour plots for testing sample 11.

Sample 12: L2T1P3; L- 0.15mm, T- 200 °C, P- 140mm/s

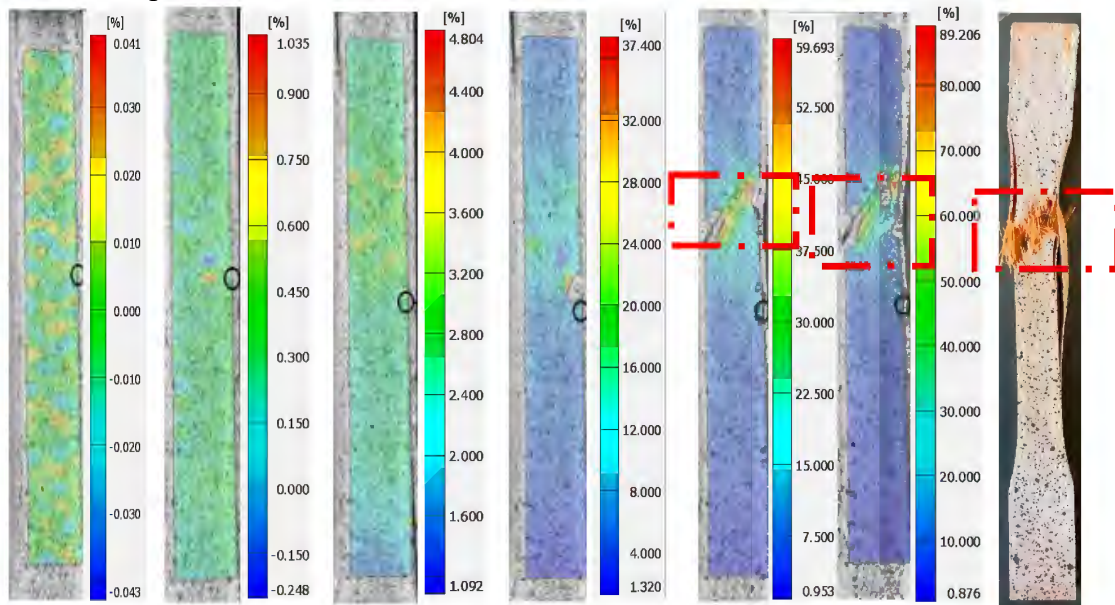


Fig. 68 Strain illustrated through contour plots for testing sample 12.

Fig. 67 and Fig. 68 show the contour plots of strain for sample 11- L2T1P2 and sample 12- L2T1P3 in the Y-direction of DIC with tensile tests over time.

Sample 13: L2T2P1; L- 0.15mm, T- 210 °C, P- 100mm/s

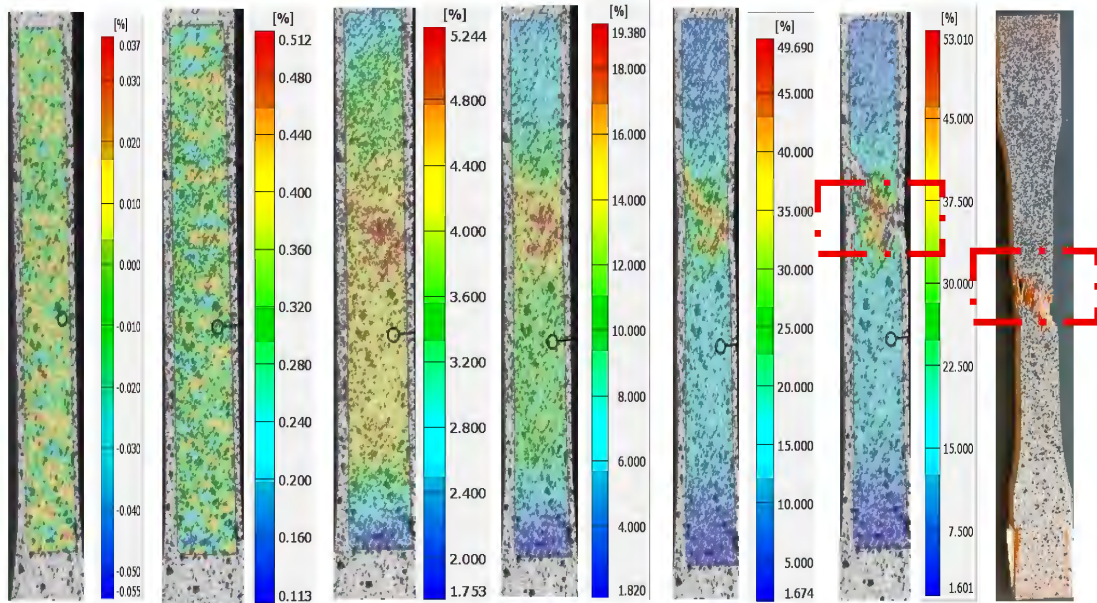


Fig. 69 Strain illustrated through contour plots for testing sample 13.

Sample 14: L2T2P2; L- 0.15mm, T- 210 °C, P- 120mm/s

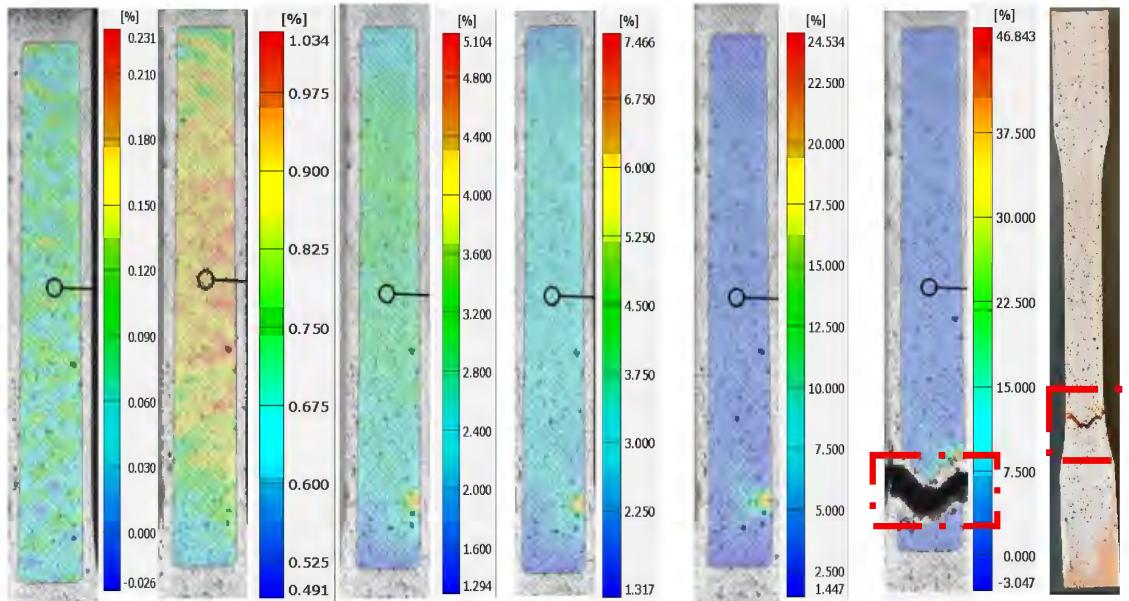


Fig. 70 Strain illustrated through contour plots for testing sample 14.

Fig. 69 and Fig. 70 show the contour plots of strain for sample 13- L2T2P1, and sample 14- L2T2P2 in the Y-direction of DIC with tensile tests over time.

Sample 15: L2T2P3; L- 0.15mm, T- 210 °C, P- 140mm/s

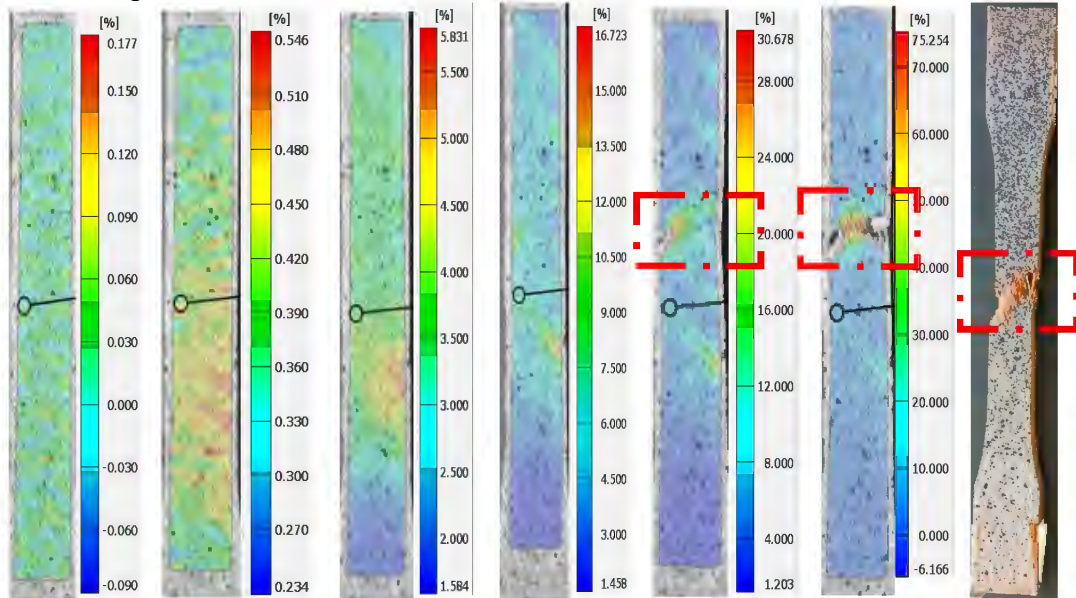


Fig. 71 Strain illustrated through contour plots for testing sample 15.

Sample 16: L2T3P1; L- 0.15mm, T- 220 °C, P- 100mm/s

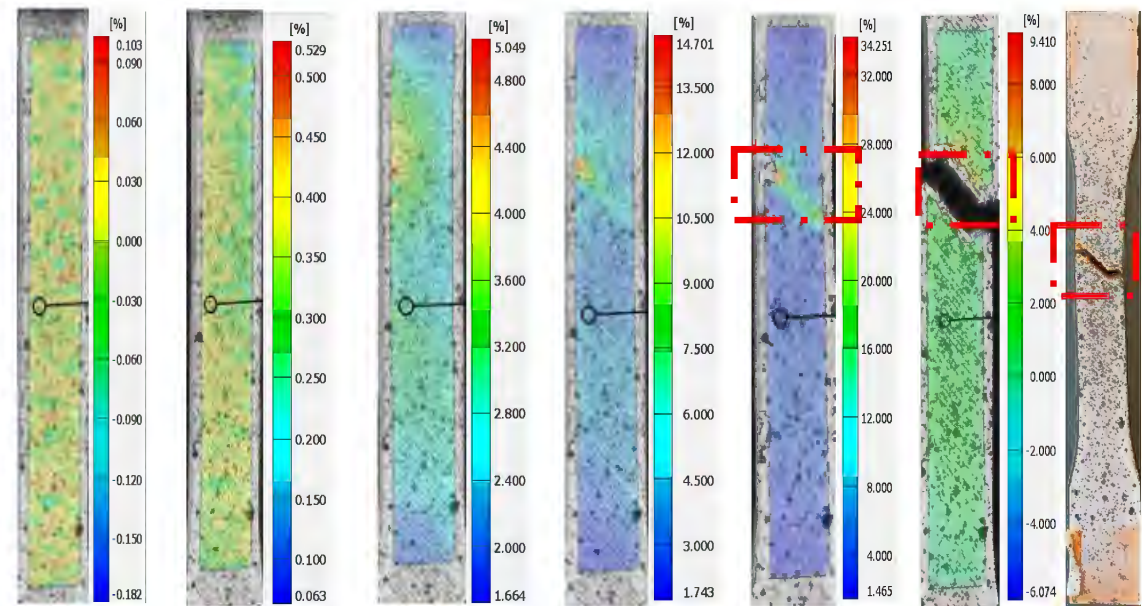


Fig. 72 Strain illustrated through contour plots for testing sample 16.

Fig. 71 and Fig. 72 show the contour plots of strain for sample 15- L2T2P3 and sample-16 L2T3P1 in the Y-direction of DIC with tensile tests over time.

Sample 17: L2T3P2; L- 0.15mm, T- 220 °C, P- 120mm/s

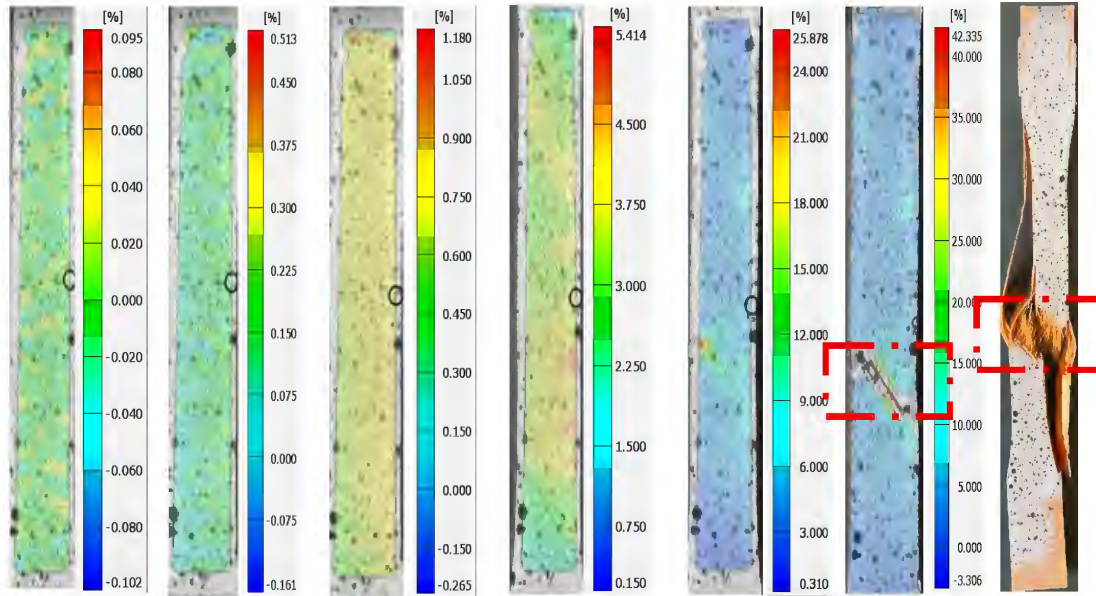


Fig. 73 Strain illustrated through contour plots for testing sample 17.

Sample 18: L2T3P3; L- 0.15mm, T- 220 °C, P- 140mm/s

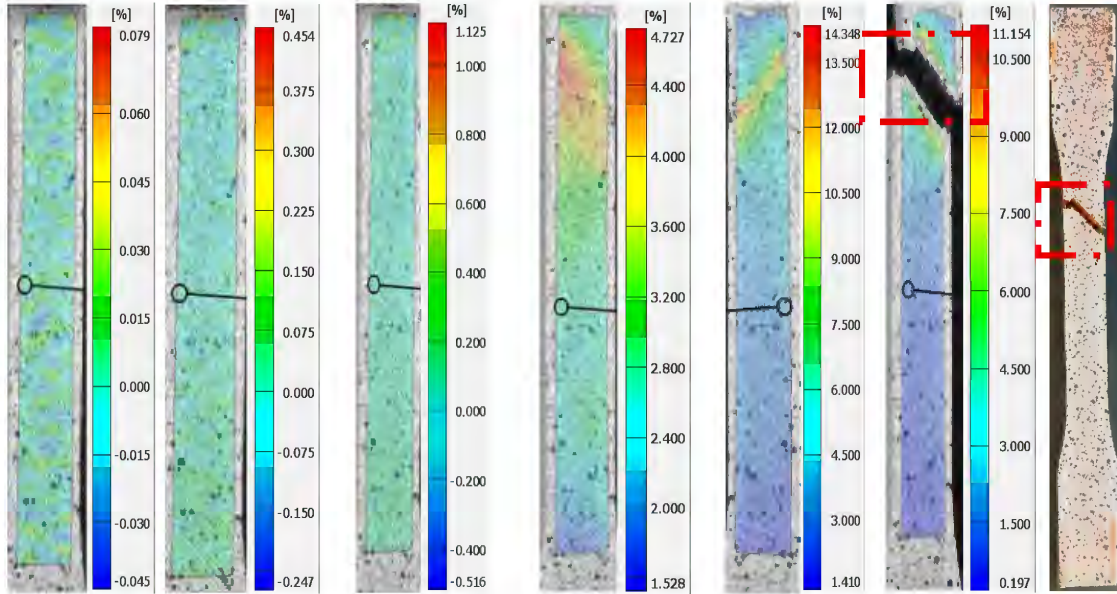


Fig. 74 Strain illustrated through contour plots for testing sample 18.

Fig. 73 and Fig. 74 show the contour plots of strain for sample 17 L2T3P2 and Sample 18- L2T3P3 in the Y-direction of DIC with tensile tests over time.

4.4.3. Strain Maps for layer thickness 0.2mm Specimens

Sample 19: L3T1P1; L- 0.2mm, T- 200 °C, P- 100mm/s

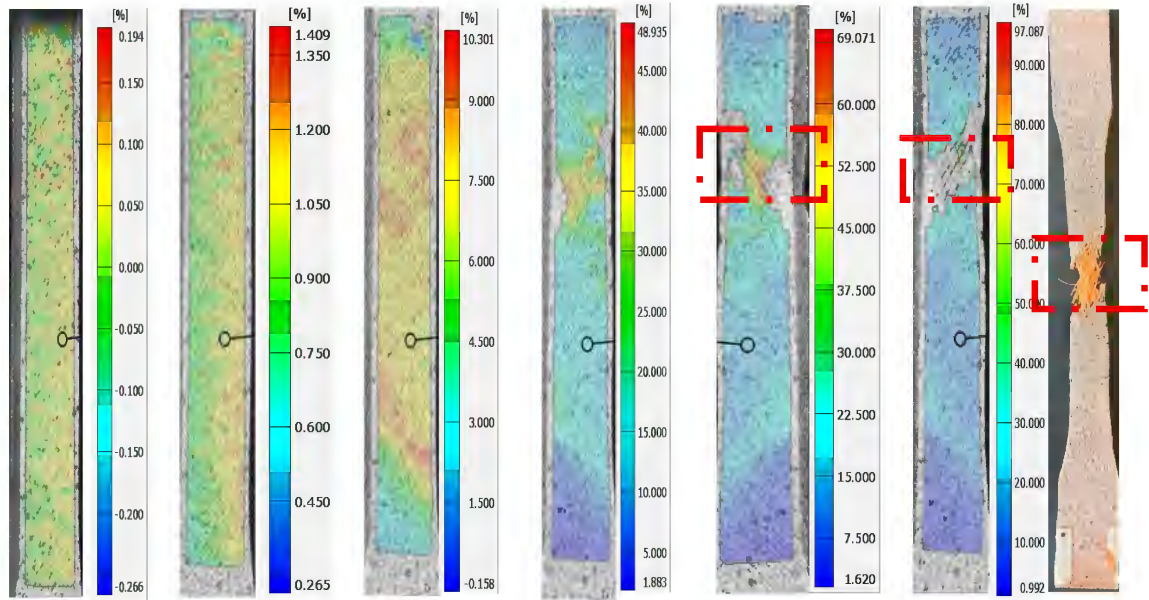


Fig. 75 Strain illustrated through contour plots for testing sample 19.

Sample 20: L3T1P2; L- 0.2mm, T- 200 °C, P- 120mm/s

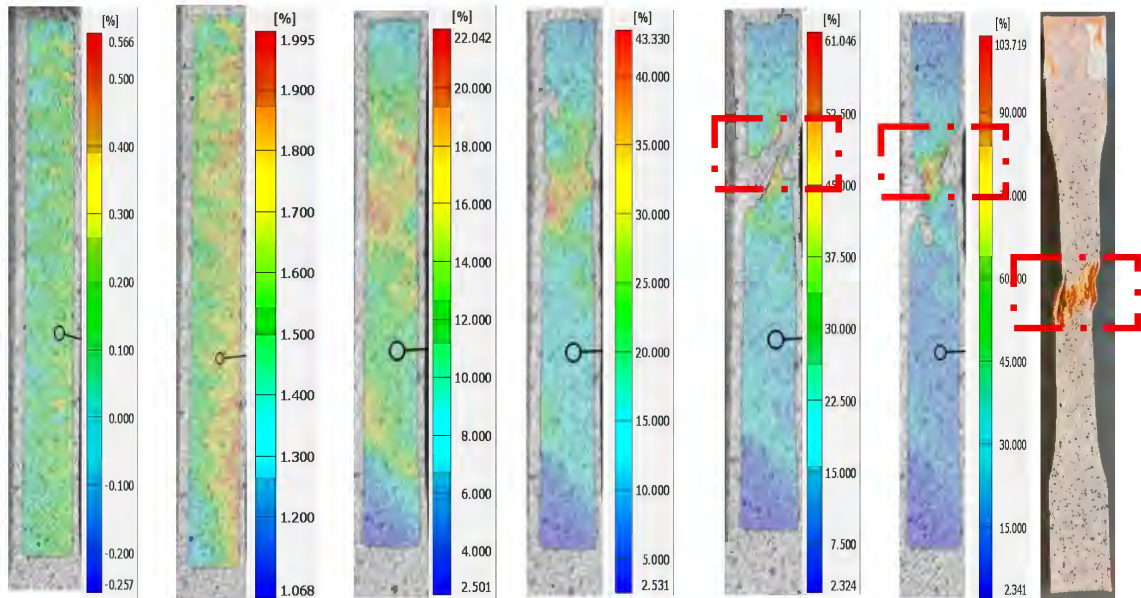


Fig. 76 Strain illustrated through contour plots for testing sample 20.

Fig. 75 and Fig. 76 show the contour plots of strain for sample 19 L3T1P1, and Sample 20 L3T1P2 in the Y-direction of DIC with tensile tests over time.

Sample 21: L3T1P3; L- 0.2mm, T- 200 °C, P- 140mm/s

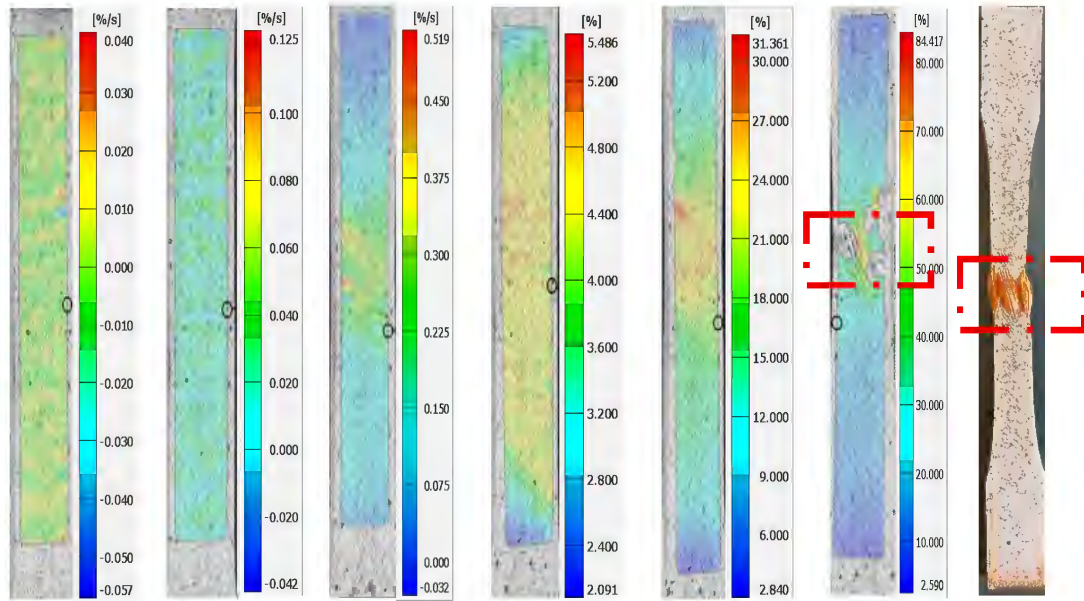


Fig. 77 Strain illustrated through contour plots for testing sample 21.

Sample 22: L3T2P1; L- 0.2mm, T- 210 °C, P- 100mm/s

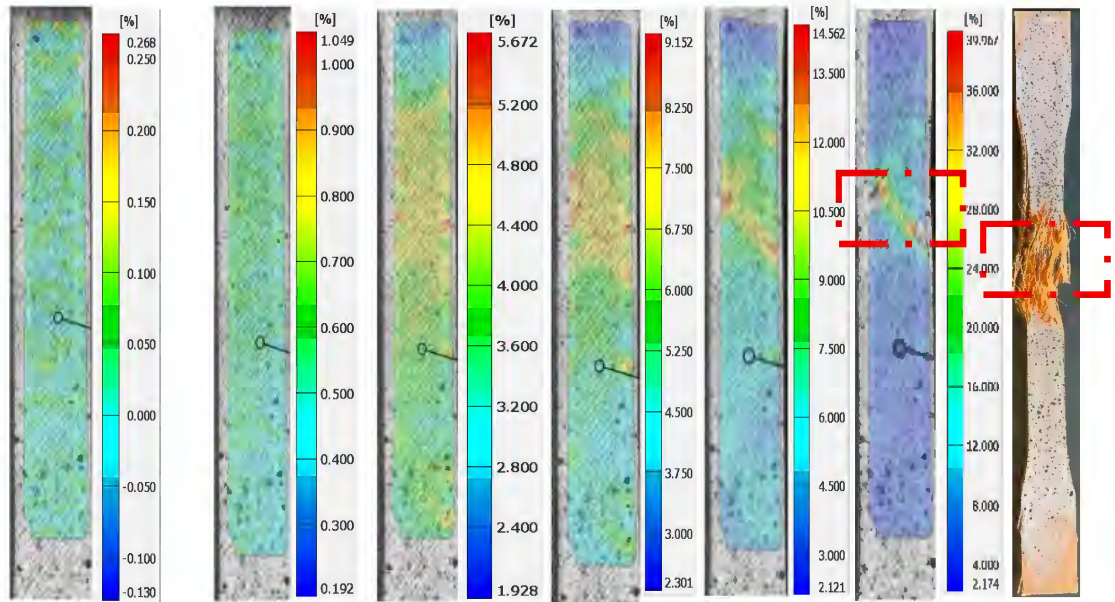


Fig.78 Strain illustrated through contour plots for testing sample 22.

Fig. 77 and Fig.78 show the contour plots of strain for sample 21 L3T1P3, and Sample 22 L3T2P1 in the Y-direction of DIC with tensile tests over time.

Sample 23: L3T2P2; L- 0.2mm, T- 210 °C, P- 120mm/s

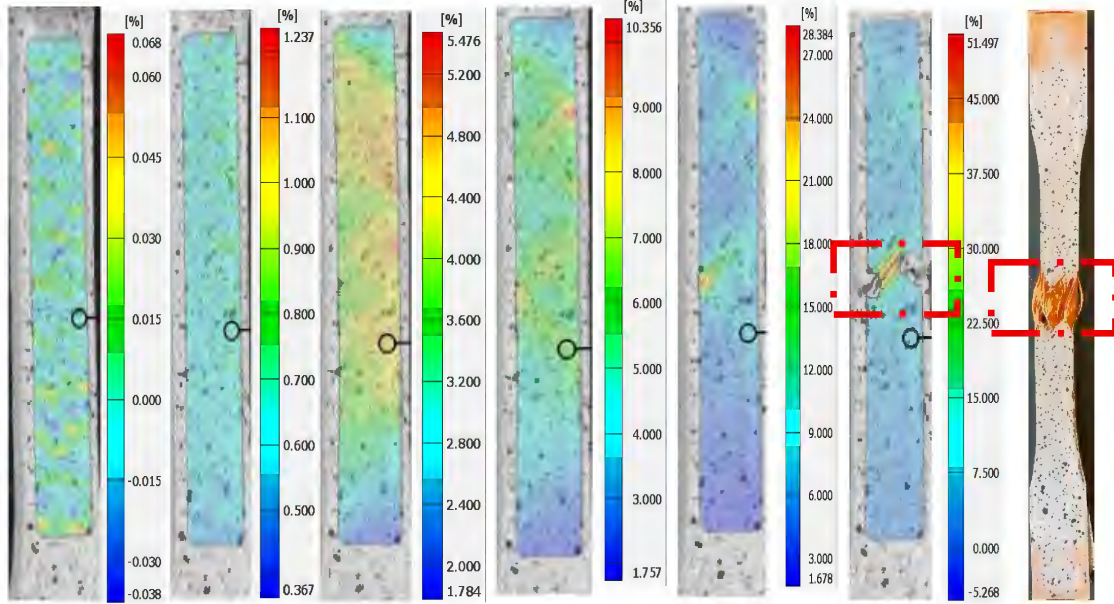


Fig. 79 Strain illustrated through contour plots for testing sample 23.

Sample 24: L3T2P3; L- 0.2mm, T- 210 °C, P- 140mm/s

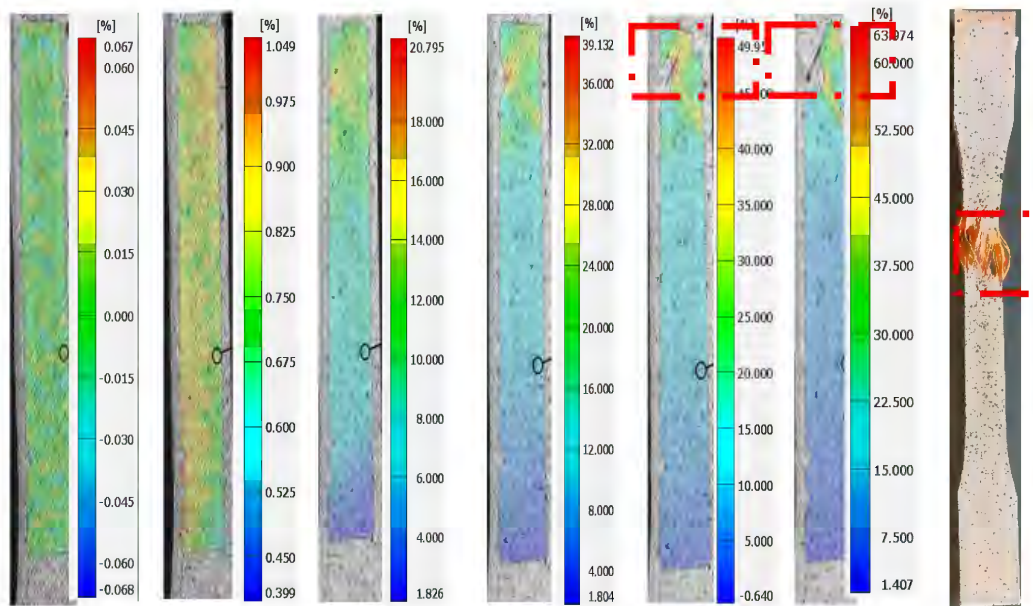


Fig. 80 Strain illustrated through contour plots for testing sample 24.

Fig. 79 and Fig. 80 show the contour plots of strain for sample 23 L3T2P2 and Sample 24- L3T2P3 in the Y-direction of DIC with tensile tests over time.

Sample 25: L3T3P1; L- 0.2mm, T- 220 °C, P- 100mm/s

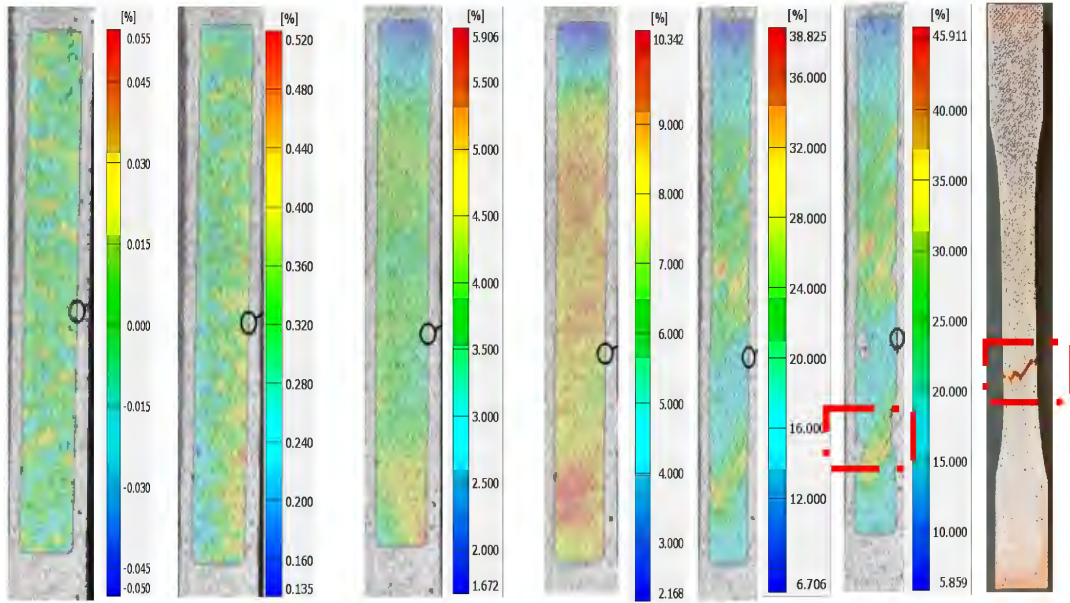


Fig. 81 Strain illustrated through contour plots for testing sample 25.

Sample 26: L3T3P2; L- 0.2mm, T- 220 °C, P- 120mm/s

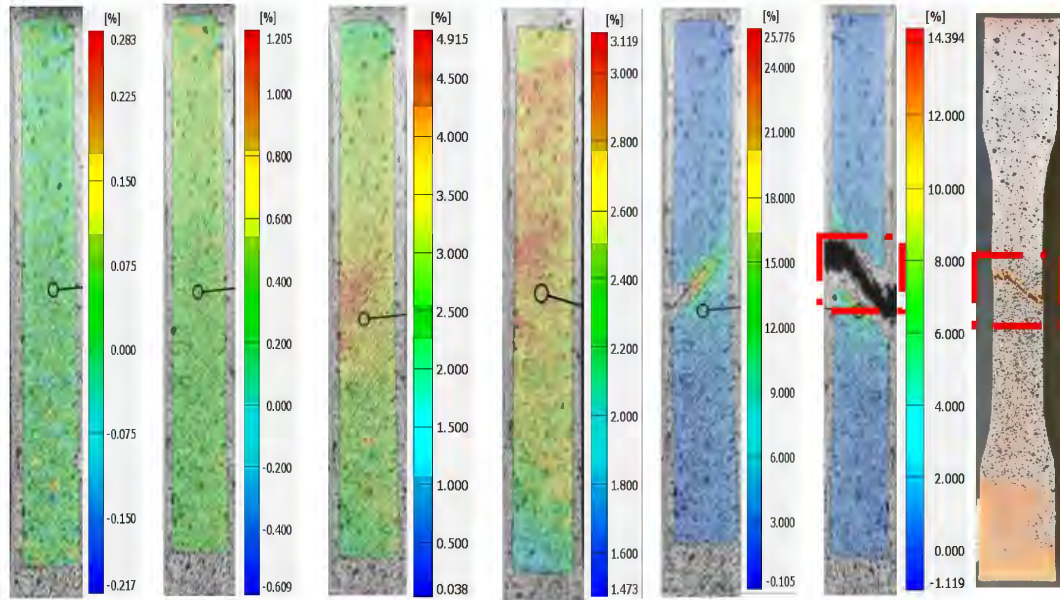


Fig. 82 Strain illustrated through contour plots for testing sample 26.

Fig. 81 and Fig. 82 show the contour plots of strain for sample 25 L3T3P1 and Sample 26 L3T3P2 in the Y-direction of DIC with tensile tests over time.

Sample 27: L3T3P3; L- 0.2mm, T- 220 °C, P- 140mm/s

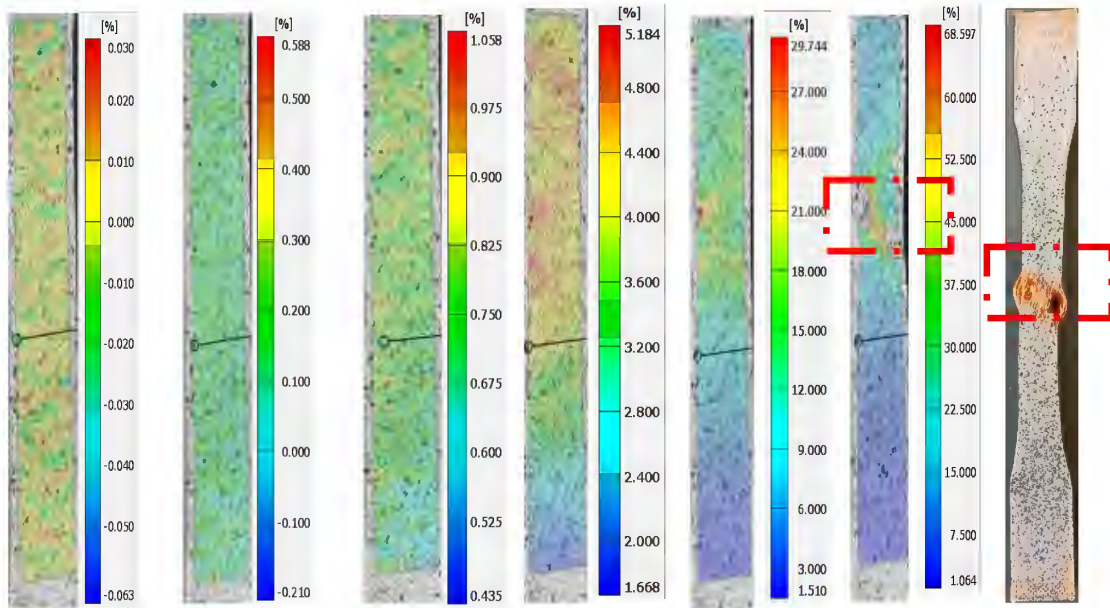


Fig.83 Strain illustrated through contour plots for testing sample 27.

Fig. 83 shows the contour plots of strain for sample 27 L3T3P3 in the Y-direction of DIC with tensile tests over time.

4.5. DIC Result Analysis

DIC is adept at measuring the full-field displacement and strain during tensile testing. It can track thousands of points on the tested specimens, providing precision that surpasses traditional extensometer techniques. Unlike these techniques, which can only obtain the average major strain value, DIC offers the capability to measure both the major and minor strains. It even has the unique ability to analyze the initiation of necking, a nearly impossible feat with traditional methods.

In this study, in terms of data visualization, the y-direction strains can be represented by a color scale bar that shows the minimum to the maximum strain values, and the red regions represent the maximum value of strains in the y-direction. Strain in the X direction is negative in the data, which means that the regions within the sample's specimens are experiencing compression or reduction in strain.

Moreover, DIC observations also indicate that in most cases, the edge of the gauge section or middle of the specimens had the largest number of neck reasons. It becomes especially noticeable at the edges of the gauge sections of the tensile specimens when the layer thickness is set to 0.1mm (see Figs. 57-65). In this case, two exceptions were noted.

For instance, testing sample-22 (L3T2P1) in Fig. 78 exhibited different behavior at a higher thickness 0.2mm, extrusion temperature 210°C, print speed 140mm/s, and sample-26 in Fig. 82 (L3T3P2) at a higher layer thickness 0.2mm, higher extrusion temperature 220°C, lower print speed 100mm/s. Conversely, in Figs. 57-83 The contour plots of strain (ϵ_{yy}) for testing samples 19-27 in the Y-direction, a layer thickness of 0.2mm, and neck primarily were observed in the middle sections of the specimens. Nonetheless, a layer

thickness of 0.15mm in Figs. 66-74 experienced neck reason in both gauge sections and the middle of the specimens.

The different printing parameters could be a possible reason for the location of the neck reason. The change in the three process parameters, and other printing settings, may introduce a potential weakness in the specimens and result in a necking reason on the edge of the gauge section or middle of the specimens. These findings highlight the impact of different printing parameters on the 3D-printed silk-PLA material's behavior under stress.

CHAPTER 5

CONCLUSION AND FUTURE WORKS

5.1. Conclusion

This study experimentally investigated the impact of various 3D printing parameters on the mechanical characteristics of silk-PLA material. Three parameters of the FDM 3D printing process were taken into account, and mechanical characteristics were focused on, such as modulus of elasticity and ultimate strength of Silk-PLA material. Additionally, the study measured and analyzed strain in both lateral (X) and longitudinal (Y) directions using the DIC method. While extensive research has been conducted on FDM process parameter optimization, relatively little focus is on investigating higher printing speeds for PLA-printed materials with the implementation of DIC. Therefore, this research was focused on determining a well-defined connection between these printing parameters, and the mechanical characteristics of silk-PLA materials. Moreover, ANOVA showed that layer thickness, nozzle temperature, and printing speed significantly affected FMD-printed silk PLA material.

This study concluded that-

- i. The ANOVA Table revealed that the layer thickness, nozzle temperature, and print speed are the key factors significantly impacting the ultimate tensile strength.
- ii. Considering the obtained P value from ANOVA, printing speed and layer thickness had no critical influence on the responses of Young's modulus.

However, the nozzle temperature significantly influenced Young's modulus value.

- iii. Higher nozzle temperatures may enhance the material's performance by improving layer adhesion, leading to an increase in tensile stress capacity, which agrees with [78] [79].
- iv. The maximum tensile strength of 40.68 MPa was achieved with the optimal combination of process parameters at testing sample 26 when a layer thickness of 0.2mm, temperature of the nozzle at 220°C, and print speed of 120mm/s.
- v. The DIC method enhanced the evaluation of mechanical properties by providing full-field strain and displacement value that traditional testing methods like extensometer or strain gauge cannot offer solely.
- vi. Different printing parameters could be a possible reason for the initiation of necking in a different location of the tensile specimens.
- vii. Thicker layers reduced the breaking strain in most cases, impacting the mechanical characteristics of the Silk-PLA material.

5.2. Printing Challenges

Printing failures were observed with printing speeds at 140mm/s. It was observed that when printing operations operated at these specific speed ranges, encountered a higher rate of printing failures issue. Tensile testing sample 4 - L1T2P1, when layer thickness is 0.1mm, nozzle temperature is 210°C, and printing speed of 140mm/s, and sample 07- L1T3P3, L1-0.1mm, T3- 220°C, and P3- 140mm/s, encountered the most printing failures as shown in Fig. 84. This printing failure could be over-extrusion or layer adhesion, when too much material is dispensed due to the higher printing speed, leading to excess filament that can disrupt the print's accuracy and quality, and poor layer adhesion and leading to individual layers of the print do not bond correctly.



Fig. 84 Printing failure sample at 140mm/s printing speed.

5.3. Future work

One key area of exploration is the optimization of process parameters to ensure better quality output. My current study highlighted the significance of maintaining the process parameters to ensure the quality of 3D-printed parts. Future studies could explore the integration of sensors into 3D printing systems. The sensors could measure crucial parameters like printing speed, printing temperature, and other parameters in real time, allowing researchers to gain insights into the printing process and make necessary adjustments to improve quality.

Another important aspect to consider is the reduction of downtime caused by print failure. This issue not only consumes valuable time but also wastes materials. This study observed frequent print failure issues at high printing speed conditions at 140mm/s. Therefore, future research will focus on the use of artificial intelligence (AI) to detect early faults to address this challenge. The printing process can be analyzed by AI algorithms to identify potential failures before they happen, which allows operators to take preventive measures and minimize disruptions. The ability to customize printing parameters holds significant potential for progress in additive manufacturing. By allowing users to tailor printing parameters during printing to specific requirements or materials, manufacturers can achieve greater flexibility and versatility in their production processes.

In conclusion, future research in additive manufacturing will consider focusing on integrating advanced sensing technologies, implementing AI for fault detection, and enabling on-the-go parameter adjustments. By embracing these advancements, FDM additive manufacturing can significantly improve quality, efficiency, and adaptability. which will lead to foster broader adoption and spur innovation across multiple industries.

REFERENCES

- [1] Mohamed, Omar Ahmed, Syed Hasan Masood, Jahar Lal Bhowmik, and Anthony E. Somers, "Investigation on the tribological behavior and wear mechanism of parts processed by fused deposition additive manufacturing process.," " *Journal of Manufacturing Processes*, no. 29, pp. 149-159, 2017.
- [2] Gibson, Ian, David W. Rosen, Brent Stucker, Mahyar Khorasani, David Rosen, Brent Stucker, and Mahyar Khorasani, *Additive manufacturing technologies*, vol. 17, Cham, Switzerland: Springer, 2021.
- [3] Wohlers, Terry, Tim Gornet, Noah Mostow, Ian Campbell, Olaf Diegel, Joseph Kowen, Ray Huff et al., "History of additive manufacturing.," 2016.
- [4] Sepasgozar, S. M. E., A. Shi, L. Yang, S. Shirowzhan, and D. J. Edwards, "Additive Manufacturing Applications for Industry 4.0: A Systematic Critical Review," *Buildings*, vol. 10, no. 12, p. 231, 2020.
- [5] Yao, Tianyun, Zichen Deng, Kai Zhang, and Shiman Li., "A method to predict the ultimate tensile strength of 3D printing polylactic acid (PLA) materials with different printing orientations.," *Composites Part B: Engineering* , vol. 163 (2019), pp. 393-402, 2019.
- [6] Carneiro, Olga S., A. F. Silva, and Rui Gomes, "Fused deposition modeling with polypropylene," *Materials & Design*, vol. 83, pp. 768-776, 2015.
- [7] Murugan, Ramu, R. N. Mitilesh, and Sarat Singamneni, "Influence of process parameters on the mechanical behaviour and processing time of 3D printing," *Int. J. Mod. Manuf. Technol*, vol. 1, pp. 21-27, 2019.
- [8] Bhosale, Vaibhav, Pranav Gaikwad, Shivam Dhere, Chinmay Sutar, and Sunil J. Raykar., "Analysis of process parameters of 3D printing for surface finish, printing time and tensile strength," *Materials Today: Proceedings*, vol. 59, pp. 841-846, 2022 .
- [9] Rao, V. Durga Prasada, P. Rajiv, and V. Navya Geethika, "Effect of fused deposition modelling (FDM) process parameters on tensile strength of carbon fibre PLA.," *Materials Today: Proceedings*, vol. 18, pp. 2012-2018, 2019.
- [10] Lanzotti, Antonio, Marzio Grasso, Gabriele Staiano, and Massimo Martorelli, "The impact of process parameters on mechanical properties of parts fabricated in PLA

- with an open-source 3-D printer," *Rapid Prototyping Journal*, Vols. 21, no. 5, pp. 604-617, 2015.
- [11] Chacón, J. M., Miguel Angel Caminero, Eustaquio García-Plaza, and Pedro J. Núñez, "Additive manufacturing of PLA structures using fused deposition modelling: Effect of process parameters on mechanical properties and their optimal selection," *Materials & Design*, vol. 124, pp. 143-157, 2017.
 - [12] Magri, Anouar El, Khalil El Mabrouk, Sébastien Vaudreuil, and Mohamed Ebn Touhami, "Mechanical properties of CF-reinforced PLA parts manufactured by fused deposition modeling," *Journal of Thermoplastic Composite Materials*, vol. 34, no. 5, pp. 581-595, 2011.
 - [13] Maguluri, Nagarjuna, Gamini Suresh, and K. Venkata Rao, "Assessing the effect of FDM processing parameters on mechanical properties of PLA parts using Taguchi method," *Journal of Thermoplastic Composite Materials*, vol. 36, no. 4, pp. 472-1488, 2023.
 - [14] Alsoufi, Mohammad S., and Abdulrhman E. Elsayed, "Surface roughness quality and dimensional accuracy—a comprehensive analysis of 100% infill printed parts fabricated by a personal/desktop cost-effective FDM 3D printer," *Materials Sciences and Applications*, vol. 9, no. 01, p. 11, 2018.
 - [15] Lei, Mingju, Qinghua Wei, Mingyang Li, Juan Zhang, Rongbin Yang, and Yanen Wang, "Numerical simulation and experimental study the effects of process parameters on filament morphology and mechanical properties of FDM 3D printed PLA/GNPs nanocomposite," *Polymers* 14, no. 15 (2022): 3081., vol. 14, no. 15, p. 3081, 2022.
 - [16] Yang, Yuan, Xilin Dai, Bo Yang, Peng Zou, Feng Gao, Jihao Duan, and Changxu Wang, "Optimization of polylactic acid 3D printing parameters based on support vector regression and cuckoo search," *Polymer Engineering & Science*, vol. 63, no. 10, pp. 3243-3253, 2023.
 - [17] Heidari-Rarani, Mohammad, Niloofar Ezati, P. Sadeghi, and M. R. Badrossamay, "Optimization of FDM process parameters for tensile properties of polylactic acid specimens using Taguchi design of experiment method," *Journal of Thermoplastic Composite Materials*, vol. 35, no. 12, pp. 2435-2452, 2022.
 - [18] Nabavi-Kivi, A., Majid R. Ayatollahi, Parham Rezaeian, and Nima Razavi., "Investigating the effect of printing speed and mode mixity on the fracture behavior of FDM-ABS specimens.," *Theoretical and Applied Fracture Mechanics*, vol. 118, p. 103223, 2022.

- [19] Napolitano, Francesco, Ersilia Cozzolino, Ilaria Papa, Antonello Astarita, and Antonino Squillace, "Experimental integrated approach for mechanical characteristic optimization of FDM-printed PLA in an energy-saving perspective.," *The International Journal of Advanced Manufacturing Technology* , vol. 121, no. 5, pp. 3551-3565, 2022.
- [20] Ł. Miazio, "Impact of print speed on strength of samples printed in FDM technology.," *Agricultural Engineering* , vol. 23, 2019.
- [21] Khosravani, Mohammad Reza, Filippo Berto, Majid R. Ayatollahi, and Tamara Reinicke. , "Characterization of 3D-printed PLA parts with different raster orientations and printing speeds.," *Scientific Reports*, vol. 12, no. 1, p. 1016, 2022.
- [22] Rezaeian, Parham, Majid R. Ayatollahi, A. Nabavi-Kivi, and Nima Razavi, "Effect of printing speed on tensile and fracture behavior of ABS specimens produced by fused deposition modeling.," *Engineering Fracture Mechanics* , vol. 266, p. 108393, 2022.
- [23] Khosravani, Mohammad Reza, and Tamara Reinicke, "Effects of raster layup and printing speed on strength of 3D-printed structural components," *Procedia Structural Integrity* , vol. 28, pp. 720-725, 2020.
- [24] Zhang, Xinzhou, Lan Chen, Tom Mulholland, and Tim A. Osswald, "Effects of raster angle on the mechanical properties of PLA and Al/PLA composite part produced by fused deposition modeling," *Polymers for Advanced Technologies* , vol. 30, no. 8, pp. 2122-2135, 2019.
- [25] M. Algarni, "The influence of raster angle and moisture content on the mechanical properties of PLA parts produced by fused deposition modeling," *Polymers* , vol. 13, no. 2, p. 237, 2021.
- [26] Sudin, Mohd Nizam, Nazri Md Daud, Faiz Redza Ramli, and Mohd Asri Yusuff, "The Effect of Nozzle Size on the Tensile and Flexural Properties of PLA Parts Fabricated Via FDM," *Science, Engineering and Technology* , vol. 3, no. 1, pp. 33-43, 2023.
- [27] Kiński, Wojciech, and Paweł Pietkiewicz, "Influence of the printing nozzle diameter on tensile strength of produced 3D models in FDM technology," *Agricultural Engineering* , vol. 24, no. 3, pp. 31-38, 2020.
- [28] Buj-Corral, Irene, Ali Bagheri, Alejandro Domínguez-Fernández, and Ramón Casado-López, "Influence of infill and nozzle diameter on porosity of FDM printed

- parts with rectilinear grid pattern," *Procedia Manufacturing* , vol. 41, pp. 288-295, 2019.
- [29] Afrose, Mst Faujiya, S. H. Masood, Pio Iovenitti, Mostafa Nikzad, and Igor Sbarski., "Effects of part build orientations on fatigue behaviour of FDM-processed PLA material," *Progress in Additive Manufacturing* , vol. 1, pp. 21-28, 2016.
- [30] Seol, Kyoung-SU, Panxi Zhao, Byoung-Chul Shin, and Sung-Uk Zhang, "Infill print parameters for mechanical properties of 3D printed PLA parts," *한국기계학회지* , Vols. 17, no. 4 , pp. 9-16, 2018.
- [31] Hsiang Loh, Giselle, Eujin Pei, Joamin Gonzalez-Gutierrez, and Mario Monzón, "An overview of material extrusion troubleshooting," *Applied Sciences* , vol. 10, no. 14, p. 4776, 2020.
- [32] Fernandez-Vicente, Miguel, Wilson Calle, Santiago Ferrandiz, and Andres Conejero, "Effect of infill parameters on tensile mechanical behavior in desktop 3D printing," *3D printing and additive manufacturing* , vol. 3, no. 3, pp. 183-192, 2016.
- [33] Gunasekaran, K. N., Vishaal Aravinth, CB Muthu Kumaran, K. Madhankumar, and S. Pradeep Kumar, "Investigation of mechanical properties of PLA printed materials under varying infill density," *Materials Today*, Vols. Volume 45, Part 2, pp. 1849-1856, 2021.
- [34] Moradi, Mahmoud, Ahmad Aminzadeh, Davood Rahmatabadi, and Alireza Hakimi, "Experimental investigation on mechanical characterization of 3D printed PLA produced by fused deposition modeling (FDM)," *Materials Research Express* , vol. 8, no. 3, p. 035304, 2021.
- [35] Lubombo, Christian, and Michel A. Huneault., "Effect of infill patterns on the mechanical performance of lightweight 3D-printed cellular PLA parts," *Materials Today Communications* , vol. 17, pp. 214-228, 2018.
- [36] Abeykoon, Chamil, Pimpisut Sri-Amphorn, and Anura Fernando, "Optimization of fused deposition modeling parameters for improved PLA and ABS 3D printed structures," *International Journal of Lightweight Materials and Manufacture* 3, vol. 3, pp. 284-297, 2020.
- [37] Samykano, M., S. K. Selvamani, K. Kadirgama, W. K. Ngui, G. Kanagaraj, and K. J. T. I. J. O. A. M. T. Sudhakar, "Mechanical property of FDM printed ABS: influence," *The International Journal of Advanced Manufacturing Technology* , vol. 102 , pp. 2779-2796, 2019.

- [38] Fernandes, João, Augusto M. Deus, Luis Reis, Maria Fatima Vaz, and Marco Leite, "Study of the influence of 3D printing parameters on the mechanical properties of PLA," *In Proc. Int. Conf. Prog. Addit. Manuf*, vol. 2018, pp. 547-552, 2018.
- [39] Wang, Y. H., J. H. Jiang, C. Wanintrudal, C. H. A. N. G. Q. I. N. G. Du, D. A. J. U. N. Zhou, Lorenzo M. Smith, and L. X. Yang, "Whole field sheet-metal tensile test using digital image correlation.," *Experimental Techniques* , vol. 34, no. 2, pp. 54-59, 2010.
- [40] Wattrisse, B., Chrysochoos, A., Muracciole, J. M., & Némot-Gaillard, M., "Analysis of strain localization during tensile tests by digital image correlation," *Experimental mechanics*, vol. 41, pp. 29-39, 2001.
- [41] Bastawros, A. F., Hi Bart-Smith, and A. G. Evans, "Experimental analysis of deformation mechanisms in a closed-cell aluminum alloy foam," *Journal of the Mechanics and Physics of Solids*, vol. 48, no. 2, pp. 301-322, 2000.
- [42] Chevalier, Luc, Sylvain Calloch, François Hild, and Yann Marco, "Digital image correlation used to analyze the multiaxial behavior of rubber-like materials," *European Journal of Mechanics-A/Solids* , vol. 20, no. 2, pp. 169-187, 2001.
- [43] Han, Yougun, Allan D. Rogalsky, Boxin Zhao, and Hyock Ju Kwon, "The application of digital image techniques to determine the large stress–strain behaviors of soft materials," *Polymer Engineering & Science* , vol. 52, no. 4, pp. 826-834, 2012.
- [44] Gao, Jianxin, and Haixia Shang, "Deformation-pattern-based digital image correlation method and its application to residual stress measurement," *Applied optics* , vol. 48, no. 7, pp. 1371-1381, 2009.
- [45] Xie, Yuxuan, Zhanyu Zhai, and Yunhuan Liu, "Characterization of the tensile behavior of continuous carbon fiber reinforced polyamide 6 under self-resistance electrical heating," *Polymer Composites* , vol. 44, no. 6, pp. 3185-3195, 2023.
- [46] Alam, Syed Yasir, Jacqueline Saliba, and Ahmed Loukili, "Fracture examination in concrete through combined digital image correlation and acoustic emission techniques," *Construction and Building Materials* , vol. 69, pp. 232-242., 2014.
- [47] Abanto-Bueno, Jorge, and John Lambros, "Investigation of crack growth in functionally graded materials using digital image correlation," *Engineering Fracture Mechanics*, vol. 69, no. 14-16, pp. 1695-1711, 2002.
- [48] Aydın, Murat, and Özkan Öz, "Application of digital image correlation technique to tensile test for printed PLA specimens," *International Journal of 3D Printing Technologies and Digital Industry 2*, vol. 2, pp. 1-7, 2018.

- [49] Schnittker, Kevin, Edel Arrieta, Xavier Jimenez, David Espalin, Ryan B. Wicker, and David A. Roberson, "Integrating digital image correlation in mechanical testing for the materials characterization of big area additive manufacturing feedstock," *Additive Manufacturing* , vol. 26, pp. 129-137, 2019.
- [50] Xu, Zhuo, Rakel Fostervold, and Nima Razavi, "Scale effect on the mechanical behavior of PLA specimens fabricated via Fused Deposition Modeling," *Procedia Structural Integrity*, vol. 33 , pp. 564-570, 2011.
- [51] Mehdikhani, Mahoor, Mohammadali Aravand, Baris Sabuncuoglu, Michaël G. Callens, Stepan V. Lomov, and Larissa Gorbatikh., "Full-field strain measurements at the micro-scale in fiber-reinforced composites using digital image correlation," *Composite Structures* , no. 140, pp. 192-201, 2016.
- [52] Cerbu, C., D. Xu, H. Wang, and I. C. Roşca, "The use of digital image correlation in determining the mechanical properties of materials," *In IOP Conference Series: Materials Science and Engineering*, vol. 399, no. 1, p. 012007, 2018.
- [53] Pellegrini, Alessandro, Maria Emanuela Palmieri, Fulvio Lavecchia, Luigi Tricarico, and Luigi Maria Galantucci, "Auxetic behavior of 3D-printed structure made in acrylonitrile butadiene styrene and carbon fiber-reinforced polyamide," *Progress in Additive Manufacturing*, vol. 9, no. 2, pp. 461-469, 2024.
- [54] K. Schnittker, "Evaluation Of Large Area Additively Manufactured Fiber Reinforced Acrylonitrile Butadiene Styrene (abs)," 2018.
- [55] Bedsole, Robert, Charles Hill, Vlastimil Kunc, Yanli Wang, and Kyle Rowe, "Structural evaluation of complex subcomponents manufactured by large scale extrusion deposition of carbon fiber reinforced aBS.," 2017.
- [56] Tucker, Michael R., Léa Deillon, Robin Forner, and Markus Bambach., "Effects of CuCr1Zr contamination on the tensile properties and microstructure of stainless steel 316L produced via laser powder bed fusion," *Progress in Additive Manufacturing* , pp. 1-21, 2024.
- [57] Wang, Y. H., J. H. Jiang, C. Wanintrudal, C. H. A. N. G. Q. I. N. G. Du, D. A. J. U. N. Zhou, Lorenzo M. Smith, and L. X. Yang., "Whole field sheet-metal tensile test using digital image correlation," *Experimental Techniques* , Vols. 34, no. 2, pp. 54-59, 2010.
- [58] Jiang, Lai, Sazidur Shahriar, Tony Grady, and Xiaobo Peng, "Woven Natural Fiber-Reinforced PLA Polymers 3D Printed through a Laminated Object Manufacturing Process.," 2023.

- [59] Petchwattana, Nawadon, Sirijutaratana Covavisaruch, and Nukul Euapanthasate, "Mechanical and thermal behaviors of the acrylic based core-shell rubber modified poly (lactic acid)," *Advanced Materials Research* , vol. 306 , pp. 340-343, 2011.
- [60] Ansari, Anis A., and M. Kamil, "Effect of print speed and extrusion temperature on properties of 3D printed PLA using fused deposition modeling process," *Materials Today: Proceedings* , vol. 45, pp. 5462-5468, 2021.
- [61] Ansari, Anis A., and M. Kamil., "Effect of print speed and extrusion temperature on properties of 3D printed PLA using fused deposition modeling process," *Materials Today: Proceedings* , vol. 45, pp. 5462-5468, 2021.
- [62] Wu, Pan, Tianyu Yu, Mingjun Chen, and David Hui, "Effect of printing speed and part geometry on the self-deformation behaviors of 4D printed shape memory PLA using FDM," *Journal of Manufacturing Processes*, vol. 84, pp. 1507-1518, 2022.
- [63] Yu, Zhu, Yingchao Gao, Jie Jiang, Hai Gu, Shuaishuai Lv, Hongjun Ni, Xingxing Wang, and Chaofan Jia, "Study on effects of FDM 3D printing parameters on mechanical properties of polylactic acid," *In IOP Conference Series: Materials Science and Engineering*, vol. 688, no. 3, p. 033026, 2019.
- [64] Pandžić, Adi, Damir Hodžić, and Aleksa Milovanović, "Effect of infill type and density on tensile properties of PLA material for FDM process," *In Proceedings of the 30th DAAAM International Symposium*, no. DAAAM International,, pp. 545-554, 2019.
- [65] Swetha, T. Angelin, V. Ananthi, Abhispa Bora, Nallathambi Sengottuvelan, Kumar Ponnuchamy, Govarthanan Muthusamy, and Ajij Arun, "A review on biodegradable polylactic acid (PLA) production from fermentative food waste-Its applications and degradation," *International Journal of Biological Macromolecules* , vol. 234 , p. 123703, 2023.
- [66] Cheung, Hoi-Yan, Kin-Tak Lau, Xiao-Ming Tao, and David Hui, "A potential material for tissue engineering: Silkworm silk/PLA biocomposite," *Composites Part B: Engineering*, vol. 39, no. 6, pp. 1026-1033, 2008.
- [67] Pastor-Artigues, Ma-Magdalena, Francesc Roure-Fernández, Xavier Ayneto-Gubert, Jordi Bonada-Bo, Elsa Pérez-Guindal, and Irene Buj-Corral, "Elastic asymmetry of PLA material in FDM-printed parts: Considerations concerning experimental characterisation for use in numerical simulations," *Materials*, vol. 13, no. 1, p. 15, 2019.

- [68] FUNMAT HT 3D PRINTER USER MANUAL, INTAMSYS TECHNOLOGY CO.,LTD.
- [69] He, F., and M. Khan, "Effects of Printing Parameters on the Fatigue Behaviour of 3D-Printed ABS under Dynamic Thermo-Mechanical Loads," *Polymers* , vol. 13, p. 2362, 2021.
- [70] Abbas, Tahseen Fadhil, Farhad Mohammad Othman, and Hind Basil Ali, "Influence of layer thickness on impact property of 3D-printed PLA," *Int. Res. J. Eng. Technol.(Irjet)* , vol. 5, no. 02, pp. 1-4, 2018.
- [71] Liu, Yanping, Wei Bai, Xian Cheng, Jiehua Tian, Donghao Wei, Yuchun Sun, and Ping Di, "Effects of printing layer thickness on mechanical properties of 3D-printed custom trays," *The Journal of Prosthetic Dentistry* , vol. 126, no. 5, pp. 671-e1, 2021.
- [72] Rajpurohit, Shilpesh R., and Harshit K. Dave, "Effect of process parameters on tensile strength of FDM printed PLA part," *Rapid Prototyping Journal* , vol. 24, no. 8, pp. 1317-1324, 2018.
- [73] Santhakumar, J., Rishabh Maggirwar, Srinivas Gollapudi, S. Karthekeyan, and Naveen Kalra, "Enhancing impact strength of fused deposition modeling built parts using polycarbonate material.," *Indian J. Sci. Technol* , Vols. 19, no. 34 , pp. 1-6, 2016.
- [74] Sood, Anoop Kumar, Raj K. Ohdar, and Siba S. Mahapatra, "Parametric appraisal of mechanical property of fused deposition modelling processed parts," *Materials & Design* , vol. 31, no. 1, pp. 287-295, 2010.
- [75] Elhatab, Karim, Sarit B. Bhaduri, and Prabaha Sikder, "Influence of fused deposition modelling nozzle temperature on the rheology and mechanical properties of 3d printed β -tricalcium phosphate (tcp)/polylactic acid (pla) composite," *Polymers* , vol. 14, no. 6, p. 1222, 2022.
- [76] Yu, Wangwang, Jianan Shi, Liwei Sun, and Wen Lei, "Effects of printing parameters on properties of FDM 3D printed residue of astragalus/polylactic acid biomass composites," *Molecules*, vol. 27, no. 21, p. 7373, 2022.
- [77] A. International, "Standard test method for tensile properties of plastics," *American Society for Testing and Materials*, 2010.
- [78] Benwood, Claire, Andrew Anstey, Jacek Andrzejewski, Manjusri Misra, and Amar K. Mohanty, "Improving the impact strength and heat resistance of 3D printed models: structure, property, and processing correlations during fused deposition

- modeling (FDM) of poly (lactic acid)," *ACS omega*, vol. 3, no. 4, pp. 4400-4411, 2018.
- [79] Thumsorn, Supaphorn, Wattanachai Prasong, Takashi Kurose, Akira Ishigami, Yutaka Kobayashi, and Hiroshi Ito, "Rheological behavior and dynamic mechanical properties for interpretation of layer adhesion in FDM 3D printing," *Polymers*, vol. 14, no. 13, p. 2721, 2022.
- [80] Hikmat, Mohammed, Sarkawt Rostam, and Yassin Mustafa Ahmed. , "Investigation of tensile property-based Taguchi method of PLA parts fabricated by FDM 3D printing technology.," *Results in Engineering*, vol. 11, p. 100264, 2021.
- [81] Dave, Harshit K., Ashish R. Prajapati, Shilpesh R. Rajpurohit, Naushil H. Patadiya, and Harit K. Raval., "Investigation on tensile strength and failure modes of FDM printed part using in-house fabricated PLA filament.," *Advances in Materials and Processing Technologies* , vol. 8, no. 1, pp. 576-597, 2022.
- [82] Hild, François, and Stéphane Roux, "Comparison of local and global approaches to digital image correlation," *Experimental mechanics* , vol. 52, no. 9, pp. 1503-1519, 2012.
- [83] Cantrell, Jason T., Sean Rohde, David Damiani, Rishi Gurnani, Luke DiSandro, Josh Anton, Andie Young et al, "Experimental characterization of the mechanical properties of 3D-printed ABS and polycarbonate parts," *Rapid Prototyping Journal* , vol. 23, no. 4, pp. 811-824, 2017.
- [84] Ma, Lian-hua, Kun Zhang, Zhi-bo Pan, Wei Zhou, and Jia Liu, "Experimental investigation on the mechanical behavior and damage of 3D printed composites under three-point bending," *Journal of Composite Materials* , vol. 56, no. 7, pp. 1019-1037, 2022.
- [85] Fraccaroli, L. O. R. E. N. Z. O., Carlo Gorla, and F. R. A. N. C. O. Concli., "Structural modelling of multilayer skis with an open source FEM software," in *In IOP Conference Series: Materials Science and Engineering*, 2021.
- [86] Dong, Y. L., and Bing Pan, "A review of speckle pattern fabrication and assessment for digital image correlation," *Experimental Mechanics* , vol. 57, pp. 1161-1181, 2017.
- [87] Chacón, J. M., Miguel Angel Caminero, Eustaquio García-Plaza, and Pedro J. Núñez, "Additive manufacturing of PLA structures using fused deposition modelling: Effect of process parameters on mechanical properties and their optimal selection," *Materials & Design* , vol. 124, pp. 143-157, 2017.

- [88] Bhosale, Vaibhav, Pranav Gaikwad, Shivam Dhere, Chinmay Sutar, and Sunil J. Raykar, "Analysis of process parameters of 3D printing for surface finish, printing time and tensile strength," *Materials Today: Proceedings* , vol. 59, pp. 841-846, 2022.
- [89] Nomani, Junior, Daniel Wilson, Mariana Paulino, and Mazher Iqbal Mohammed, "Effect of layer thickness and cross-section geometry on the tensile and compression properties of 3D printed ABS," *Materials Today Communications* , vol. 22, p. 100626, 2020.
- [90] Wu, Wenzheng, Peng Geng, Guiwei Li, Di Zhao, Haibo Zhang, and Ji Zhao, "Influence of Layer Thickness and Raster Angle on the Mechanical Properties of 3D-Printed PEEK and a Comparative Mechanical Study between PEEK and ABS," *Materials*, Vols. 8, no. 9, pp. 5834-5846, 2015.
- [91] Jeon, Haejoon, Jihoon Park, Sunju Kim, Kyungho Park, and Chungsik Yoon, "Effect of nozzle temperature on the emission rate of ultrafine particles during 3D printing," *Indoor Air* , vol. 30, no. no. 2 , pp. 306-314, 2020.
- [92] Sabik, Agnieszka, Magdalena Rucka, A. Andrzejewska, and Erwin Wojtczak, "Tensile failure study of 3D printed PLA using DIC technique and FEM analysis," *Mechanics of Materials* , vol. 175, p. 104506, 2022.
- [93] A. S. f. T. a. Materials, Standard test method for tensile properties of plastics., American Society for Testing and Materials, 2010.
- [94] Mishra, Debashis, and Anil Kumar Das, "Linear model analysis of fused deposition modeling process parameters for obtaining the maximum tensile strength in acrylonitrile butadiene styrene (ABS) and carbon fiber polylactic acid (PLA) materials," *Multidiscipline Modeling in Materials and Structures* , vol. 17, no. 5, pp. 915-930, 2021.
- [95] Tung, Shih-Heng, Ming-Hsiang Shih, and Jui-Chao Kuo, "Application of digital image correlation for anisotropic plastic deformation during tension testing," *Optics and Lasers in Engineering*, vol. 48, no. 5, pp. 636-641, 2010.

CURRICULUM VITAE

Razaul Islam rislam1@pvamu.edu

EDUCATION

- Ph.D. Mechanical and Aerospace Engineering, Oklahoma State University, OK, Ongoing
- M.S. Mechanical Engineering, Prairie View A&M University, Prairie View, TX, 2024
- B.S. Aeronautical Engineering, Shenyang Aerospace University, China, 2016

WORK EXPERIENCE

- Company: Sky Capital Airlines, Bangladesh
Position: Trainee Engineer, 2021 – 2022
- Company: United College of Aviation, Science and Management, Bangladesh
Position: Lecturer 2018 - 2020

PROFESSIONAL, AND WORK-RELATED SKILLS

- Computer-Aided Design: CATIA V5, SOLIDWORKS, Autodesk Fusion360
- Simulation & Data Analytics: ANSYS, MATLAB, MINITAB, Sigma Plot
- Programming: C, Python
- DIC Analysis: GOM Snap, GOM Professional

PUBLICATIONS AND PRESENTATIONS

1. **R. Islam**, Saquib Shahriar, Jaejong Park, Xiaobo Peng, "Effect of Process Parameters on Mechanical Properties of the 3d Printed Silk-Pla Specimens Fabricated via Fused Deposition Modeling" ASME (IMECE) 2024 (Accepted for publication)
2. Cori Yancy, Saquib Shahriar, **R. Islam**, Rambod Rayegan, Alok Sutradhar, Jaejong Park, "Identifying Correlation between Thermal Gradient and Major FDM Printing Parameters for Enhanced Mechanical Properties" Progress in Additive Manufacturing Journal (Technical Paper on review).
3. Saquib Shahriar, **R. Islam**, Jaejong Park, "Enhancing the Structural Performance of 3d Printed Objects Through G Code Optimization via FEA in the FDM Process" ASME(IMECE) 2024 (Accepted for publication).
4. **R. Islam**, J. Park, "An Experimental Investigation of Printing Speed, Layer Thickness, and Nozzle Temperature On The Mechanical Properties of PLA-Printed Specimens," ASME (IMECE2023), New Orleans, Louisiana, October 29-November 2, 2023 (Presentation).
5. J. Park, **R. Islam**, C. A. King, L. Jiang, X. Peng, B. Yalvac, "Work In Progress: Virtual Reality For Manufacturing Equipment Training For Future Workforce Development," ASEE Annual Conference & Exposition, Baltimore, Maryland, June 25-28, 2023.